RAYTHEON

# RESEARCH ON THE CHEMISTRY AND SINGLE CRYSTAL GROWTH OF MAGNETIC OXIDES

H.J. Van Hook
A.E. Paladino
B.D. Roiter
T. Kohane
R.L. Mozzi

Research Division
Raytheon Company
Waltham 54, Massachusetts

FINAL REPORT
AF 19 (604)-5511

June 5, 1961



ELECTRONICS RESEARCH DIRECTORATE
AIR FORCE CAMBRIDGE RESEARCH LABORATORIES
OFFICE OF AEROSPACE RESEARCH
UNITED STATES AIR FORCE
BEDFORD, MASSACHUSETTS

# RESEARCH ON THE CHEMISTRY AND SINGLE CRYSTAL GROWTH OF MAGNETIC OXIDES

H. J. Van Hook
A. E. Paladino
B. D. Roiter
T. Kohane
R. L. Mozzi

Research Division
Raytheon Company
Waltham 54, Massachusetts

Final Report
AF 19(604)-5511
5 June 1961

Prepared for
Electronics Research Directorate
Air Force Cambridge Research Laboratories
Office of Aerospace Research
UNITED STATES AIR FORCE
Bedford, Massachusetts

Requests for additional copies by Agencies of the Department of Defense, their contractors, and other Government agencies should be directed to the:

ARMED SERVICES TECHNICAL INFORMATION AGENCY
ARLINGTON HALL STATION
ARLINGTON 12, VIRGINIA

All other persons and organizations should apply to the:

U. S. DEPARTMENT OF COMMERCE
OFFICE OF TECHNICAL SERVICES
WASHINGTON 25, D. C.

Research on the Chemistry and Single Crystal Growth of Magnetic Oxides

H. J. Van Hook
A. E. Paladino
B. D. Roiter
T. Kohane
R. L. Mozzi

## ABSTRACT

Phase relationships in the liquidus range under different oxygen partial pressures are described for the oxide systems involving yttrium-iron garnet and yttrium-gadolinium-iron garnet phases. These data are applied to an analysis of the conditions for crystal growth of the incongruently melting garnet phase from oxide liquids as concerns the temperature-composition-oxygen pressure range for stable growth, and the composition of garnets crystallized under these conditions. Some preliminary results are presented on single crystal growth of yttrium-iron garnet by a modification of the Czochralski technique.

The conductivity mechanism in magnetite-derived spinels is strongly dependent on oxygen stoichiometry and cation distribution. Phase equilibrium data in the systems Ni-Fe-O and Co-Fe-O are described with emphasis on the conditions necessary to prepare the spinel solid solutions $Fe_3O_4$-$NiFe_2O_4$ and $Fe_3O_4$-$Co_3O_4$. Cation distribution studies by x-ray diffraction techniques are given for single phase spinels in the system Mg-Fe-O as well as preliminary data for spinel composition preparation in the system Fe-Al-O. The effect of substitution of the cations $Ni^{2+}$, $Co^{2+}$, $Mg^{2+}$ and $Al^{3+}$ for divalent and/or trivalent iron on electrical conductivity in magnetite is discussed. Resistivity and thermoelectric data are given for a series of nickel ferrous ferrites and the results are analyzed quantitatively.

TABLE OF CONTENTS

TABLE OF CONTENTS (Cont' d. )

TABLE OF CONTENTS (Cont'd.)

## LIST OF FIGURES

LIST OF FIGURES (Cont'd.)

LIST OF FIGURES (Cont'd.)

## LIST OF TABLES

## I. GENERAL INTRODUCTION

Experimental studies of crystal growth of ferromagnetic garnets and the chemistry of magnetic oxides have been the subject of continued research under the present contract. At this point it appears appropriate to review the progress made over the past two years in phase equilibrium studies, and the programs being initiated in physical measurements and crystal growth as a result of the equilibrium work.

At its present stage, the program can be divided into two major areas: 1) liquidus equilibrium relations and single crystal growth in garnet-type oxide systems, and 2) subsolidus equilibria with electrical conductivity measurements made on spinel solid solutions. Each of these projects can be further subdivided into an initial phase of acquiring pertinent equilibrium data and a later phase where these results are applied in preparing known crystalline compositions under specific conditions.

The importance of equilibrium data as a necessary precursor to studies of electrical and magnetic properties and to crystal growth has not always been fully appreciated in the past. The importance of preliminary studies is particularly true in systems involving the transition metal oxides where large changes in oxygen content arise within the temperature range for the preparation of both polycrystalline and single crystal materials. The preliminary studies in this laboratory have, therefore, dealt in some detail with the thermal stability and chemical composition of certain magnetic oxide phases under the variable conditions of temperature, oxygen pressure, and total composition; these phase equilibrium data comprise the bulk of the factual data in this report.

The data obtained in the garnet systems are in support of a program on crystal growth from the melt and are confined primarily to the high temperatures where oxide liquids are stable. This section is followed by a very general

discussion of crystal growth and of the factors which may be expected to influence most significantly the kinetics of the growth process. The discussion does not consider the limitations in composition or temperature-stability of the garnet phase as shown by the various phase diagrams; the situation as described can be readily extended to take these factors into consideration.

The second part of this report describes phase equilibrium data for systems containing ferrimagnetic spinels and the application of these data to the preparation of spinels having known compositions for electrical measurements. Electrical conductivity in magnetite-derived spinels has been traditionally attributed to the exchange of valence electrons between $Fe^{2+}$ and $Fe^{3+}$ occupying octahedral sites in the structure. This point of view has prevailed ever since the earily conductivity studies by Verwey.[1]

The explanation given for conductivity in ferrites has been largely based on the work in magnetite. It has been assumed that the firing of ferrites at elevated temperatures is accompanied by oxygen loss, ferrous ion formation, and conduction via the valence exchange process. Qualitatively this description has considerable appeal, but the detailed analysis of such a process has not been rigorously made with the possible exception of Jonker's[2] studies in the magnetite-cobalt ferrite series. Any real attempt to develop a suitable model applicable to all spinels of necessity requires samples of explicitly defined composition, structure, and cation distribution. Therefore, as a prelude to any serious attempt to analyze conductivity processes in spinels, phase relations and ionic distribution where applicable will be required.

With the above objectives in mind, several spinel systems derived from magnetite have been considered as suitable for conductivity studies. The reasons for selecting each will be briefly outlined in addition to the detailed description of the phase relations determined during the course of the current program. In one system, the cation distribution studies have been started and will be discussed in relation to the conductivity program. In addition, data on conductivity in one simple system will be presented with an explanation of the results based on a tentative model.

## II. GARNET SYSTEMS

### A. Phase Equilibria in Garnet-Type Oxide Systems

The system iron oxide-yttrium oxide serves as the focal point for studies of crystal growth of pure yttrium-iron garnet and for further research on phase relations in more complex systems involving substitution of other cations for yttrium and iron. Because of its critical importance, the system $Fe_2O_3$-FeO-$YFeO_3$ has been studied in detail in the temperature range of 1400°C to 1650°C and in several oxygen atmospheres. The methods used to define the critical points on the phase diagram are described in this final report as well as in Scientific Report No. 1 (January, 1960).[3] A follow-up of the original work on the air isobaric section with two other oxygen sections has resulted in a more complete picture of the system $Fe_2O_3$-FeO-$YFeO_3$ as a whole as described in Scientific Report No. 2 (January, 1961).[4]

Since the completion of the work on the yttrium-iron-oxygen system, a similar method of analysis has been used to study the effect of gadolinium substitution in yttrium-iron oxide compositions. A comparison of our early results with findings in the literature was contradictory so that a re-investigation of the system $Fe_2O_3$-FeO-$GdFeO_3$ was necessary before proceeding with experiments in the quaternary system. The phase relations for the air isobar in the four-component system Y-Gd-Fe-O are included in this report along with the proposed relationships for other oxygen pressure sections deduced from a knowledge of the limiting ternary systems. This line of investigation is continuing with studies on the effect of aluminum oxide substitutions in yttrium-iron garnet in a portion of the quaternary system Y-Al-Fe-O. The following discussion will summarize the experimental findings in the yttrium-iron-oxygen and yttrium-gadolinium-iron-oxygen systems.

## 1. The System $Fe_2O_3$-FeO-$YFeO_3$

### a. Introduction

The purpose of the phase equilibrium studies in this system was to locate the temperature-composition-oxygen pressure range for the coexistence of yttrium-iron garnet and oxide liquid, to determine the solubility of the garnet in oxide liquid as a function of temperature and pressure, to ascertain any deviation of the garnet phase from the stoichiometric formula $Y_3Fe_5O_{12}$ within the limits of measurement, and finally to determine the thermal stability of the garnet phase as influenced by oxygen pressure.

Previous studies by Muan,[5] Grieg,[6] and others[7, 8] have served as the basis for the investigation of non-condensed iron oxide containing systems and the form of the resulting phase diagrams. The original study of the system $Fe_2O_3$-$YFeO_3$ was made by Nielsen and Dearborn[9] in the course of their investigation of the effect of lead oxide addition on the melting relations. Since their work on this system was tentative and rather brief, it was felt that a more detailed investigation would be useful.

### b. Experimental Procedure

The furnace used in this study was a conventional platinum-rhodium wound resistance furnace with two concentric alumina muffles. The inner muffle of the furnace was sealed against the atmosphere. Ambient atmospheres other than air were achieved by a continuous gradual flow (1.5 liters per hour) of the desired gas through the furnace.

Samples in the form of powder were packed in platinum-rhodium vials and suspended at the thermal center of the furnace from platinum quench leads, the temperature gradient being about 1°C over the length of the sample vial (10 mm) at 1500°C. The sample was centered directly opposite a 95 percent Pt - 5 percent Rh vs 80 percent Pt - 20 percent Rh measuring thermocouple. This thermocouple was calibrated frequently during the investigation because

of the known tendency of iron-containing mixtures to contaminate platinum thermocouples after prolonged exposure at high temperatures and/or low partial oxygen pressures. The calibrants were diopside ($CaMgSi_2O_6$, melting point 1391.5°C)[10] and wollastonite ($CaSiO_3$, melting point 1544°C).[10] The melting point of these standard materials was determined to within ±1°C by quenching followed by microscopic examination and the temperature versus millivolt curve corrected correspondingly. The results of periodic checks have shown that this thermocouple is very stable in operation except where accidentally in direct contact with the oxide melt.

The oxide samples were contained in 80 percent Pt - 20 percent Rh vials approximately 10 mm in length made from 4 mm diameter tubing by sealing one end. Since the amount of material was limited (0.2 - 0.3 gm) by the crucible size, it was very important to provide as homogeneous a starting mixture as possible. Several different preparation techniques were tried. Mechanical mixtures of $Fe_2O_3$ and $Y_2O_3$ were found to be non-uniform and unsuitable for the quench runs. Chemical co-precipitation of the oxalates gave material with very fine particle size but, due to solubility differences of ferrous and yttrium oxalate and especially to the high solubility of ferric oxalate, mixtures varied considerably from the desired compositions and this method was also rejected. The hydroxides, however, are both quite insoluble in alkaline solution, forming an intimate co-precipitation mixture, and seemed to be much superior for the purpose at hand. Starting compositions were prepared by dissolving weighed amounts of yttrium and ferric nitrate in de-mineralized water and adding the solution slowly to concentrated $NH_4OH$. The mixed hydroxide precipitate was filtered, dried, and fired at 700°C before chemical analysis. Final compositions showed some variation from the theoretical input and a chemical analysis was run on each mixture to be certain of total composition. Deviation from the theoretical values was to be expected since the nitrate salts were hydrated with somewhat variable water content. Wet chemical analyses were made for both yttrium and iron; critical mixtures bracketing the garnet composition were analyzed until a standard deviation of ±0.1 mole percent was attained. Other analyses are considered to be accurate to within ±0.5 mole percent.

The phases present at melting temperatures were determined by the familiar quenching technique where a given starting composition is held at one temperature until equilibrium is achieved between the condensed phases and the ambient atmosphere before quenching or cooling rapidly to room temperature. For very fast quenching, provision was made to burn off the fine platinum wire holding the vial and drop the samples directly into the water below the furnace. Slower quenching rates were often desirable and could be achieved by lifting the sample out of the hot zone of the furnace and allowing it to cool in a stream of the gas used in the specific experiment. The advantage of slower cooling is that the liquid phase develops a characteristic eutectic-type intergrowth which is easier to identify in comparison with the crystalline phases than is the very fine-grained quenched liquid formed during faster cooling.

In experiments where a liquid phase was present, one hour runs were found to be long enough to assure equilibrium; below melting temperatures much longer periods were necessary. The lowest temperature runs below 1400°C were held 48 hours.

The phases present in the quenched specimens were identified optically in polished sections and by X-ray diffraction techniques. For the microscopic study, the sample and containing platinum vial were mounted and polished together so as to get a section representative of the entire specimen. Etching was not found to be necessary in identifying phases under the microscope.

X-ray diffraction patterns were taken as a general check on microscopic identification and in the more specific study of the solubility limits in yttrium garnet. To assure close control of composition for X-ray studies, two hydroxide mixtures were carefully analyzed for yttrium and iron to ±0.1 mole percent after conversion to the sesquioxide by firing to 700°C. The samples were then refired to 1100°C and reground, with special care being taken to avoid introducing impurities, especially iron, during grinding. Weighed amounts of these fired materials totaling about 2 grams were then mixed together and prefired at 1350°C for 12 hours. After regrinding, one-half gram samples were packed in platinum-rhodium vials and held at temperatures ranging from 1400°C to 1540°C before the final quenching in water.

A GE XRD5 X-ray diffractometer with cobalt radiation was used to measure the position of (12, 6, 0) garnet diffraction peak at about 151°2Θ. With a slow speed trace (0. 2° per min) and silicon powder as standard, the accuracy of the diffraction peak measurements is believed to be within the limits of ±0. 03°2Θ or ±0. 001 Å.

Although the composition of the various phases is known in terms of starting mixtures of $Fe_2O_3$ and $Y_2O_3$ from quenching data, the total oxygen content of the samples cannot be determined in this way. The amount of loss or gain of oxygen by the oxide mixtures was determined for seven critical compositions by thermogravimetric (weight loss) studies in different oxygen atmospheres by the gradual flow of air, oxygen, and $CO_2$ gases through the closed furnace tube. The unit (Fig. 1) is similar to the one described by White[11] having a standard analytical balance mounted on a table above a platinum wound furnace. The oxide samples were packed in platinum crucibles and suspended in the thermal center of the furnace by a wire connected to one pan of the balance. The hole for this wire was kept as small as possible to avoid back diffusion of air. With samples weighing 3 - 5 grams, the balance sensitivity of ±0. 3 mg corresponds to ±0. 1 percent change in weight.

The principle error in weight loss measurements is the volatilization loss of the platinum crucible which reaches a significant level above 1400°C. Samples near the yttrium-iron garnet composition required firings for extended periods of time because oxygen loss and gain is very slow in these samples. Due to platinum volatilization, these data are not as reliable as compositions higher in iron where weight gains and losses could be measured in shorter time intervals. The oxygen fraction data in the various oxygen atmospheres given in this report are therefore primarily based on an extrapolation of composition along the garnet + magnetite and garnet + liquid tie lines.

c. Experimental Results

The data obtained in quenching experiments are shown graphically in Fig. 2, the isobaric section through the ternary system. The lower diagram

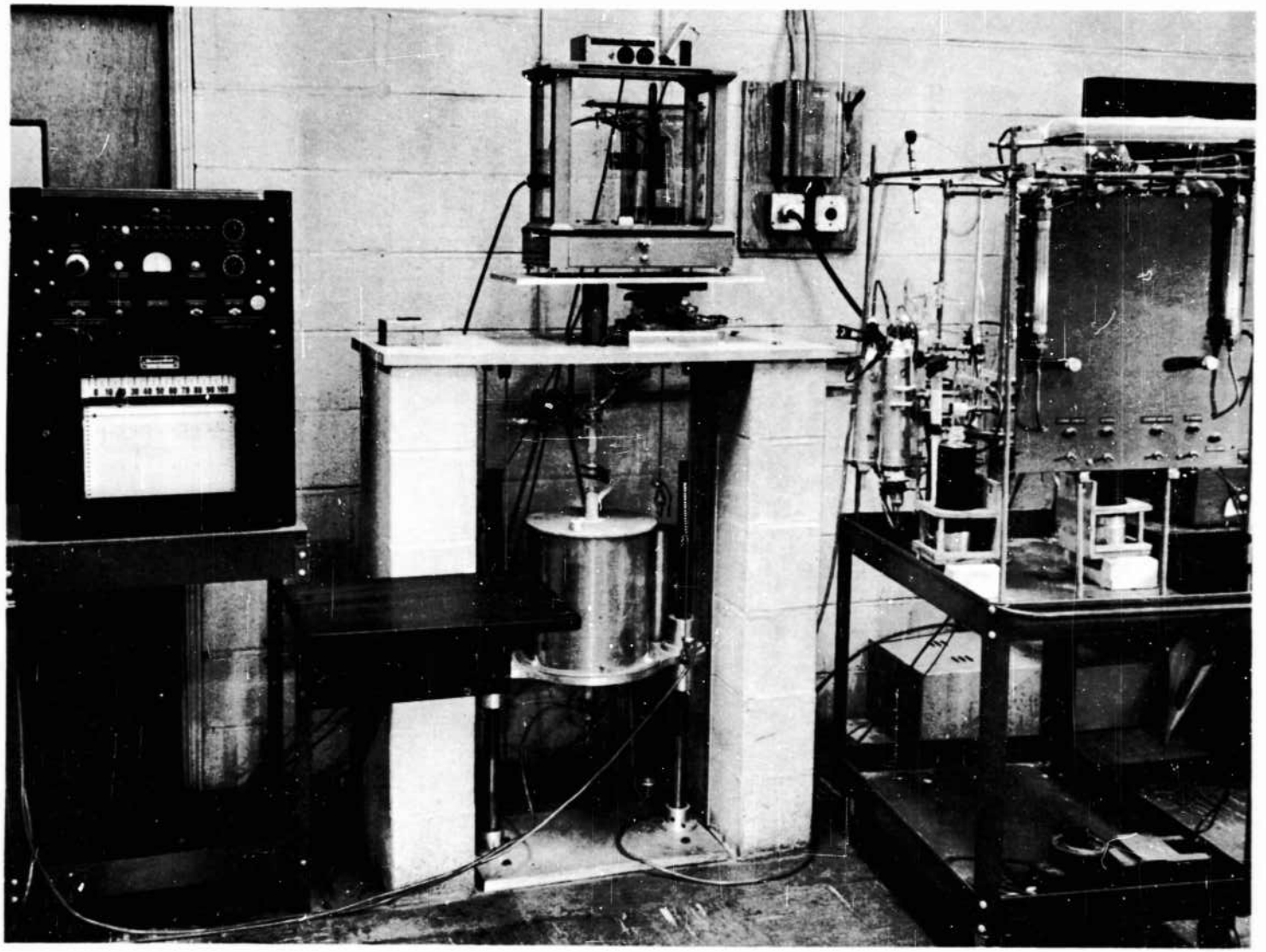

THERMOBALANCE UNIT. AMPLIFIER AND RECORDER ON LEFT,
GAS MIXING TRAIN ON THE RIGHT.

FIGURE I

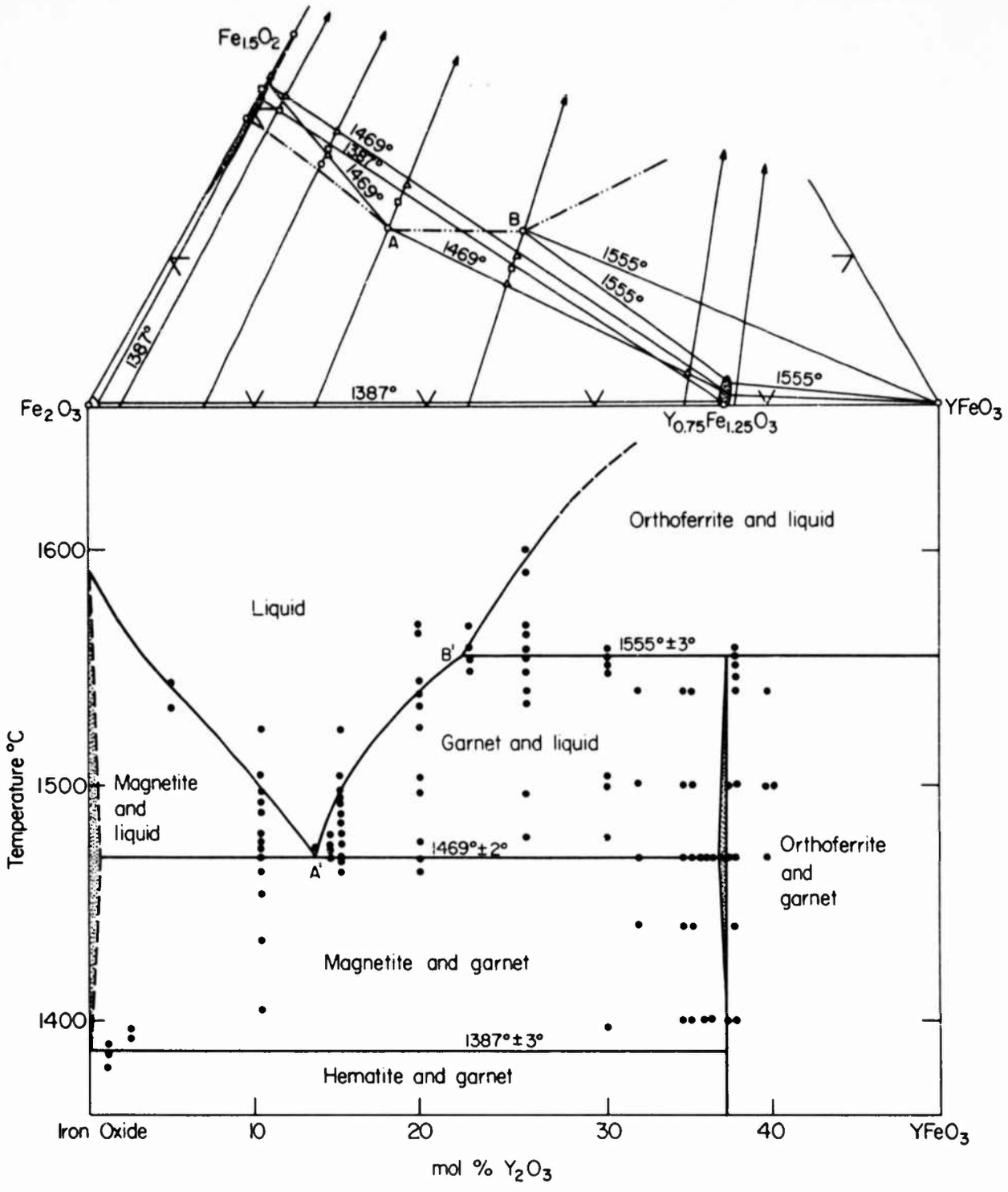


Phase relations in the system $Fe_2O_3$-FeO-$YFeO_3$ in air. The lower diagram shows phases present as a function of temperature and initial composition; the triangular diagram shows the ternary composition of the liquids (dash double-dot line) and of the crystalline garnet and magnetite phases (strippled areas). The light lines with arrows in the triangular plot are oxygen reaction lines, the isothermal reaction points with temperatures indicated are discussed in the text.

FIGURE 2

gives the appearance of a binary system with a "eutectic" at 1469°C ±2°C and 13.5 mole percent $Y_2O_3$ and a "peritectic" at 1555°C ±3°C and 22 mole percent $Y_2O_3$. The compositions given above are values in terms of starting mixtures of $Y_2O_3$ and $Fe_2O_3$ as originally analyzed, however, and are not true compositions of these melts since some oxygen has been lost at high temperature. The eutectic and peritectic points are actually the intersection of the air isobar with univariant boundary curves in the ternary system involving liquid, two crystalline phases and a gas with fixed partial oxygen pressure. The ternary composition of the condensed liquid and crystalline phases is shown above in mole percent of the components $Fe_2O_3$, FeO, and $YFeO_3$. In air there are three reaction temperatures involving three condensed phases and an atmosphere with a partial oxygen pressure of 159 mm Hg. These points appear as horizontal lines in the projection and as three phase triangles in the ternary plot. With increasing temperature the first reaction point in air occurs at 1387°C involving hematite, magnetite, and yttrium-iron garnet, $Y_{0.740}Fe_{1.250}O_{2.980}$. The second reaction point having the appearance of a eutectic point in the projected binary diagram occurs at 1469°C between magnetite, garnet, $Y_{0.745}Fe_{1.255}O_{2.970}$, and oxide liquid, $Y_{0.27}Fe_{1.73}O_{2.87}$. Yttrium-iron garnet decomposes in air at 1555°C giving rise to a third reaction point with yttrium orthoferrite, garnet, $Y_{0.745}Fe_{1.250}O_{2.960}$, and liquid of composition, $Y_{0.44}Fe_{1.56}O_{2.88}$. The oxygen reaction lines[5] in the figure represent compositions of fixed Y:Fe ratio which have lost variable amounts of oxygen in moving into the ternary system.

Polished sections were the most convenient means for routine phase identification and for locating critical phase boundaries in the quenching study. Photographs of some representative samples quenched in air from different temperature-composition regions are shown in Fig. 3. All of the samples in the figure were permitted to cool relatively slowly so that the liquid phase would develop the characteristic eutectic intergrowth. The sample in the first photograph was quenched from the two phase region magnetite + liquid. The magnetite crystals show white lamellae of hematite parallel to (111) planes resulting from partial oxidation on cooling. Magnetite crystals were always found near the surface of the quenched melt indicating that their density was lower than the liquid density. Photograph II shows primary garnet crystals

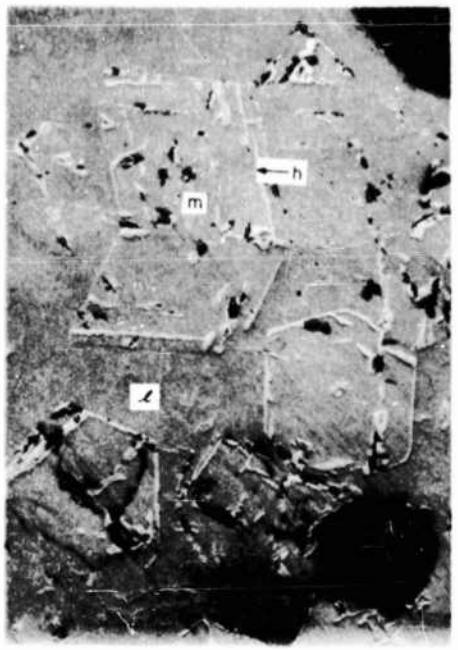


I MAGNETITE (m) WITH LAMELLAE OF HEMATITE (h) FORMED DURING COOLING IN A MATRIX OF QUENCH LIQUID (ℓ). DARK AREAS IN THE SECTION ARE HOLES

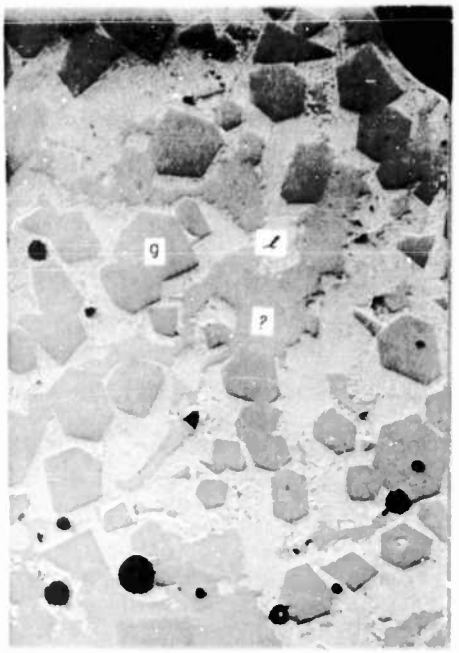


II PRIMARY YTTRIUM GARNET (g) IN MATRIX OF QUENCH LIQUID (ℓ). IRREGULAR GRAY AREAS "?" ARE PROBABLY A SURFACE COATING

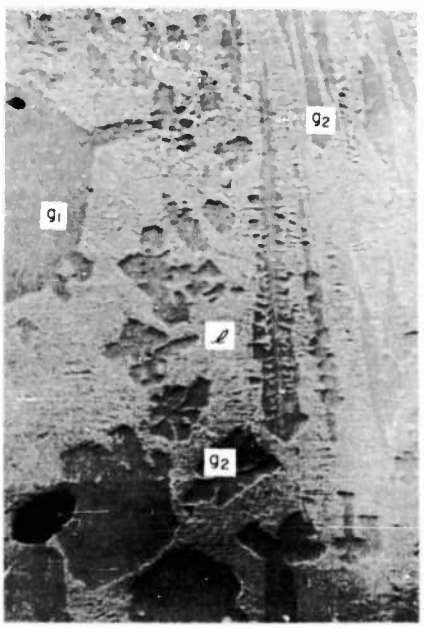


III WELL FORMED PRIMARY $g_1$, AND SKELETAL QUENCH GARNET $g_2$ SURROUNDED BY QUENCH PHASE (ℓ)

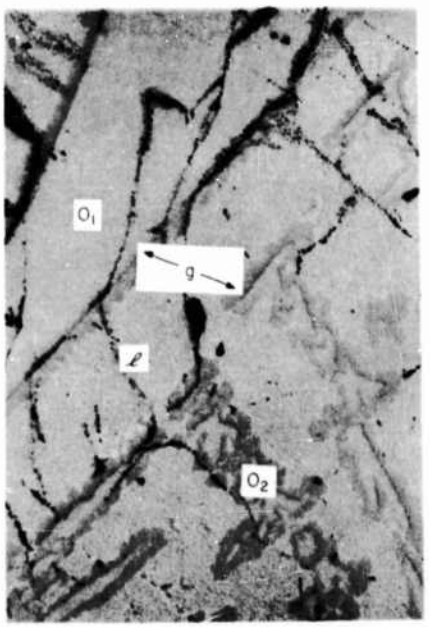


IV PRIMARY $O_1$, AND SECONDARY $O_2$ (quench crystals) OF YTTRIUM ORTHOFERRITE SURROUNDED BY GARNET (g) AND QUENCHED LIQUID (ℓ)

REPRESENTATIVE POLISHED SECTIONS OF QUENCHED SAMPLES, 500X

FIGURE 3

and melt quenched from just above the "eutectic" temperature. The garnet appears as well developed dodecahedral crystals in section and with a somewhat lower reflectivity (darker) than the magnetite phase. Garnet crystals were always found at the bottom of the vials, apparently being more dense than the melt in air at the quenching temperature.

Secondary garnet crystals formed during cooling are quite different in habit from the primary phase, as can be seen by comparing the skeletal quench crystals with the equant primary crystals in Photograph III. The quench crystals show characteristic changes in size and orientation proceeding from the crucible wall, where rapid cooling occurs, to the interior which retains the heat longer, and their abundance depends on the temperature range of the liquid during cooling. Photograph IV is an example of both the differences in habit of quench and primary phases and of the "reaction rims" of garnet which form about the orthoferrite crystals as a result of the "peritectic" reaction. The orthoferrite phase usually appears as elongated light grey crystals somewhat rounded in shape as is the large grain at the top of the photograph. The small irregular grains are secondary $YFeO_3$ formed during cooling and the dark grey crystallites surrounding both primary and secondary orthoferrite are garnet crystals resulting from the peritectic reaction of orthoferrite + liquid to form garnet. Orthoferrite crystals were not found at any particular level in the vials and are probably nearly equal to the melt in density.

The experimental results on the X-ray diffraction study of compositions near 37.5 mole percent $Y_2O_3$ are summarized in Fig. 4. The lattice parameters given are for approximately one-half gram samples quenched in water from the temperatures indicated. Assuming that the range in lattice parameter is indicative of compositional variation, the solubility of iron oxide in stoichiometric yttrium-iron garnet is a maximum at 1470°C in air and decreases from this value at both higher and lower temperatures. The solubility of yttria in garnet was below the limits of detection. The range in composition for a single phase garnet at the "eutectic" temperature in air is 37.0 - 37.5 ±0.15 mole percent $Y_2O_3$ in terms of the starting ratios of $Y_2O_3$ and $Fe_2O_3$. The precision of the X-ray data from one series to the next is not as high as comparative results

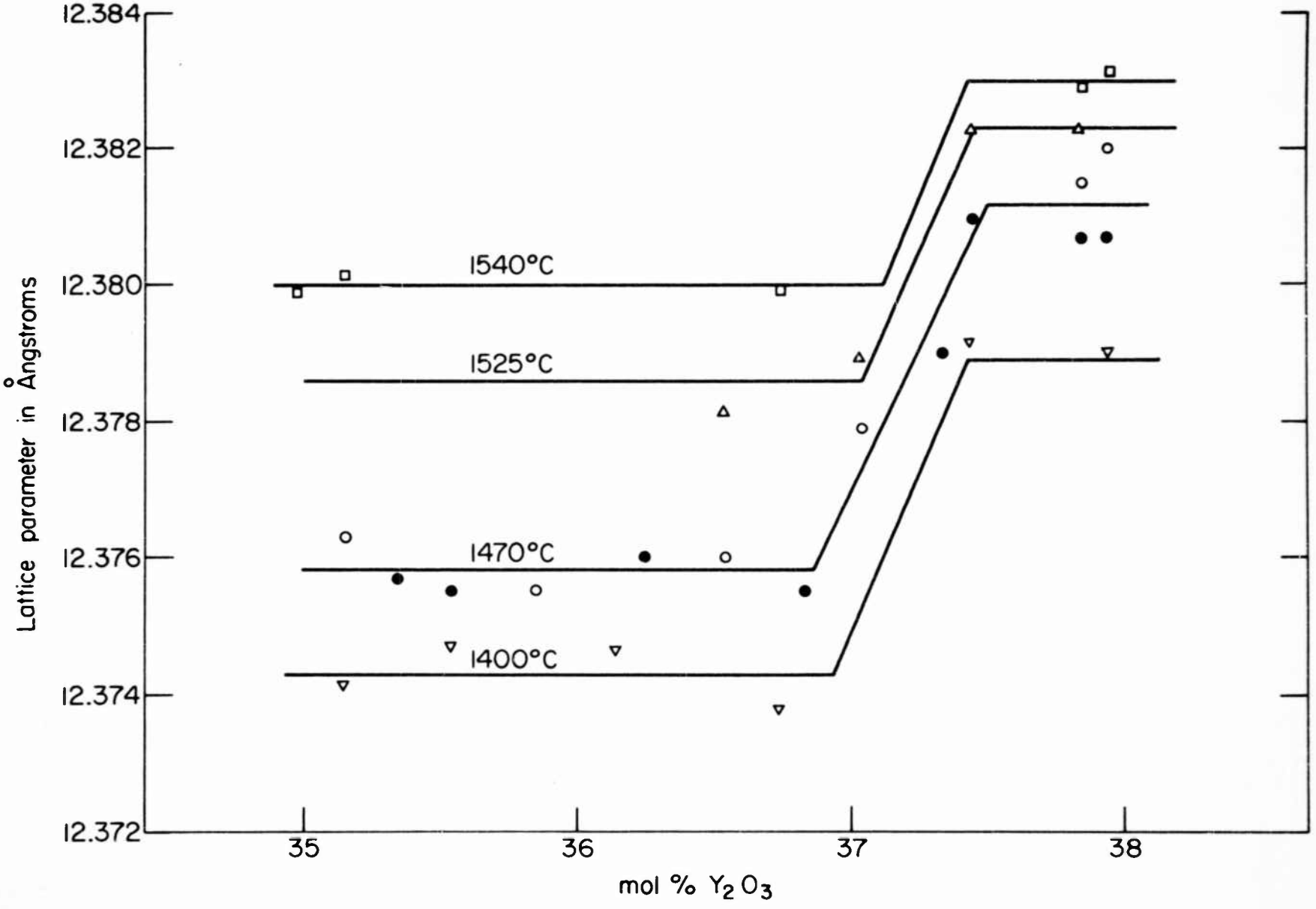


LATTICE PARAMETER OF THE GARNET PHASE IN AIR AS A FUNCTION OF TEMPERATURE

FIGURE 4

on samples fired together, as shown by the two separate runs (shaded and open circles) at 1470°C. The changes in X-ray spacing with temperature and composition, however, are seen to be considerably larger than the error (±0.001 Å) in measurement of peak position.

A study of Fig. 4 will reveal that the variations in unit cell parameter are a function of temperature as well as of composition. These results, in conjunction with weight loss data, are interpreted as changes resulting from reduction of the garnet, i.e., formation of $Fe^{2+}$, at high temperatures. The increase in cell parameter with temperature may be a consequence of a change in composition or possibly of disordering of cations on the various lattice sites. If thermal disorder were the predominant cause for the increase in lattice parameter, then one would not expect large differences in $a_o$ for samples held at the same temperature in equilibrium with different oxygen pressures. Cell values, however, did vary considerably under these conditions, changing from $a_o$ = 12.375 Å in oxygen to $a_o$ = 12.380 Å in $CO_2$ at 1470°C which is almost as large as the total variation observed with temperature from 1400°C to 1540°C. From this one may conclude that changes in oxygen content are the dominant cause for the variation in the lattice parameter with temperature. An attempt was made to determine the extent of this reduction by measurements of loss in weight as a function of temperature. As mentioned previously, the adjustment to an equilibrium oxygen content was very slow for compositions near YIG compositions and the results of the weight loss studies in this range must be considered tentative. If reoxidation of the yttrium garnet is as slow as this preliminary work suggests, it may prove impractical to fill the oxygen deficiencies formed during growth at high temperatures. A more thorough re-examination of weight gain and loss in garnet single crystals pulled from the melt will prove interesting in this respect.

Phase equilibria have been studied using the same techniques as described above in an atmosphere of pure oxygen gas ($P_{O_2}$ = 760 mm Hg) resulting in the oxygen isobar diagram, Fig. 5. A comparison of this diagram with the previous figure shows that a change in oxygen pressure from 159 mm Hg to 760 mm Hg has a marked effect on liquidus relationships in this system. The

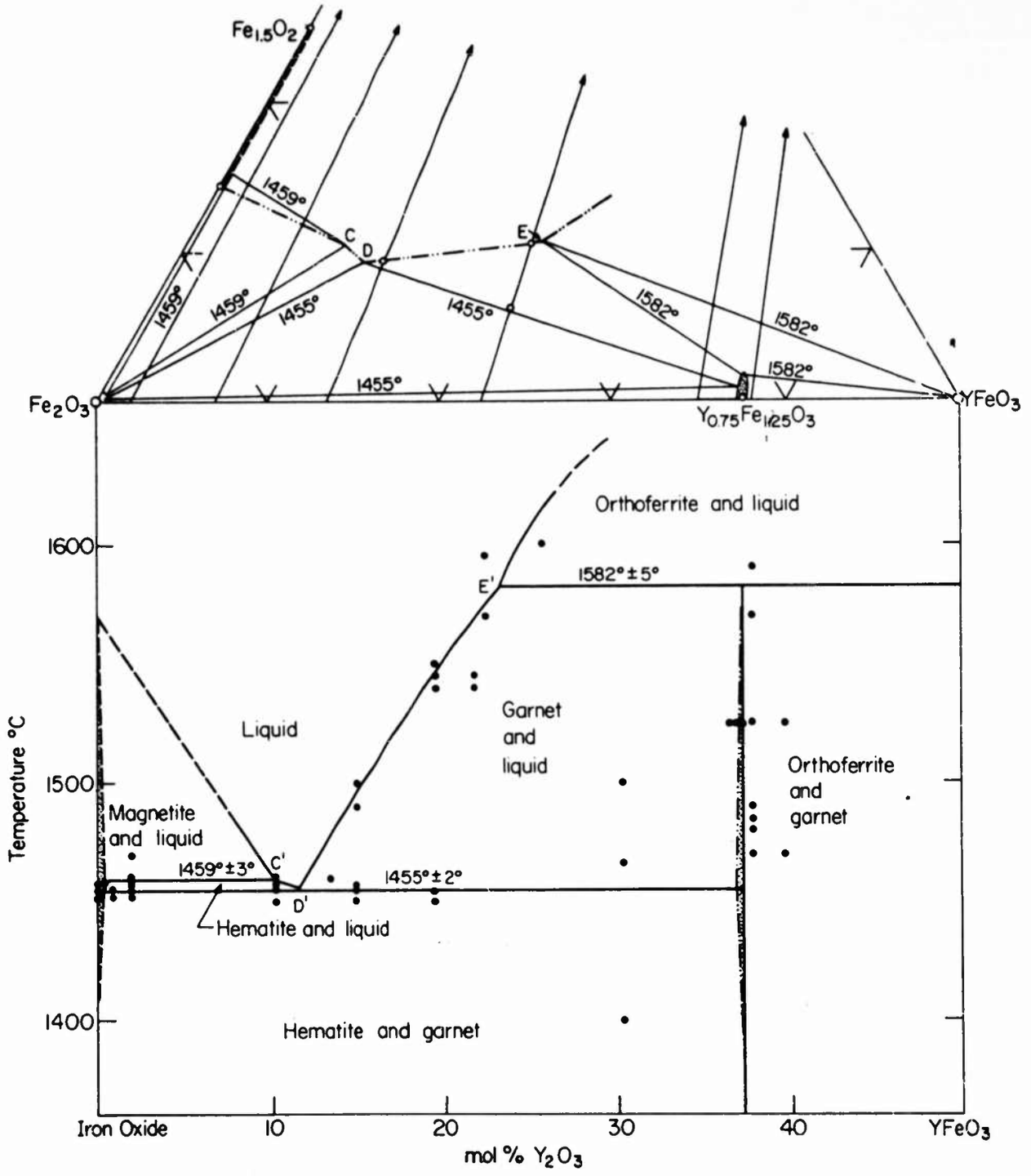


Phase relations in the system $Fe_2O_3$-FeO-$YFeO_3$ in oxygen. The relation of upper to lower diagram same as in Fig. 1, with the oxygen isobar (dash double-dot line) giving liquid compositions, lines with arrows as oxygen reaction lines, and isothermal reaction points labeled with appropriate temperature.

FIGURE 5

hematite magnetite transition has been raised by increased oxygen pressure to a point just above the minimum melting temperature, resulting in a small primary crystallization field for the hematite phase. The minimum melting temperature is 1455°C and the decomposition temperature of yttrium-iron garnet is 1582°C. Thus, the temperature range for the stable coexistence of garnet and an oxide liquid is extended to 127°C in oxygen as compared to 86°C in air. Three reaction points involving two crystalline phases, a liquid, and oxygen gas (Fig. 2) are as follows: hematite + garnet, $Y_{0.740}Fe_{1.250}O_{2.975}$ + liquid, $Y_{0.25}Fe_{1.75}O_{2.90}$ at 1455°C; hematite + magnetite + liquid, $Y_{0.22}Fe_{1.78}O_{2.89}$ at 1459°C; and orthoferrite + garnet, $Y_{0.745}Fe_{1.250}O_{2.945}$ + liquid $Y_{0.46}Fe_{1.54}O_{2.88}$ at 1582°C.

Although melting relations are changed appreciably by changes in oxygen pressure, no measurable differences could be found in composition of the garnet crystallizing from liquids in air or oxygen ambients. Lattice parameter studies (Table I) and measurements of loss in weight indicate solubility of excess iron oxide and loss of oxygen to be essentially the same in both atmospheres within experimental error.

The oxygen partial pressure in an atmosphere of carbon dioxide gas varies according to temperature[12] and hence cannot be considered isobaric. In the temperature range of interest in Fig. 6, the partial oxygen pressure increases from 0.96 mm Hg at 1450°C to 2.14 mm Hg at 1600°C. The temperature range for stable coexistence of garnet and liquid has been reduced considerably in a $CO_2$ atmosphere as shown in Fig. 3. Significant changes have also taken place in the oxygen content of both liquid and crystalline phases. Two invariant situations involving the garnet phase arise; at 1475°C and $P_{O_2}$ = 1.1 mm Hg with magnetite, garnet, $Y_{0.750}Fe_{1.245}O_{2.945}$ and liquid, $Y_{0.30}Fe_{1.70}O_{2.70}$ and at 1495°C and $P_{O_2}$ = 1.3 mm Hg with orthoferrite, garnet $Y_{0.75}Fe_{1.25}O_{2.945}$ and Liquid $Y_{0.35}Fe_{1.65}O_{2.78}$. Although the garnet phase is oxygen deficient at melting temperatures, a comparison of lattice parameter data with iron oxide and with yttria in excess (Table I) indicates very little deviation from stoichiometry in the metal atom ratio of 3:5.

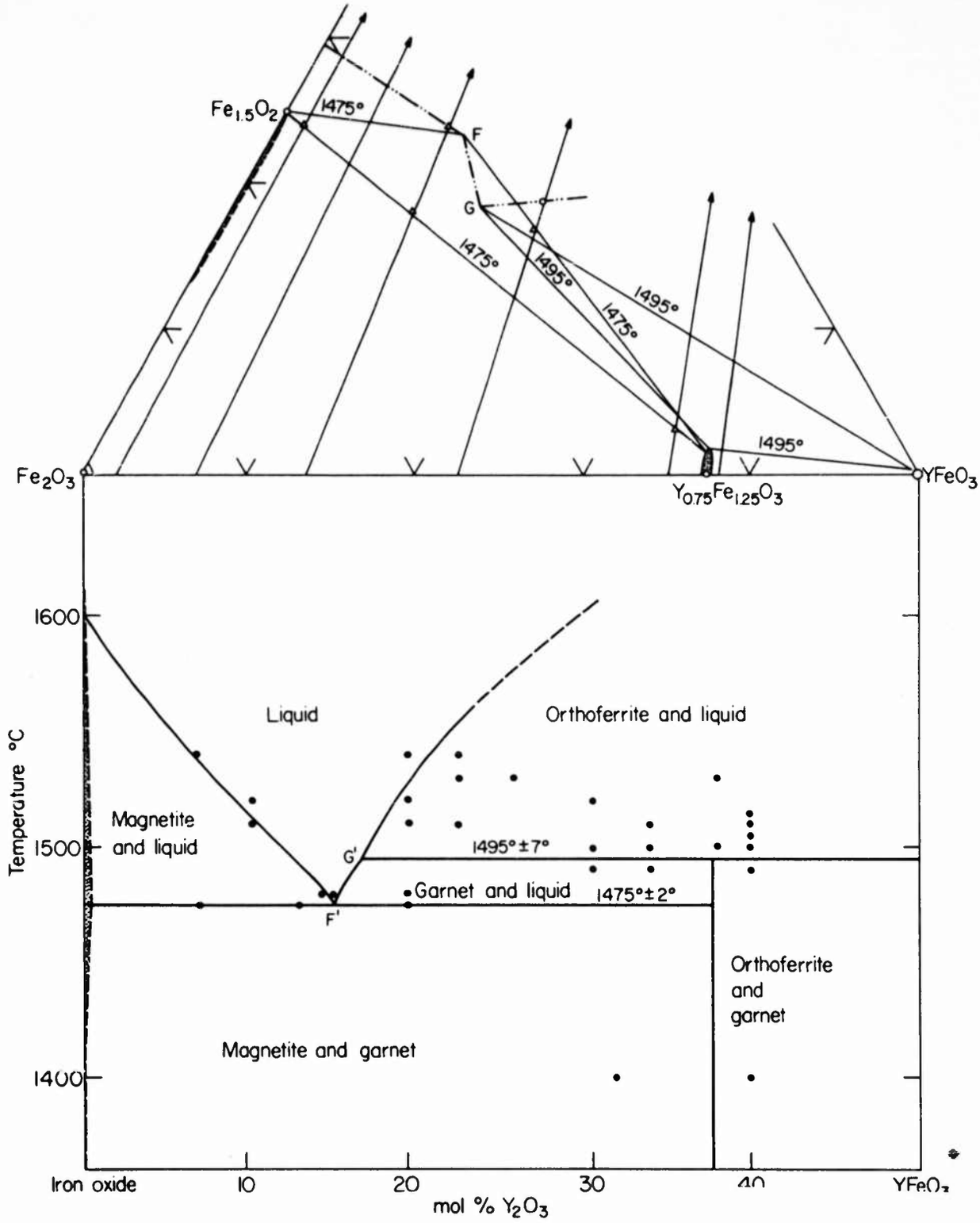


Phase relations in the system $Fe_2O_3$-FeO-$YFeO_3$ in $CO_2$. The section is not strictly isobaric as explained in the text. Symbols and lines same as in previous figures.

FIGURE 6

TABLE I

LATTICE PARAMETER OF YTTRIUM-IRON GARNET SOLID SOLUTIONS

| | Oxygen | | Air | | $CO_2$ | |
|---|---|---|---|---|---|---|
| Temperature (°C) | Excess $Fe_2O_3$ | Excess $Y_2O_3$ | Excess $Fe_2O_3$ | Excess $Y_2O_3$ | Excess $Fe_2O_3$ | Excess $Y_2O_3$ |
| 1400 | 12.374 | 12.380 | 12.374 | 12.379 | 12.378 | 12.381 |
| 1440 | --- | --- | 12.375 | 12.381 | --- | --- |
| 1470 | 12.375* | 12.381 | 12.376+ | 12.381 | 12.381- | 12.382 |
| 1525 | 12.378 | 12.383 | 12.378 | 12.382 | --- | --- |
| 1540 | --- | --- | 12.380 | 12.383 | --- | --- |

*$Y_{0.74}Fe_{1.25}O_{2.975}$

+$Y_{0.745}Fe_{1.245}O_{2.970}$

-$Y_{0.745}Fe_{1.245}O_{2.945}$

d. Discussion of Results

The experimental results on melting relations in the three oxygen pressure sections cited above demonstrate the controlling effect of oxygen atmosphere on melting relations. The reason for this will be apparent from a study of the ternary system as a whole. Figure 7 summarizes the data in the form of a ternary diagram with oxygen isobars drawn on the liquidus surface. The intersection of each isobar (dash double-dot lines) with the liquidus surface fixes the composition of the melt in equilibrium with crystals, as well as the temperature and composition for the intersection with the ternary boundary curves (heavy solid lines). Liquidus isotherms are shown as light solid lines. This figure may be compared with the solid model (Fig. 8) to give a better indication of the shape of the liquidus surface.

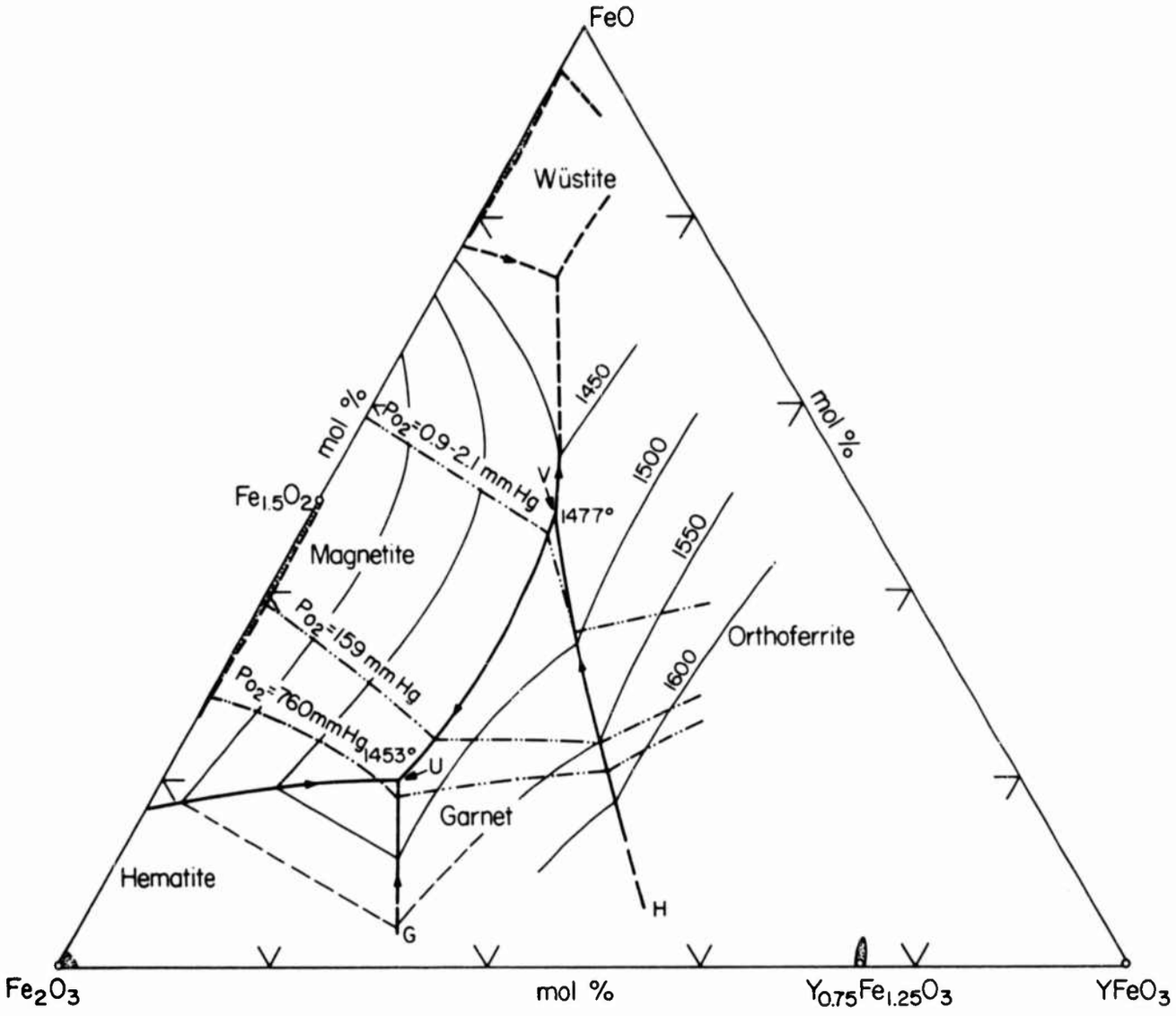


Diagram summarizing relationships in the system $Fe_2O_3$-FeO-$YFeO_3$ as deduced from three isobaric sections. The heavy lines are boundary curves separating primary crystallization fields, the dash-double dot lines indicate intersection of the isobars with liquidus surface, and light lines indicate liquidus isotherms. Points U and V are ternary eutectic and peritectic points respectively. Stippled areas are crystalline single phase areas at liquidus temperatures. Dashed lines represent inferred relationships.

FIGURE 7

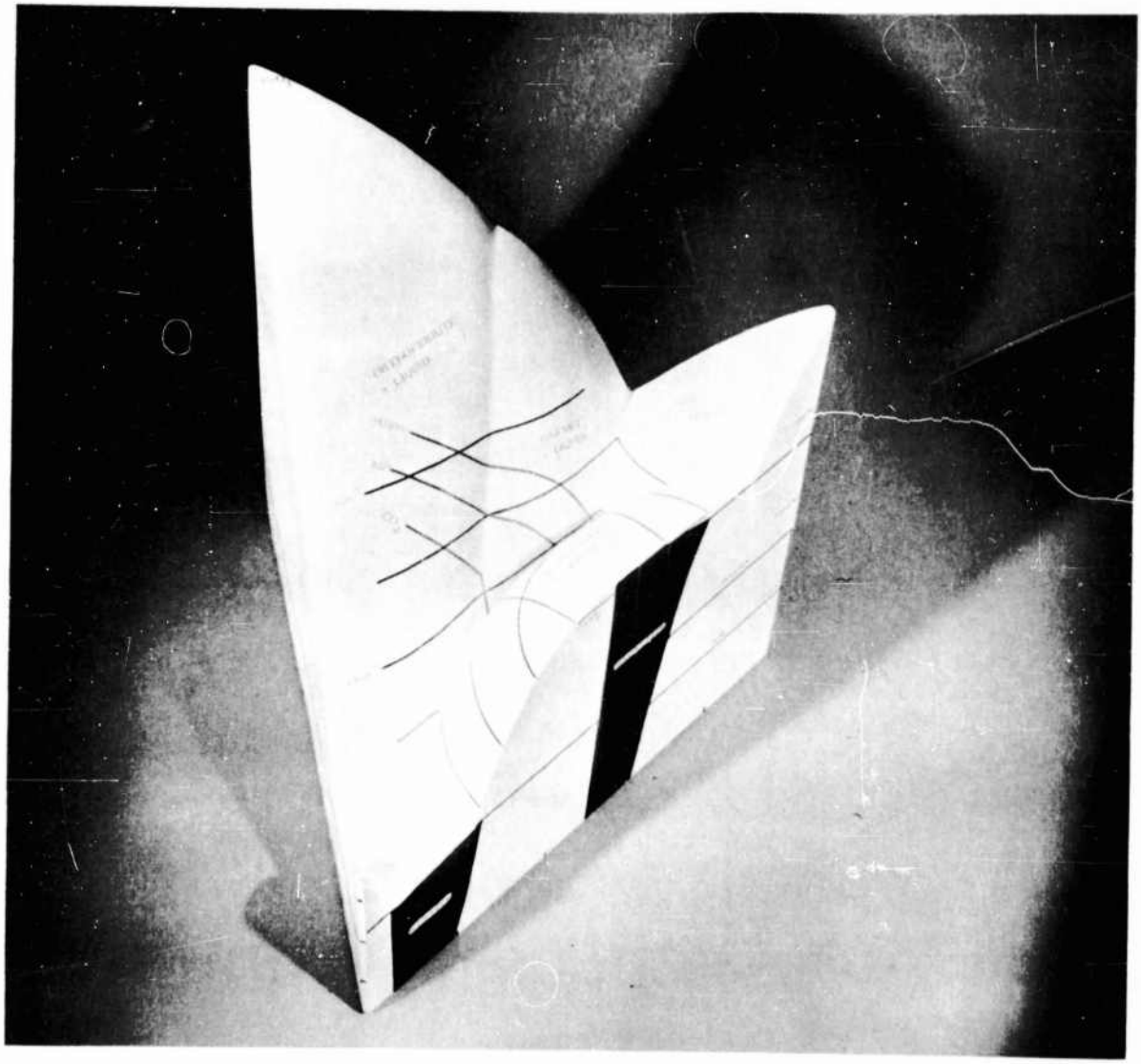

SOLID MODEL OF THE TERNARY SYSTEM $Fe_2O_3$-FeO-$YFeO_3$.
FIGURE 8

The boundary curves separating the primary crystallization fields present a unique situation since four phases are present and, for a given oxygen partial pressure, conditions are invariant. The intersections with boundary curves give rise to the eutectic and peritectic reaction points, i. e., points A through G in Figs. 2, 5, and 6, for each isobar shown in the preceeding diagrams. It follows that there is a unique oxygen isobar that passes directly through the ternary eutectic U and another through the peritectic point V. These two points represent true invariant equilibrium with five coexisting phases (gas, liquid and three crystalline phases) in contrast to the four-phase reaction points cited above. The ternary invariant points U and V are important because they define the critical limits for the stable coexistence of yttrium-iron garnet phase and liquid; point U fixes the minimum liquidus temperature in the system, and point V the minimum oxygen partial pressure. The ternary eutectic occurs at approximately 1453°C and 680 mm Hg oxygen pressure and the peritectic at an estimated 1477°C in an oxygen atmosphere somewhat below that given by $CO_2$ dissociation at that temperature, approximately 0. 25 mm Hg. The temperatures and oxygen pressures at these critical points can be estimated most readily from a plot of the four-phase boundary curves as a function of log $P_{O_2}$ vs T.

The equilibrium relations shown in Fig. 7 can be used to predict the situation at oxygen pressures higher and lower than those studied in this work. At pressures slightly lower than $P_{O_2}$ = 0. 25 mm Hg the garnet phase will decompose on heating to a mixture of magnetite and yttrium orthoferrite below the liquidus, and the two latter phases will present a simple eutectic situation at the melting temperature in the isobaric projection. This means that the isobars will intersect the orthoferrite plus magnetite plus liquid boundary curve at some point above V in Fig. 7. At oxygen pressures exceeding 680 mm Hg, the isobar in question will intersect the ternary boundary curve GU at some temperature above 1453°C and HV above 1575°C. Both the minimum melting temperature and the decomposition temperature of the garnet will be increased by higher pressures due to intersection of isobars with the boundary curves which are ascending in temperature as the $Fe_2O_3$-$YFeO_3$ sideline is approached.

There is some uncertainty as to whether the peritectic boundary curve (HV) will change in direction towards $YFeO_3$, possibly leading to congruent melting of yttrium-iron garnet at very high pressures although this does not appear likely from the projected trend of the curve. At any rate this situation is experimentally inaccessible at present since very high temperatures (>1600°C) and high oxygen pressures would be required. High pressures of oxygen gas are likely to increase the temperature range for coexisting garnet plus liquid because of very rapidly increasing temperatures along the boundary curve HV.

The composition of the garnet phase crystallizing from an oxide melt also shows a dependence on oxygen pressure. Measurable deviations from stoichiometry do occur in air which can be followed by measurement of loss in weight and by changes in lattice parameter. The same is true for the two other pressure sections described in this report. Experimentally, it is observed that solubility of iron oxide in excess of stoichiometry decreases the lattice parameter of yttrium-iron garnet while loss of oxygen increases its value (see Table I).

A comparison of lattice constant and weight loss of samples fired in oxygen with those fired under equivalent conditions in air did not reveal any measurable changes (Table I) indicating that solubility relations are the same in both ambients within experimental error. In a $CO_2$ atmosphere, however, the results show changes of some significance; first, the small variation in lattice parameter for garnet with excess iron oxide compared with garnet having yttria excess (as $YFeO_3$) suggests a lower solubility of iron oxide, and second, larger lattice parameter values indicate greater loss in oxygen content which was borne out by weight loss studies. From these observations one can deduce that the garnet solubility surface at liquidus temperatures extends into the ternary system through loss of oxygen and that the fieldwidth narrows through decreasing solubiiity of excess metal oxide as shown in Fig. 7. At low oxygen pressures the garnet phase is essentially stoichiometric in metal ratio, but is oxygen deficient, whereas at higher pressures oxygen loss is lessened but solubility of iron is increased (Table I). These deviations from stoichiometry are unavoidable during equilibrium growth from an oxide

liquid and may have important consequences in the mechanism of the growth of the garnet crystals as well as on their physical properties.

The limited temperature range for garnet in the presence of liquid, coupled with the small but quite probably significant variations in composition with temperature, makes it imperative that the temperature be known exactly and controlled very closely during the growth process. A large thermal gradient over the growing crystal would also favor zoning and should be avoided if at all possible.

## 2. The System $Fe_2O_3$-FeO-$GdFeO_3$

### a. Introduction

The study of phase relations involving gadolinium and iron oxide represents the first extension to other garnet-type oxides from the original work on the yttrium-iron-oxygen system. It was expected that the chemical similarity of gadolinium and yttrium would result in comparable phase relations and that the essential features of the diagram could be determined much more rapidly. The choice of gadolinium oxide rests on the fact that the oxide is stable at high temperature and that substitutional solid solutions are complete in both orthoferrite $(YGd)FeO_3$ and garnet $(YGd)_3Fe_5O_{12}$ crystalline phases.[13] The extent of crystalline solubility can be followed readily by changes in lattice parameter, in density, and in magnetic properties.[14] Gadolinium, therefore, would appear to be ideally suited to an investigation of the effect of a rare earth substitution for yttrium on the general melting relations. Roy and Warshaw[15] have reported that the gadolinium-iron garnet melts congruently which, if true, would lead to melting relations involving yttrium-gadolinium garnet solid solutions without excess iron oxide in the liquid. It was expected that this situation would be simpler to deal with in single crystal growth, especially growth by Verneuil or zone melting techniques. Before proceeding to the quaternary Y-Gd-Fe-O, it was decided to reinvestigate the end member Gd-Fe-O system to verify the melting relations preposed by Roy and Warshaw.

### b. Experimental Procedure and Results

The methods of material preparation and phase and composition determination have been described in the previous section on the yttrium-iron system. The system was studied in some detail in air (Fig. 9) and only briefly in atmospheres of oxygen and $CO_2$ gas. The similarity of the air isobar of the gadolinium-iron oxide system to the corresponding isobar in the yttrium system (Fig. 2) is apparent in both temperature and composition of the invariant points except that the decomposition of the gadolinium-iron garnet is about 60°C lower in temperature. The peritectic reaction temperature (or garnet

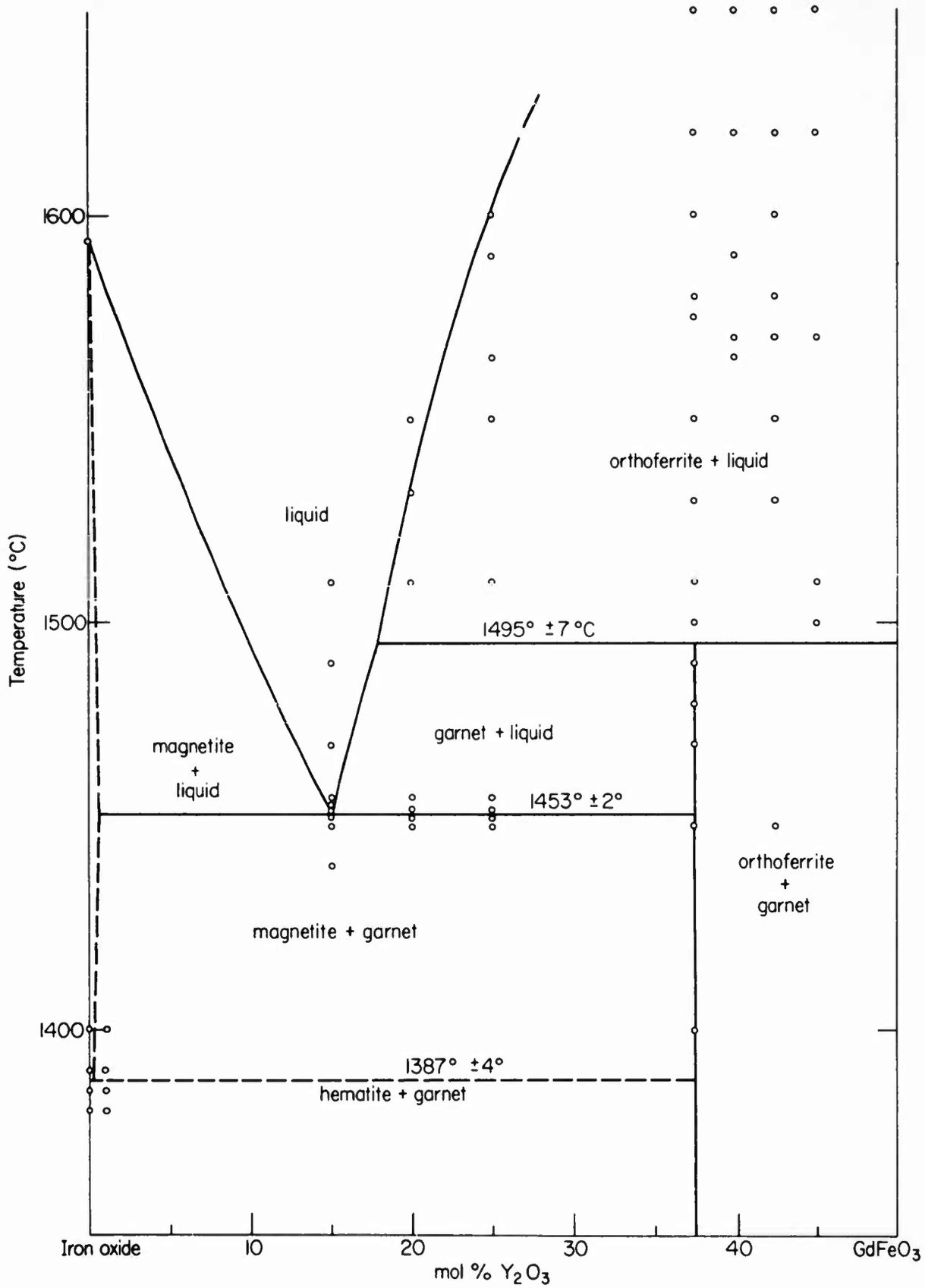


THE SYSTEM $Fe_2O_3$-FeO - $GdFeO_3$ IN AIR. CIRCLES REPRESENT SEPARATE QUENCH RUNS

FIGURE 9

decomposition temperature) was difficult to locate with precision better than ±7°C because of the tendency for the orthoferrite ($GdFeO_3$) to form and to persist metastably. The temperature was determined by reacting separate samples, one of orthoferrite + iron oxide and one of garnet at a series of temperatures to determine which of the two assemblages is the stable one at each point.

The resulting diagram does not agree with the published findings of Roy and Warshaw,[15] particularly as regards the congruent melting of the garnet phase. The authors heated oxide mixtures rapidly on a strip, resistance furnace and found that both gadolinium garnet and orthoferrite phases melted congruently at 1650°C and 1710°C, respectively. These results are not in agreement with the present findings where the garnet phase decomposes at 1495°C ±5°C. The reason for this lack of agreement may rest in differences in oxygen content in the samples. Warshaw and Roy pointed out that their diagram is intended to represent melting relations approaching the binary $Gd_2O_3$-$Fe_2O_3$ join under conditions in which limited oxygen loss has occurred because of rapid heating, whereas this representation is for the equilibrium situation in air where oxygen loss has been extensive for all compositions.

The solubility of iron oxide in yttrium-iron garnet has been determined to be 0.5 mole percent at 1469°C on the basis of a series of samples near the garnet composition fired under the same conditions. The solubility results in a change in lattice parameter of 0.005 Å ±0.001 or 0.001 Å per 0.1 mole percent iron oxide in excess of stoichiometry. The change in lattice parameter of gadolinium-iron garnet from iron excess to gadolinium excess was found to be 0.001 Å, approximately the limit of experimental accuracy. Assuming solubility of iron oxide in gadolinium-iron garnet has the same effect on lattice parameter as in yttrium-iron garnet, the fieldwidth at 1495°C is 0.1 mole percent iron oxide or less.

Two other oxygen isobars were studied briefly and the combined results are represented in Fig. 10. A comparison of this figure with Fig. 7 will indicate that the primary crystallization field of gadolinium iron garnet is

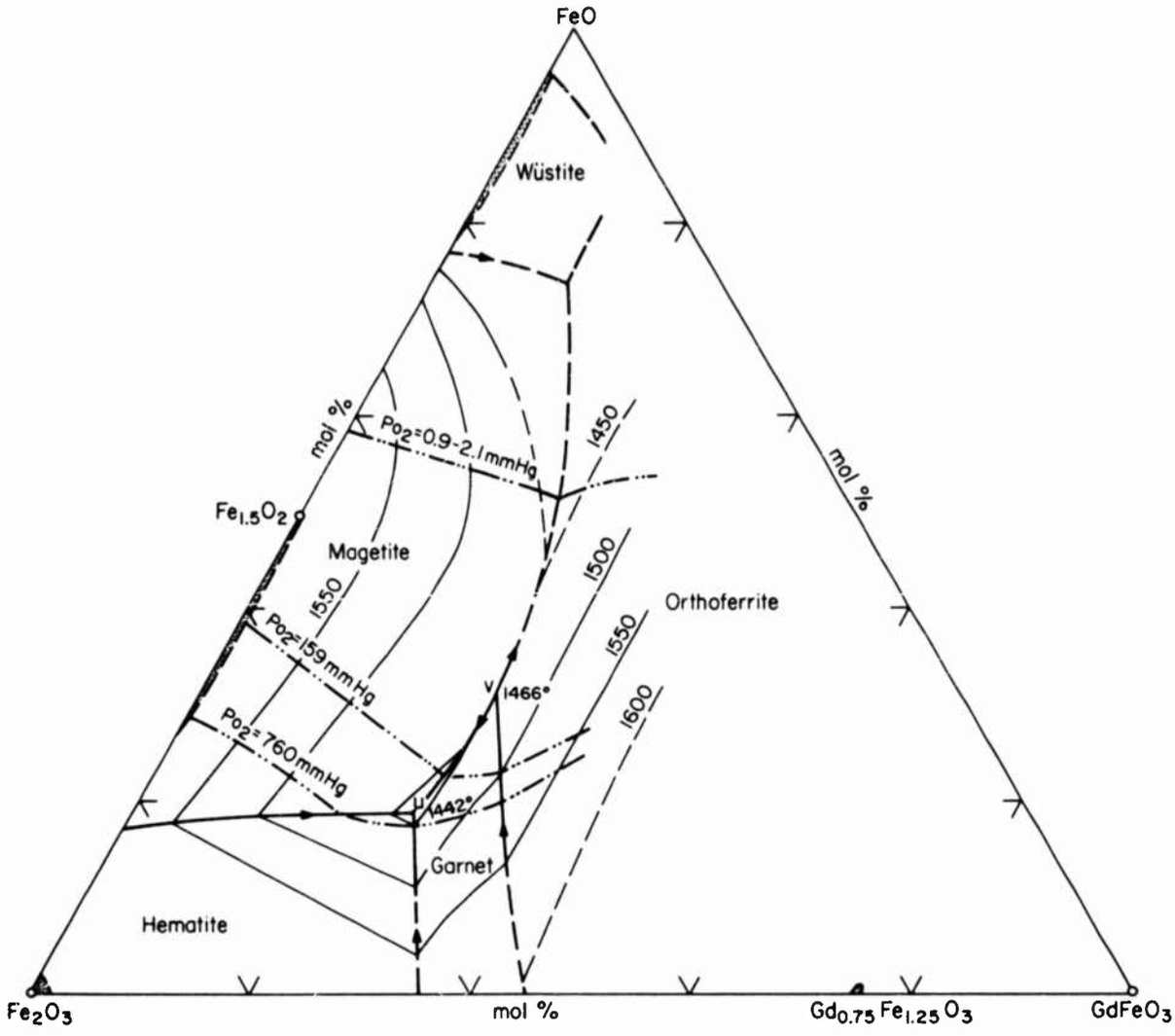


Diagram summarizing relationships in the system $Fe_2O_3$-FeO-$GdFeO_3$ as deduced from three isobaric sections. The heavy lines are boundary curves separating primary recrystallization fields, the dash-double dot lines indicate intersection of the isobars with liquidus surface, and light lines indicate liquidus isotherms. Points U and V are ternary, eutectic and peritectic points respectively. Stippled areas are crystalline single phase areas at liquidus temperatures. Dashed lines represent inferred relationships.

FIGURE 10

much more restricted than its yttrium counterpart; indeed the field does not exist in an oxygen partial pressure generated by $CO_2$ at melting temperature. The phase decomposes at approximately 1350°C which is far below liquidus temperatures. In air the temperature interval for garnet + liquid is 42°C, in oxygen gas the interval is 60°C. These data lead to the conclusion that GdIG is more susceptible to decomposition than YIG and that crystal growth of compositions close to GdIG would present difficulties owing to the very short temperature region of stability in the melting range.

### 3. The System $Fe_2O_3$-FeO-$YFeO_3$-$GdFeO_3$

#### a. Experimental Results

The quaternary system was the goal of the study originated with the Gd-Fe-O system. The experimental results of quenching studies for the air isobar in the four component system are shown in Fig. 11. At liquidus temperatures the orthoferrite solid solutions are seen to be the dominant crystalline phase. In this ternary projection of the air isobar, the boundary curve for coexisting garnet, orthoferrite and liquid solutions decreases uniformly from 1555°C for yttrium-iron garnet to 1495°C for gadolinium-iron garnet. The eutectic boundary curve decreases from 1469°C to 1453°C without any minimum. Oxygen loss again has not been shown in this projection and is quite probably extensive as in the limiting ternary systems Y-Fe-O and Gd-Fe-O. Lattice parameter studies on the yttrium-gadolinium-iron garnet solid solutions have indicated solubilities of iron oxide intermediate between that of the two end members.

#### b. Discussion and Results

The data on oxygen and $CO_2$ isobars in the limiting ternary systems Y-Fe-O and Gd-Fe-O are combined with the results of the air isobar to give a picture of the quaternary system as a whole. This is shown diagramatically in Fig. 12 in terms of the four chosen components. The garnet + liquid region appears as a volume in the tetrahedron. The various isobars intersect this liquidus volume and, after projection back down on the $Fe_2O_3$-$YFeO_3$-$GdFeO_3$ base, can be represented as, for example, the ternary projected air isobar in Fig. 11. One may note that the garnet plus liquid field pinches out below the $CO_2$ oxygen pressure section in the diagram, i. e., there is no garnet + liquid field for compositions high in gadolinium in a $CO_2$ atmosphere. The oxygen isobaric section cuts a larger section of the garnet + liquid volume than the air isobar and would appear correspondingly larger in the ternary projection onto the base of the tetrahedron.

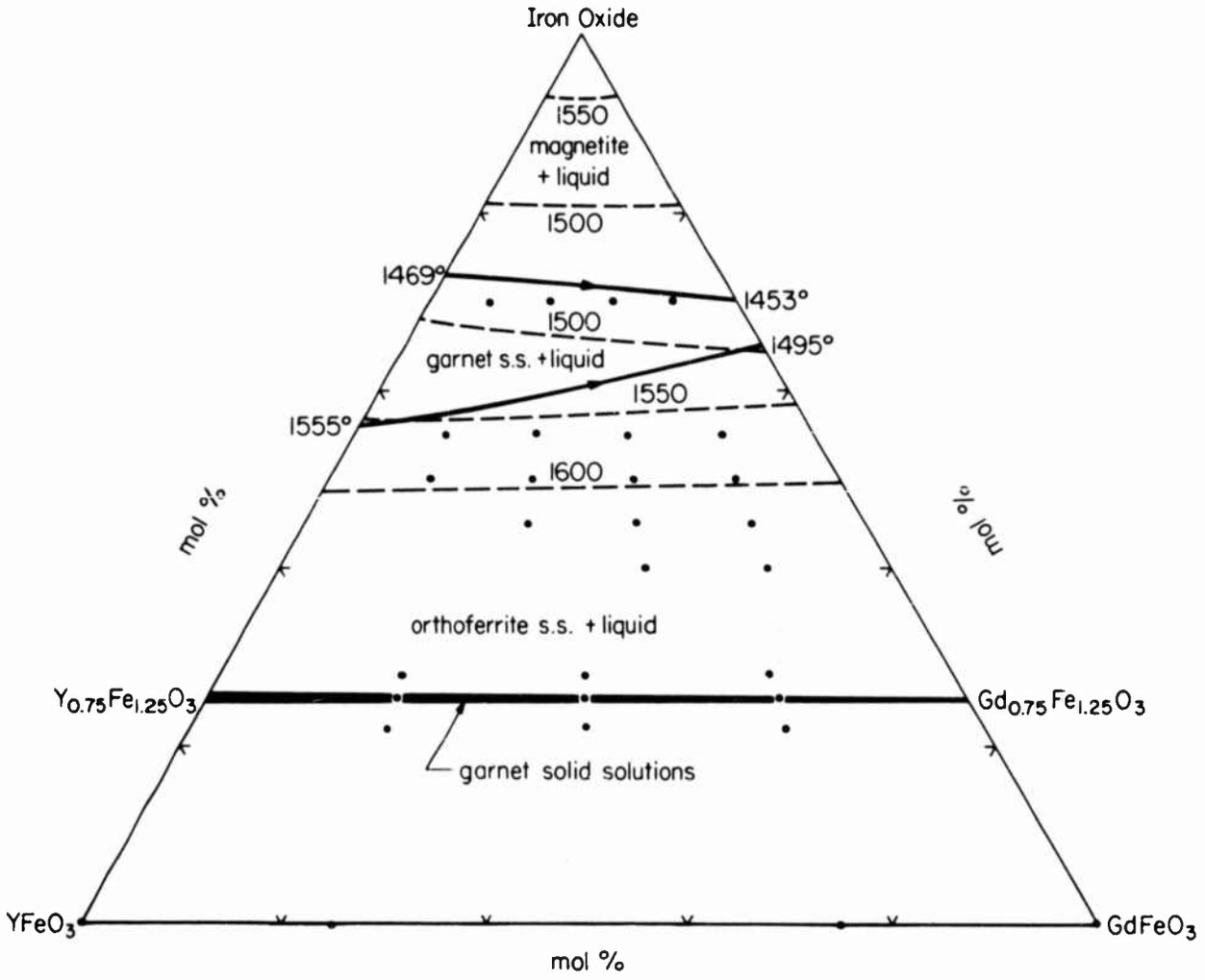


Dashed lines represent isotherms on the liquidus surfoce ond heavy lines with orrows are eutectic and peritectic boundory curves for the isobar

THE AIR ISOBARIC SECTION OF A PART OF THE SYSTEM Y-Gd-Fe-O

FIGURE 11

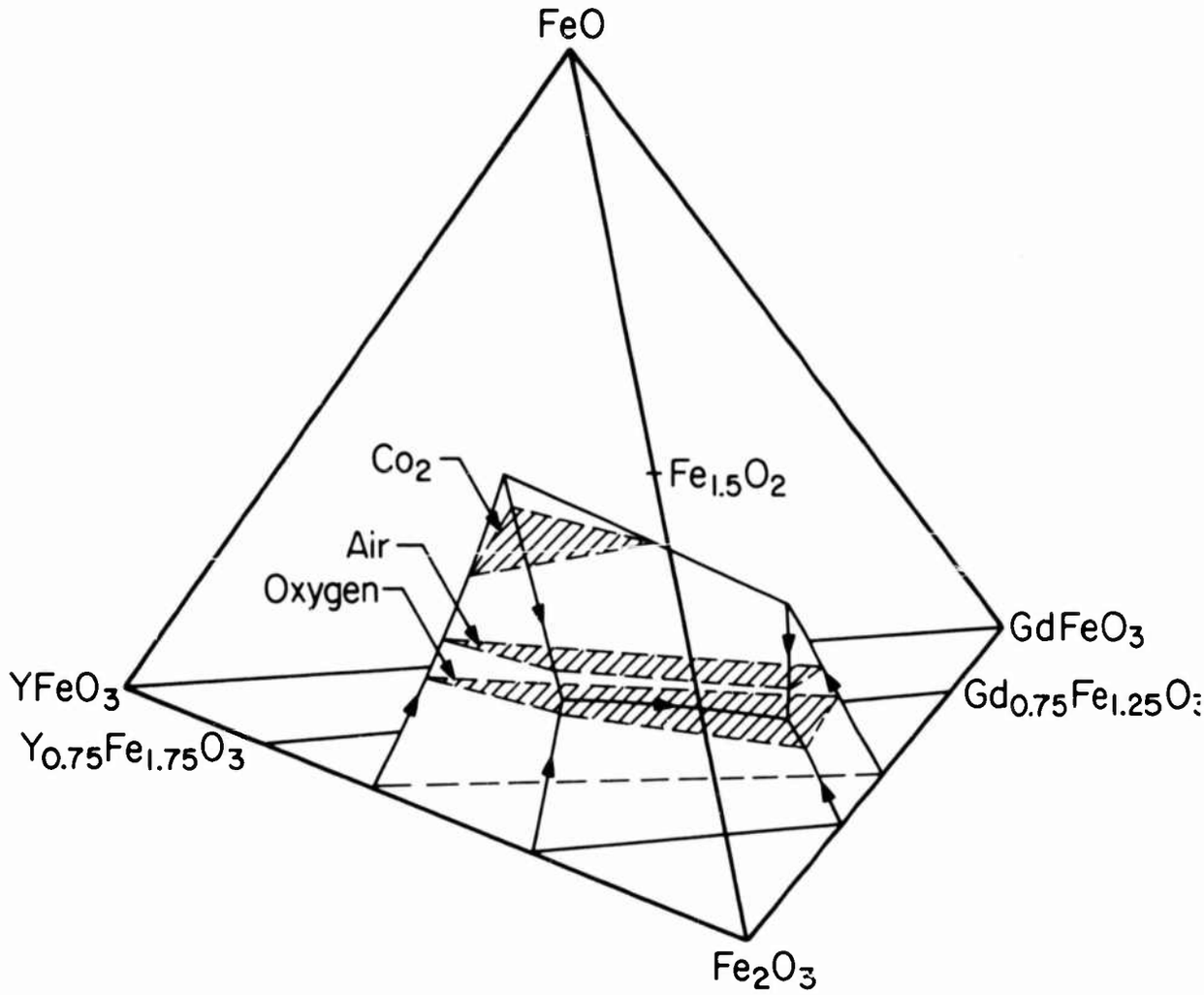


QUATERNARY REPRESENTATION OF LIQUID COMPOSITION IN EQUILIBRIUM WITH YIG - Gd I G SOLID SOLUTIONS. THE INTERSECTION OF OXYGEN, AIR AND $Co_2$ ISOBARIC SURFACES WITH THE LIQUIDUS VOLUME ARE SHOWN

FIGURE 12

With such extensive liquid and solid solutions, there existed the possibility of changes in the Y:Gd ratio of the condensed phases at various temperatures, that is, a progressive variation in ratio between liquid and solid phases with changing temperature. This tendency for fractionation is common in solid solutions and often results in zoning of crystals during cooling of the melt. Experiments, however, have shown that there is no preferential incorporation of gadolinium or yttrium in the crystals with temperature, the Y:Gd ratio remaining constant throughout in solid and liquid phases within the limits of lattice parameter measurement (±1 mole percent). It appears that $(Y, Gd)_3Fe_5O_{12}$ solid solution crystals can be grown from oxide liquids without zoning by the same slow cooling technique as might be used to grow either end member garnet.

## 4. Implications of Phase Equilibria on Crystal Growth of the Garnets

Phase relations in Y-Fe-O and Gd-Fe-O systems as well as intermediate Y-Gd-Fe-O compositions have demonstrated that the garnet phase melts incongruently in ambient atmospheres of air, oxygen, and carbon dioxide. Extrapolation of the data to higher oxygen pressures indicates that melting is probably incongruent at high pressures also. Crystal growth, therefore, will necessarily take place in melt compositions significantly different from that of the crystallizing solid. In garnet systems considered above, the liquid contains excess iron and is oxygen deficient. The rate of growth will, therefore, depend on the transport of yttrium and/or gadolinium and oxygen to the crystal interface as well as the rate of their incorporation in the solid. This is in contrast to congruently melting compounds where solid and liquid are equal in composition and growth depends primarily on the rate of accommodation or rearrangement of the disordered liquid into the ordered crystal structure. Whatever the technique used in growth from the melt, i. e., Verneuil, Bridgmann, zone melting or Czochralski method, the rate of growth will depend on the rate of transport through iron oxide rich liquids. High temperatures increase the solubility of yttrium and gadolinium in the liquid and high oxygen pressures increase oxygen solubility, both leading to a more favorable melt composition.

We have also seen that the composition of the garnet crystallizing from these oxide liquids is not of fixed stoichiometric composition, but varies, depending on pressure and temperature. The garnet composition in equilibrium with the iron rich liquid in air contains iron in excess of the ideal 3:5 ratio by as much as 2. 96:5. 04 and is also deficient in oxygen. Oxygen deficiency in melt grown crystals can perhaps be remedied by annealing in high oxygen pressures, but excess iron cannot, of course, be physically removed. This excess iron will probably exsolve as $Fe_2O_3$ (maximum $\approx$ 1 percent $Fe_2O_3$ phase in air) after annealing for extended periods at low temperatures.

The fact that all of the garnets studied melt incongruently places a further limitation on the possible composition range of crystals grown from a liquid. With congruent melting of binary or higher order compounds, crystals

can be grown from melts on either side of stoichiometry. Since the solubility surface of the solid is necessarily different under these conditions, a range of solid compositions are possible. This variable composition effect was aptly demonstrated by Bloem and Krogger[16] for lead sulfide which may be grown from lead rich or sulfur rich liquids. Changes in composition could not be measured chemically, but could be detected by electrical measurements. Similar deviation from stoichiometry undoubtedly do arise to some degree in all crystalline solids. When a compound melts incongruently, however, liquids with excess of one component in equilibrium with the compound are not stable, so that one side of the solid solubility surface is not available for the study of the variation of composition in crystals grown from solution.

One rather obvious implication for crystal growth which can be deduced from the phase diagrams is the temperature-composition limits of garnet and liquid phases and the effect of changes in oxygen atmosphere on these limits. The minimum possible melting temperatures occur at just below one atmosphere oxygen pressure in YIG and GdIG systems and any change in $P_{O_2}$ will raise this minimum temperature. Higher oxygen pressures are favorable since they suppress the decomposition (incongruent melting) of the garnet phase; oxygen partial pressures below that given by pure $CO_2$ dissociation are unfavorable since they result in decomposition of garnet before melting temperatures are reached.

It has been assumed implicitly throughout this discussion that equilibrium conditions are essentially maintained during crystal growth. The growth process in itself implies an imbalance in equilibrium to provide the driving force for the reaction. The deviation from equilibrium during orderly crystal growth, however, is probably quite small since a large variance would disrupt growth. Considering the temperatures involved (1450° - 1650°C) and the observed high fluidity of the oxide liquids, the assumption of virtual equilibrium would appear to be quite safe.

## B. CRYSTAL GROWTH

### 1. General Conditions of Growth

When an embryonic crystal nucleus forms within a homogeneous phase, as for example a liquid, the high surface to volume ratio tends to make it unstable due to the high surface energy. Therefore, a certain degree of supercooling or supersaturation below the equilibrium liquidus temperature is necessary to overcome the inherent instability of the nucleus. A plot of the rate of crystal growth or nucleation versus supercooling (Fig. 13, Curve A) characteristically indicates a negligibly small rate until a critical saturation level is reached whereupon the process occurs very rapidly. In accordance with these observations, the theories on the homogeneous process[17] predict an exponential dependence of rate of nucleation (I) on the degree of supercooling $(T_o - T_I)$, viz.,

$$I \approx I_o \exp \frac{-\text{const}}{(T_o - T_I)^2} \quad . \tag{1}$$

In many cases, however, preexisting surfaces such as insoluble impurities or container walls act as sites for the nucleation of the second phase. These surfaces reduce the retarding effect of surface energy and thereby reduce the degree of supercooling required for the formation and growth of a stable nucleus. The greater the similarity in crystal structure between the preexisting phase and the material crystallizing, the more pronounced will be the tendency for crystal growth at low supersaturations. Examples of this phenomena can be found in seeding rainclouds with cadmium iodide crystals and in epitaxial growth of many compounds on substrates of similar atomic structure.

Once a stable growing crystal is formed, the continued growth will depend on the transport of material to the solid interface and the rate of its incorporation in the crystal. If a nucleus of critical size must form on an

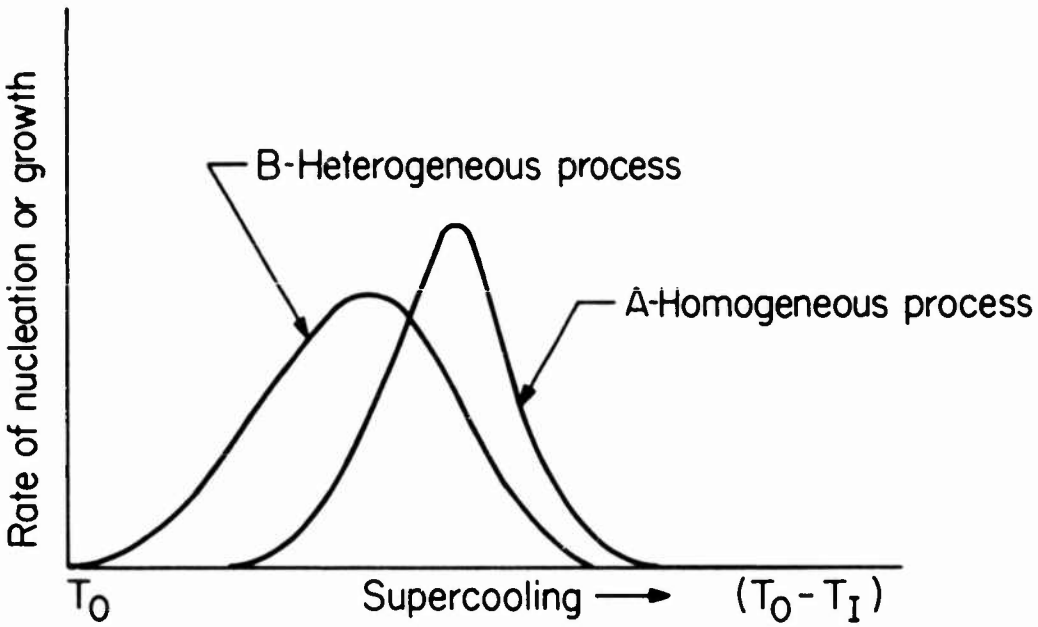


RATE OF GROWTH AS A FUNCTION OF SUPERCOOLING

FIGURE 13

atomically flat crystal surface for each successive layer of growth, one would expect a rate of growth similar to the homogeneous nucleation process (Fig. 13, Curve A) where a certain degree of supercooling is necessary to support continued growth.[17] In most heterogeneous systems, however, nucleation and growth do occur at measurable velocities even at low supersaturations (Fig. 13, Curve B) and several approaches have been developed to reconcile theory with experiment.

The theories of growth can be divided for convenience into two groups; those in which the rate of growth is controlled mainly by the rate at which material is built into the crystal, and those in which transport of the solute is the predominant factor.

a. Interface Controlled Growth

In the surface controlled rate theories, the formation of steps or discontinuities on the surface of a crystal growing in solution plays an important role in entrapping the rapidly moving solute atoms or atomic groups which impinge on or diffuse across the solid interface. Since these sites would be rapidly filled and annihilated during growth leading to flat surfaces and "homogeneous" growth rates, Frank[18] and others[19] have proposed self-perpetuating steps generated by dislocations which would continually entrap the solute material. The density of these stable steps or growth sites is believed to increase with the degree of supersaturation of the liquid. Hillig and Turnbull[20] have proposed screw dislocation and uniform rough surface models where growth at very small undercoolings would be proportional to the square of the degree of undercooling as compared to measured rates proportional to $(T_o - T_I)^{1.7}$ at nominal undercoolings. The critical importance of active growth centers has been emphasized by Sears[21] and Stranski[22] in demonstrating that growth may be greatly inhibited by certain impurities which apparently accumulate in these regions.

Another interface controlled reaction affecting crystallization velocity is the absorption or dissipation of the enthalpy of freezing. If the direction of heat flow is through the crystal and uniform, a simplified model[17] predicts a

growth rate directly proportional to the degree of undercooling. Radiation of solid and liquid and heat transfer in the liquid through convection would probably alter this simple heat conduction mechanism at high temperatures.

The crystallographic orientation of the solid interface has an important influence on the linear growth rate in both solution and melt-grown crystals. It is well known that rapidly growing crystal faces tend to annihilate themselves leaving the slow growing faces on crystals grown from solution.[19] In growth from the melt the dependence of growth velocity on orientation has been verified by numerous investigations, and, in fact, the Czochralski method was originally devised to determine the effect of orientation of the rate of crystallization in metals.

b. Transport Controlled Growth

The rate of transfer of material to growing crystal can, in many cases, have a controlling effect on the kinetics of the process. The early theories on growth[19] assumed that the diffusion of solute controlled the growth rate without any barrier to incorporation of material at the interface. Under steady state conditions, the extraction of solute by the growing crystal sets up a concentration gradient (Fig. 14) which is controlled by the rate of diffusion of material from the bulk of the liquid at concentration $C_o$. In Fig. 14 $C_\ell$ is the solute concentration at the solid-liquid interface which we will assume is equal to the equilibrium solute concentration at that temperature. The equilibrium solubility at any temperature, $T_I$, is given simply by the value on the liquidus curve of the phase diagram in question. In Fig. 14 the degree of supersaturation (or supercooling) is given by the concentration difference $C_o - C_\ell$ which is seen to increase with distance from the interface. For a diffusion controlled process the early theories[23] predict a dependence of linear growth rate U on the concentration difference

$$U \approx DS(C_o - C_I) \qquad (2)$$

where S is a surface area term and D the diffusion constant. From studies of growth in alloy systems, Tiller et al.[23] have derived an expression for the solute

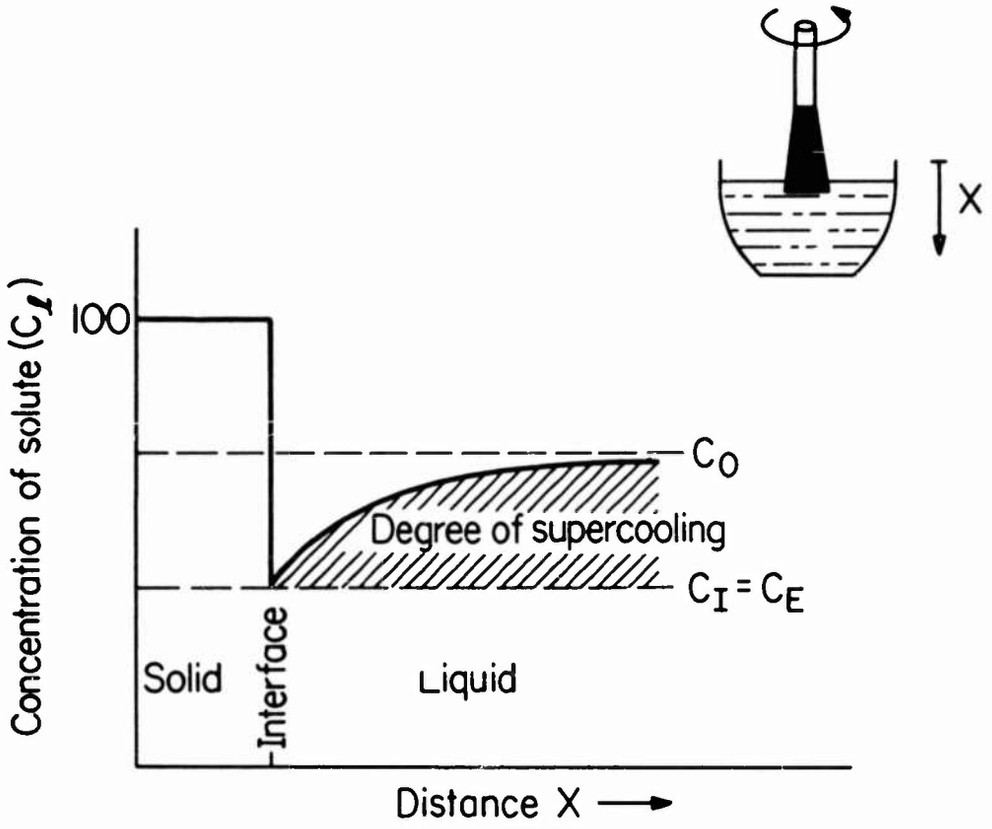


CONCENTRATION PROFILE DEVELOPED DURING DIFFUSION CONTROLLED GROWTH AT CONSTANT TEMPERATURE

FIGURE 14

concentration as a function of distance x' from the solid interface. The concentration values $C_\ell$, $C_I$, and $C_o$ have the same meaning as before, that is,

$$C_\ell = C_1 \exp\left(\frac{R}{D} x'\right) + C_o \quad . \tag{3}$$

From this expression, assuming stable growth conditions, one can predict that an increased rate of growth must be balanced by a steeper concentration profile in the melt. A high concentration gradient near the interface, however, can lead to unstable growth conditions as shown by Chalmers,[23] since any portion of the crystallizing solid momentarily in advance of the planar interface will find itself in a region of greater supersaturation and will tend to grow more rapidly. The planar growth interface will then break down as these protuberances or fast growing regions advance into the melt as dendritic or cellular shapes leaving slower growing areas behind. The liquid phase is entrapped between fast growing regions and freezes out as elongate worm-like areas parallel to the general growth direction. To discourage this unstable type of crystal growth, the degree of supersaturation or "constitutional supercooling"[24] of the melt in advance of the interface must be controlled This can be done by imposing a gradient of increasing temperature from the solid into the liquid phase. Since the solubility in the liquid increases with temperature, a sharp temperature gradient will decrease the supercooling to a region very close to the planar crystal liquid interface. The effect of this gradient on reducing the area of supersaturation in the liquid (ruled area, Fig. 14) is shown in Fig. 15. The equilibrium solubility in the liquid (dashed line) for a given temperature gradient is given by the liquidus line of the phase diagram. Any rapidly growing area in advance of the interface will soon find itself in an area of higher temperature and decreasing or non-existent supersaturation which will tend to slow its rate of advance, thus maintaining a planar interface and stable growth conditions. High temperature gradients near the interface will also increase diffusion of solvent and solute, thereby discouraging the entrapment of liquid as inclusions in the growing crystal.

In addition to the interaction of growth rate and diffusion rate on the concentration profile in the liquid, convection currents and mechanical stirring

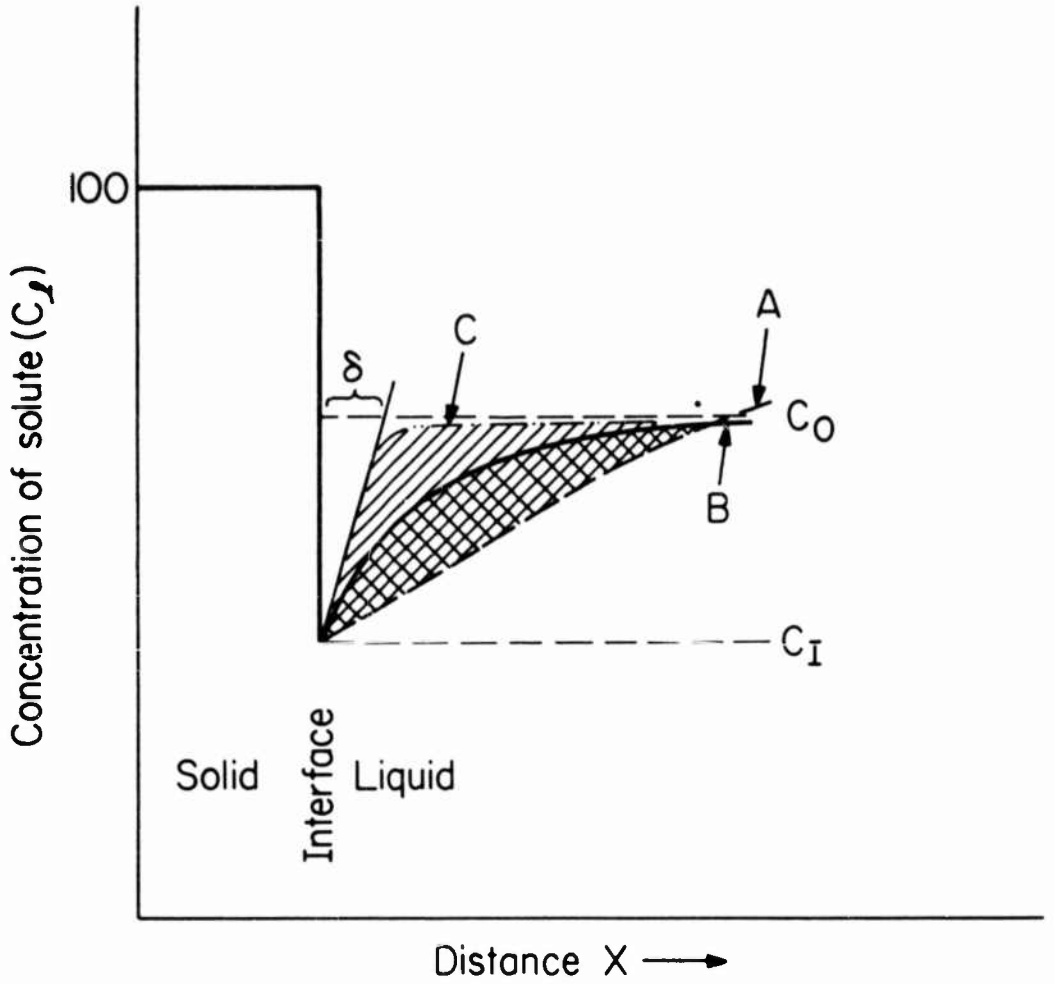


Curve A - Equilibrium concentration curve for given temperature gradient in crucible

Curve B - Concentration profile for diffusion controlled growth mechanism

Curve C - Concentration curve for growth modified by diffusion, convection and stirring; $\delta$ is effective boundary layer thickness

VERTICAL CONCENTRATION GRADIENTS IN A LIQUID DURING CRYSTAL GROWTH

FIGURE 15

make additional contributions to the distribution of solute. Convection arises from density differences in the liquid as controlled by temperature and composition gradients. Changes in viscosity also effect both convection and diffusion rates. Although the interaction of temperature, viscosity, convection, and diffusion is quite complex[25, 26] the overall effect is to increase the concentration gradient adjacent to the interface by the rapid flow of liquid. The resulting boundary layer (Curve A, Fig. 15) is considerably sharper than the diffusion gradient controlled concentration profile (Curve B, Fig. 15). This boundary layer can be very narrow for fluid liquids with high temperature gradients and high fluid flow velocities. The film thickness is defined by the tangent to the concentration profile at the interface. The rate of transfer of solute from liquid to solid will be greatly increased across this high concentration gradient. The growth rate equation can be modified to take the increased concentration gradient into account through dividing by the effective film thickness $\delta$ [19]

$$U \approx \frac{D}{\delta} (C_o - C_I) \quad . \tag{4}$$

Stirring the solution will reduce the effective film thickness even further. In aqueous solutions the boundary layer between homogeneous liquid and solid may be a fraction of a millimeter;[26] indeed, some investigators[27] feel that this stagnant boundary layer is practically non-existent in stirred solutions (10 to 100 Å thick). However, the entrapped liquid and generally poorer quality of crystals grown from unstirred liquids force the conclusion that an effective concentration gradient does arise from the depletion of solute from the liquid and that diffusion across this gradient is a factor in crystal growth.

## 2. Oxide Single Crystal Growth

Practieally all of the teehniques presently employed to produce refraetory oxide single erystals ean be grouped into one of two categories: 1) from melt, or 2) solution growth. The distinetion between these two situations is generally made on the basis of concentration of the material crystallizing from the liquid phase. In growth from the melt, the major component or solvent crystallizes, whereas in growth from solution, the phase separating from the liquid is the minor constituent or solute. Growth of garnet crystals from solution would involve the intermediate case where solvent and solute occur in roughly comparable concentrations. Growth under these conditions may be expected to involve factors which are operative in both dilute solution and melt so that a review of the faetors affecting growth in the latter two situations may be of some use.

Growth of oxide crystals from aqueous solution has been extended to high temperatures as hydrothermal growth, but is limited, in general, because of low solubility and the necessity of high pressure autoclave design. A notable exeeption to this is quartz ($SiO_2$) which is reasonably soluble under alkaline conditions. According to the preliminary findings of Laudise[28] the linear growth rate in quartz is directly proportional to supersaturation, and at constant saturation the rate of growth varies exponentially with temperature. The rate is of the order of 2 mm per day. This situation can be described by the formula[17]

$$U \approx k(C_o - C_I) \cdot \exp\left(-\frac{Q}{T_I}\right) \tag{5}$$

where U = growth rate, Q is the growth aetivation energy and $T_I$ the growth temperature.

Molten salts have been used as a solvent in producing barium titanate[29] and related oxide materials. Lead oxide-fluoride solvents have been used similarly to dissolve spinel and garnet compositions.[9] In these systems the supersaturation required for growth is provided both by volatilization of solvent and by slowly lowering the temperature. Since both volatilization and

temperature affect the supersaturation of liquid at any point during cooling, it is difficult to assess the relative importance of each on growth rate. Moreover, a number of crystals of different sizes are generally formed throughout the crucible during cooling which would indicate that either the rate of crystallization was not uniform, that crystals began growing at various times, cr perhaps that the liquid phase itself was not uniform. Because of these possible complications, it seems unlikely that any real insight relating to the general problem of crystal growth will develop from a study of crystallization under these conditions.

The most extensive application of crystallization from the melt in producing refractory oxide single crystals has been the Verneuil or flame fusion process. This method has been used in the commerical production of sapphire, and in the laboratory synthesis of many other oxides.[30] The rate of growth in the Verneuil process for comparable materials is orders of magnitude greater than growth from solution. A quantitative accessment of the factors controlling growth of the boules is difficult, however, because the degree of supercooling at the solid-liquid interface cannot be measured accurately nor can it be changed significantly without causing a breakdown of the stable interface. The zone melting or floating zone technique[31] is very similar in principal to the Verneuil process. As in the Vernueil method, the overall rate of growth can be measured accurately, but the factors controlling the growth rate cannot be measured directly nor can the growing conditions be varied sufficiently to give some indication of the rate controlling steps.

The phase diagrams of the oxide systems investigated thus far have shown that the garnet phase at equilibrium must be grown from melts high in iron oxide which implies growth from concentrated solution. After considering the possible alternative methods described in the preceding section, the Czochralski technique was decided upon because it would permit the greatest flexibility in investigating what are considered the important variables controlling growth. These factors are 1) the interface temperature $T_I$, 2) the temperature gradient in the liquid $T_\ell$ and the attendant constitutional supercooling, 3) the orientation of the crystal seed, 4) the rotation and pulling rates, and 5) the temperature drop through the crystal from melt to pulling rod, i.e.,

thermal conduction through the crystal. A further advantage of the Czochralski technique is that the crystalline perfection is generally higher where close control of growth temperature is maintained and extreme temperature gradients are avoided. The major disadvantage of Czochralski growth lies in the possible contamination of melt and crystal by gradual solution of the crucible material. Other materials are being developed in a parallel program to minimize crucible contamination, but for the present, platinum seems most convenient and will be used in the preliminary studies deferring this problem to a later stage of the project.

A Czochralski furnace and pulling assembly has been designed and built in this laboratory specifically to attempt the growth of single crystals of yttrium iron and related garnets; it is expected that this equipment will be used in growing other refractory oxide materials in the future. The furnace, pictured in Fig. 16, is heated by six Kanthal-Super hairpin elements surrounding a three-inch diameter, 30-inch vertical alumina muffle. The muffle is sealed at both ends with water-cooled brass units to permit atmosphere control. The pulling rod "O" ring seal and quartz sighting window are in the top assembly through which a stainless steel-alumina pulling rod projects down into the furnace. The platinum crucible containing the melt sits on an alumina pedestal which can be positioned at different heights within the furnace allowing for variation in the vertical thermal gradient in the crucible. Temperature is measured by several thermocouples positioned in the vicinity of the crucible.

Some representative boules that have been grown under these conditions are pictured in Fig. 17. The garnet area of the boules is generally crystallographically continuous, but often contains inclusions of frozen liquid which indicate that the optimum conditions for stable growth have not been achieved. The growth interface of boules pulled from the liquid is remarkably similar to the cellular interface in metals as described by Chalmers.[24] From the results of these preliminary experiments and the findings of previous studies in crystal growing, a number of variables may be stated which would seem to influence most significantly the rate of growth and the stability of growth conditions.

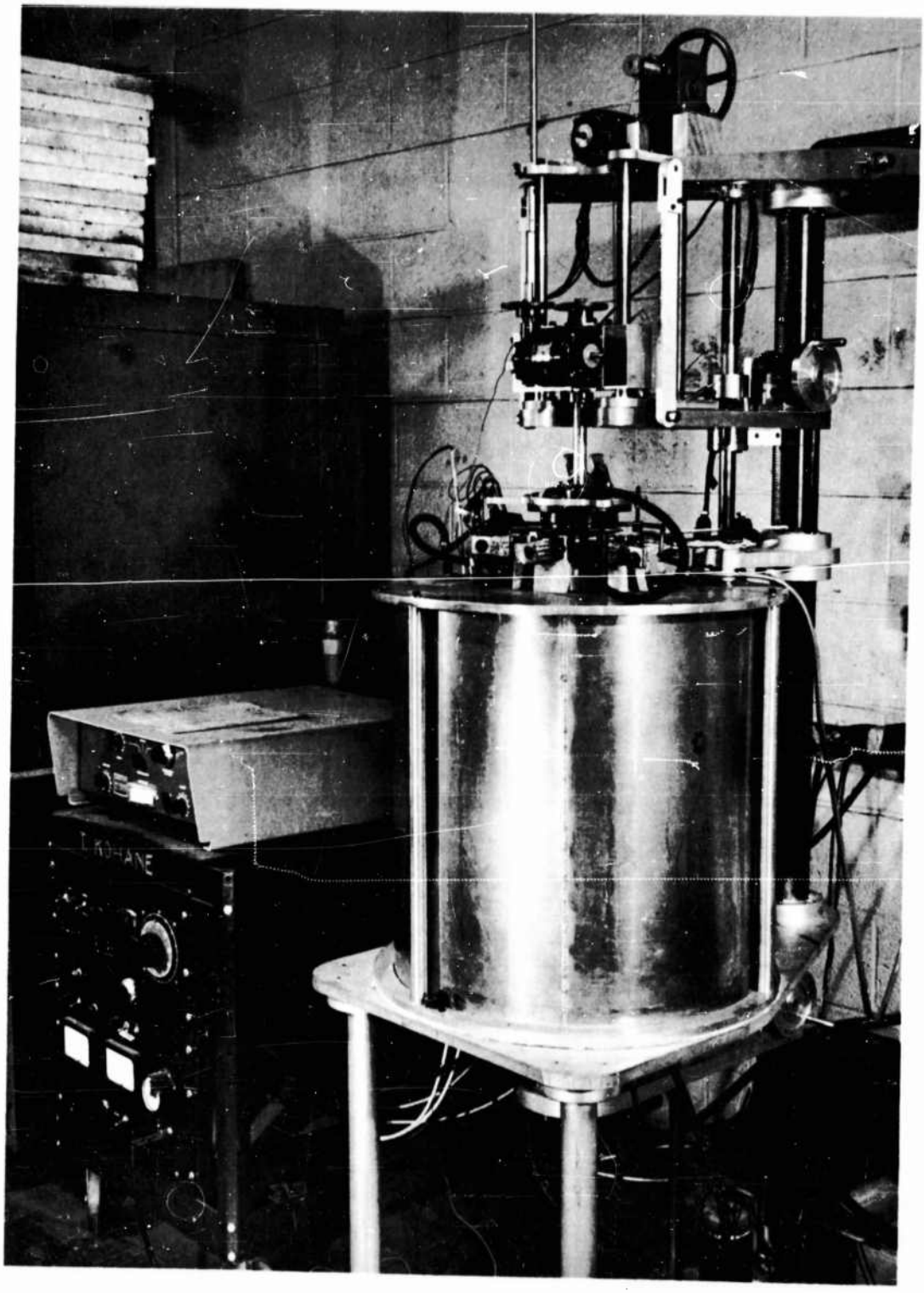

CZOCHRALSKI CRYSTAL PULLING APPARATUS.
FIGURE 16

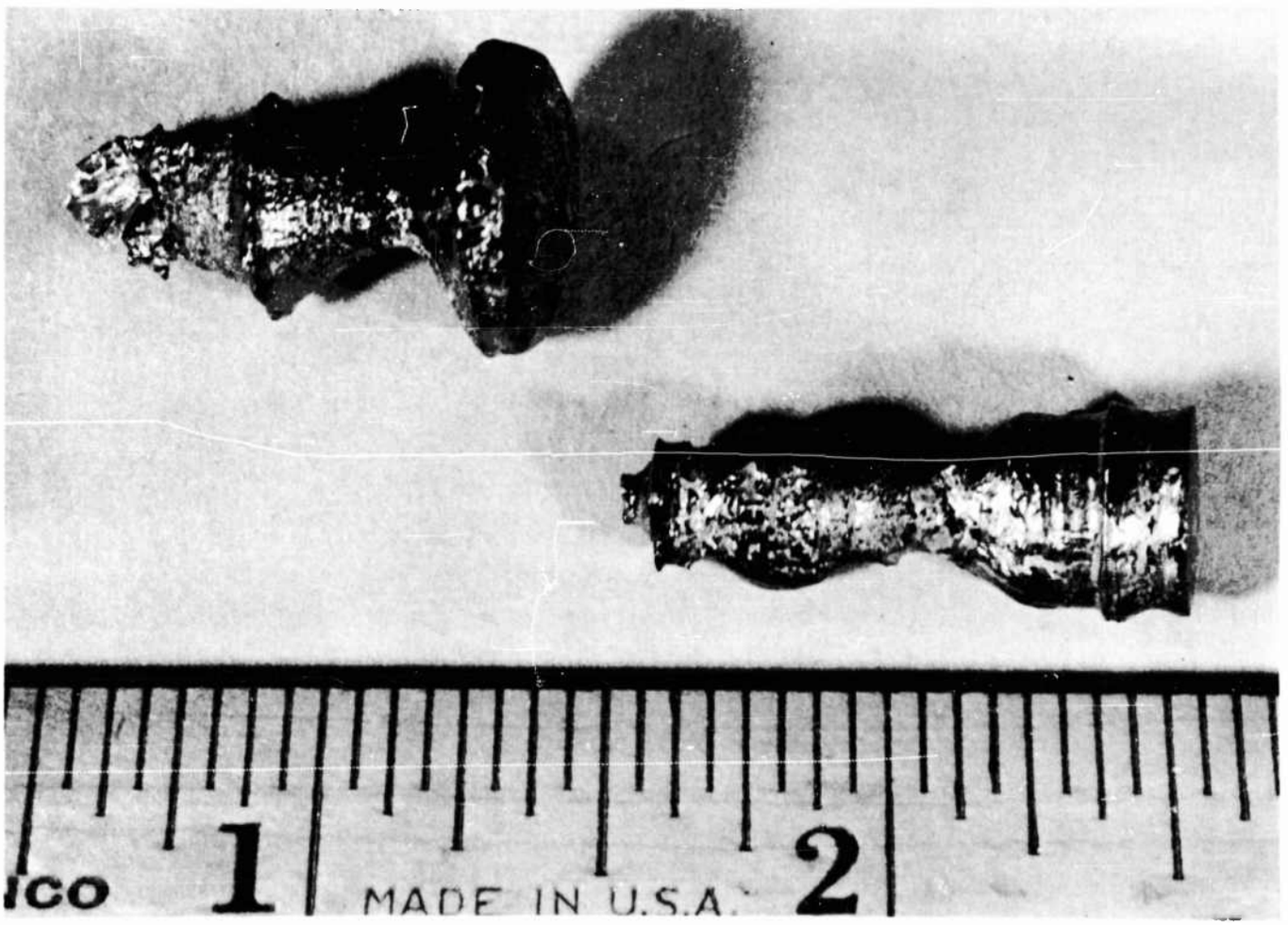


YTTRIUM - IRON GARNET BOULES GROWN BY CZOCHRALSKI TECHNIQUE.

FIGURE 17

a. Degree of supercooling. This is the most important factor. The transport models predict a direct proportionality of supercooling or supersaturation $(C_o - C_I)$ to growth velocity; surface controlled growth models predict a higher dependence $(C_o - C_I)^2$. An excessive supersaturation can result in unstable growth. This instability cannot be corrected by a slower extraction rate because the crystal grows excessively large in lateral direction making handling very difficult. Increased supercooling increases both diffusion and convection transport, the latter because of density differences resulting from concentration differences in solution;

b. Rotation rate. Rotation is expected to lead to more uniform and stable growth because the stirring evens out radial temperature-concentration gradients. High rotation speeds may increase growth rate slightly through reducing the boundary layer film at the solid-liquid interface;

c. Growth temperature. The rate of growth increases with temperature. Since growth is an activated process the rate varies exponentially as $1/T$;

d. Heat conduction. Since heat must be expelled during crystallization, growth will depend on the efficiency of heat conduction and/or radiation;

e. Crystal orientation. The effect of crystallographic orientation on growth rate is perhaps the easiest variable to investigate. For simple face-centered cubic metals Chalmers[24] has predicted growth rates in the ratio 2.0:1.5:1.0 for the directions [110], [100], and [111], respectively.

The factors considered above are summarized qualitatively in the

following formula

$$U \approx \frac{k}{\Delta H_v} \cdot \frac{D_o}{\delta} \cdot a_{hk\ell} (C_o - C_I)^n \exp \frac{-Q}{T_I} \qquad (6)$$

where U is the crystallization velocity, k the thermal conductivity, $\Delta H_v$ the enthalpy of freezing, $D_o$ the diffusion coefficient, $\delta$ the effective boundary layer thickness, $a_{hk\ell}$ the crystal orientation factor, $(C_o - C_I)^n$ the degree of supersaturation with n varying from 1 to 2 and the exponential term containing surface controlled growth activation energy Q and the interface temperature $T_I$.

A study of growth with regard to the variables outlined above will indicate the range of conditions under which stable growth can be maintained. The macroscopic perfection of the crystalline boules can then be correlated with changes in certain of these variables. As the growth technique is improved it is expected that the more sensitive physical, electrical, and magnetic properties will be measured which will yield more insight into the details of the growth process.

## III. SPINEL-TYPE OXIDE SYSTEMS

### A. Phase Equilibria

Selection of various spinel systems for phase studies has been based primarily on whether the spinel solid solutions appeared suitable for simple analysis of the conductivity process. For example, solid solutions of the form $Fe^{2+}_{1-y}Me^{2+}_{y}Fe^{3+}_{2}O_4$ where the cation $Me^{2+}$ substituting for $Fe^{2+}$ located only on one site would obviously be least complicated in formulating a suitable conductivity model. Two such cations which may be substituted in this simple manner are nickel and cobalt. In the case of nickel, substitution occurs only up to $NiFe_2O_4$, whereas with cobalt, solid solution exists from $Fe_3O_4$ through $CoFe_2O_4$ to $Co_3O_4$. With these substitutions, presumably the number of carriers changes as y varies, if only the variable valence of iron contributes electrons for conduction.

Another type of substitution is represented by $Fe^{2+}Fe^{3+}_{2-y}Al^{3+}_{y}O_4$, where the carriers are maintained constant (again assuming the carriers are proportional to the ferrous ion content) but the octahedral sites containing trivalent iron available for conduction are dependent upon the value of y. In this system, a fraction of the aluminum ions can also occupy the tetrahedral sites. The distribution of aluminum ions between tetrahedral and octahedral sites depends upon the "effective" temperature at which the material is prepared. Therefore, at constant composition, the ferric ions participating in octahedral conduction can be varied by proper heat treatment assuming that the $Fe^{2+}$ ions are confined to an octahedral environment. Of necessity then, cation distribution studies will have to compliment the phase studies in this system for a complete analysis of conductivity in aluminum substituted magnetites.

Finally, another system offers further interesting variations. Magnesium extends the magnetite field on both sides of stoichiometry, viz., oxygen excess and oxygen deficient spinels exist in this system.[32] In addition,

the distribution of magnesium ions on the A and B sites is temperature dependent, and the degree of this disorder apparently depends upon the concentration of magnesium in the spinel. Consequently, in this system divalent substitution for $Fe^{2+}$ will vary the number of carriers, and at constant composition the number of ferrous and ferric ions participating in the conduction process will depend upon the fraction of magnesium ions in octahedral positions. Also in this system, the effects of nonstoichiometry on conductivity can be ascertained.

## 1. The System $FeO$-$NiO$-$Fe_2O_3$

### a. Introduction

This is perhaps the simplest of all systems to investigate conductivity processes because of the independence of cation distribution on heat treatment. Once the chemistry is defined, the conductivity dependence of ferrous ion content can be ascertained, and hopefully quantitatively analyzed.

Suitable explanations of results obtained in this system should provide some rational basis for interpreting conductivity in other spinel systems.

The phase relations in the system Fe-Ni-O below 1300°C between 1.0 and 0.01 atmospheres have been previously determined,[8] and serve as a basis for extending such studies to higher temperatures and lower pressures. Most important of all, it has been shown that in the vicinity of nickel ferrite the spinel field has little or no width, but with the continuous replacement of nickel by iron, the field widens in the direction of higher oxygen content.. This deviation from the stoichiometric formula, $M_3O_4$, cannot be tolerated if conductivity measurements are to be meaningful. The excess oxygen in the high iron spinels is assumed to correspond to cation vacancies as in oxygen excess magnetite. Ideally, the preparation of solid solutions according to the formula $Ni^{2+}_{1-x}Fe^{2+}_{x}Fe^{3+}_{2}O_4$ is desirable for quantitative interpretation of the conduction process in this series. The ensuing discussion will be concerned primarily with the preparation of such solid solutions, and reference will be made to values of x in the above formula rather than to the starting compositions in terms of NiO and $Fe_2O_3$.

b. Experimental Procedure

Baker's Reagent Grade iron oxide and nickel oxide were mixed in various proportions by tumbling in methanol followed by rapid drying under an infrared heating lamp. The material was then reacted at 1300°C for 24 hours, and the furnace cooled to room temperature. A second mixing and heating was used to insure good homogeneity. Samples were then placed in platinum thimbles, held at various temperatures and oxygen pressures, water quenched, and then subjected to x-ray analysis.

c. Discussion and Results

As stated above, it was desired to prepare solid solutions of $NiFe_2O_4$ and $Fe_3O_4$, and the phase studies were restricted to conditions considered to correspond to those necessary to prepare this series of solid solutions. In particular, the objective was to find an oxygen isobar that would originate in binary magnetite field at $Fe_3O_4$ and extend into the ternary spinel field for some distance before emerging into the spinel wüstite area. Fig. 18 summarizes the available data on the temperature-pressure relations in the magnetite field of the binary Fe-O system.[33] It is immediately apparent that the oxygen pressures generated by $CO_2$ decomposition above 1300°C will provide appropriate atmospheres to produce nearly stoichiometric $Fe_3O_4$. With increasing temperature the oxygen pressure from the dissociation of $CO_2$ is changing, but the magnetite phase is getting closer to the ideal $Fe_3O_4$ composition. For example, at 1300°C an oxygen pressure of $10^{-3.4}$ atmosphere is in equilibrium with magnetite having a mole fraction of $Fe_3O_4$ of 0.9862, and at 1393°C, the oxygen pressure is $10^{-3.08}$ atmosphere at an $Fe_3O_4$ mole fraction of 0.9968. In terms of FeO and $Fe_2O_3$, which will be plotted on the ternary diagram, this corresponds to 49.66% and 49.92% FeO at the two respective temperatures. Consequently, in the ternary construction this isobar will be drawn originating in the binary magnetite field at $Fe_3O_4$. Although the equilibrium oxygen pressure for $CO_2$ decomposition changes with temperature, the following discussion will make reference to the "$CO_2$ isobar" as though it corresponded to a constant oxygen pressure on the diagram.

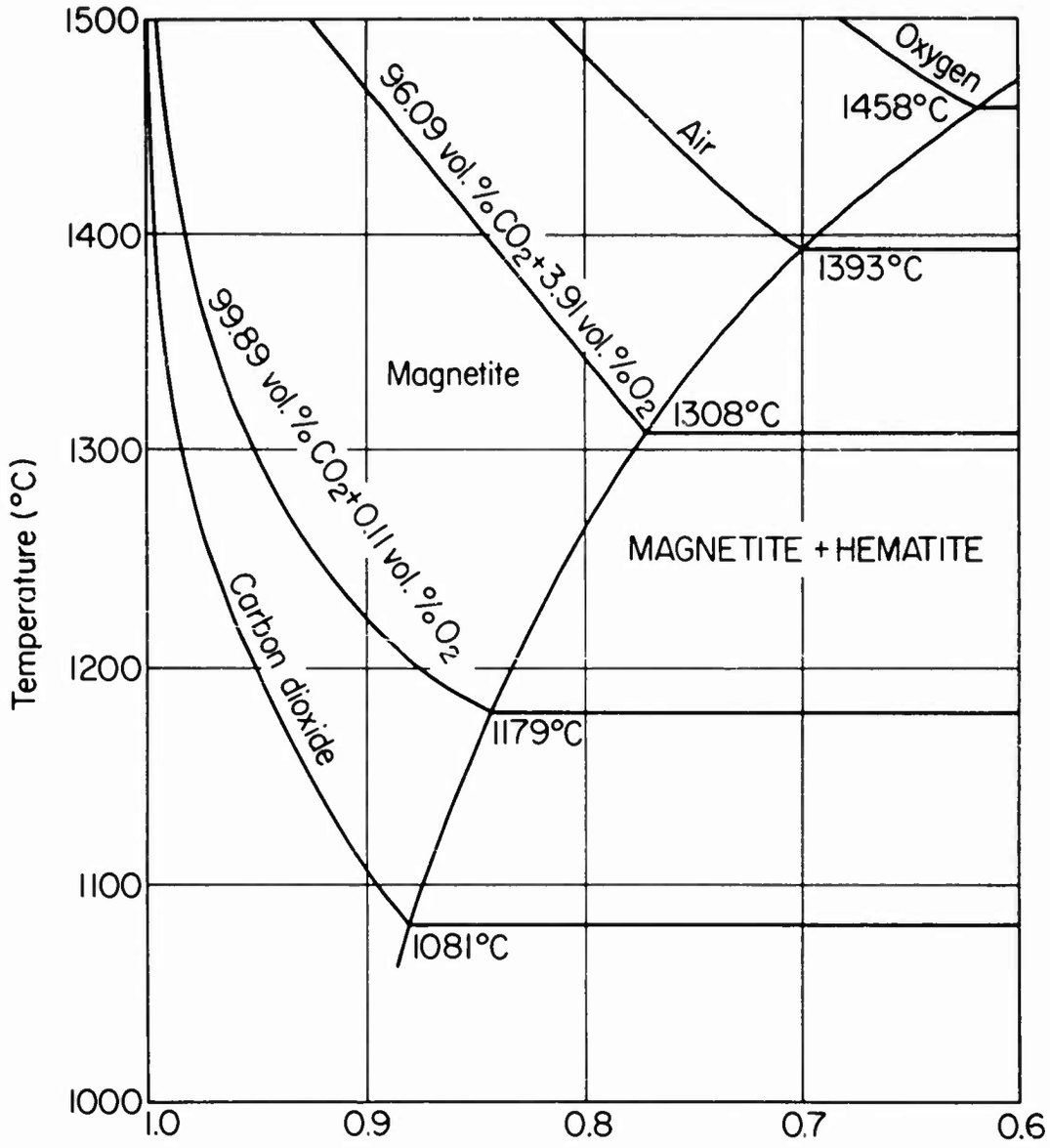


COMPOSITION OF MAGNETITE ($N_{Fe_3O_4}$ IS THE MOL FRACTION OF $Fe_3O_4$, THE OTHER COMPONENT BEING $Fe_2O_3$) IN EQUILIBRIUM WITH VARIOUS ATMOSPHERES[33]

FIGURE 18

Since the spinel field in the vicinity of $NiFe_2O_4$ has little or no width, an oxygen isobar originating in the binary magnetite field at low oxygen partial pressures would extend into the ternary diagram along the spinel boundary and then emerge into the spinel + wüstite field. With increasing temperature, a given oxygen isobar would emerge further down from $NiFe_2O_4$ in the direction of $Fe_3O_4$. With increasing temperature, however, the $O_2$ pressure for pure $CO_2$ decomposition increases so that this "isobar" moves down slower than a constant oxygen isobar would move.

Lattice parameter measurements were used to determine where the $CO_2$ isobar emerged from the spinel field and are plotted in Fig. 19. The (751) reflection was measured with Co Kα radiation and was scanned at 0.2°2Θ per minute. Powdered silicon was used as a standard. Lattice parameters were measured to within ±0.0006Å and the larger deviations in Fig. 19 at fixed x values are considered to be due to variations in composition caused by non-equilibrium with the gas phase prior to quenching. The nickel ferrite lattice constant was taken as 8.3385Å and $Fe_3O_4$ as 8.3890Å with the above limit of ±0.0006Å. In addition to a $CO_2$ atmosphere, pure oxygen was used at 1300°C and 1400°C for compositions x = 1 and 0.1. From Fig. 19 it is evident that the lattice constant varies linearly between $NiFe_2O_4$ and $Fe_3O_4$. Therefore, the composition of the spinel phase in equilibrium with wüstite is determined by reading off directly from this plot the composition corresponding to a particular lattice constant. For example, a composition initially consisting of only $NiFe_2O_4$ quenched from 1400°C in $CO_2$ had an $a_o$ of 8.3466Å, and for x = 0.1, an $a_o$ of 8.3468Å, so that a horizontal line intersects the oblique line at an x value of 0.15. This gives the composition of the spinel in equilibrium with wüstite of an undetermined composition.

From these data and those of reference 8, a part of the phase diagram of the system $FeO$-$NiO$-$Fe_2O_3$ has been constructed in Fig. 20. In addition, the location of the 1400°C spinel-hematite field boundary and the oxygen tie line for the spinel-hematite equilibrium have been estimated. Quite surprisingly, the $CO_2$ isobar emerges from the spinel field at very low ferrous content, and is not very far from the oxygen isobar at 1300°C and 1400°C. The composition of the spinel phase in equilibrium with wüstite is given in Table II, both in

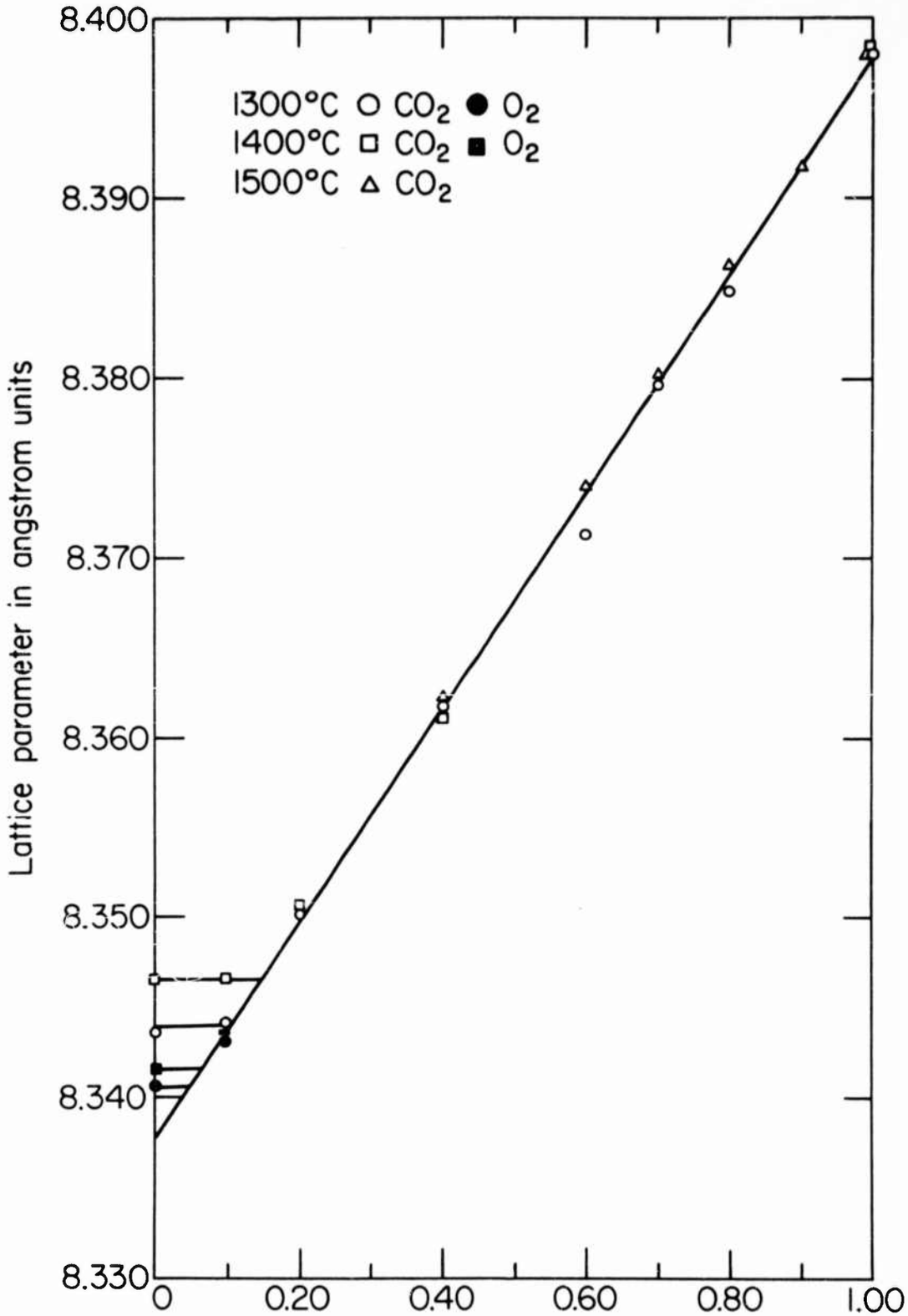


LATTICE PARAMETER AS A FUNCTION OF X IN THE SERIES $Ni_{1-X}^{2+} Fe_X^{2+} Fe_2^{3+} O_4$

FIGURE 19

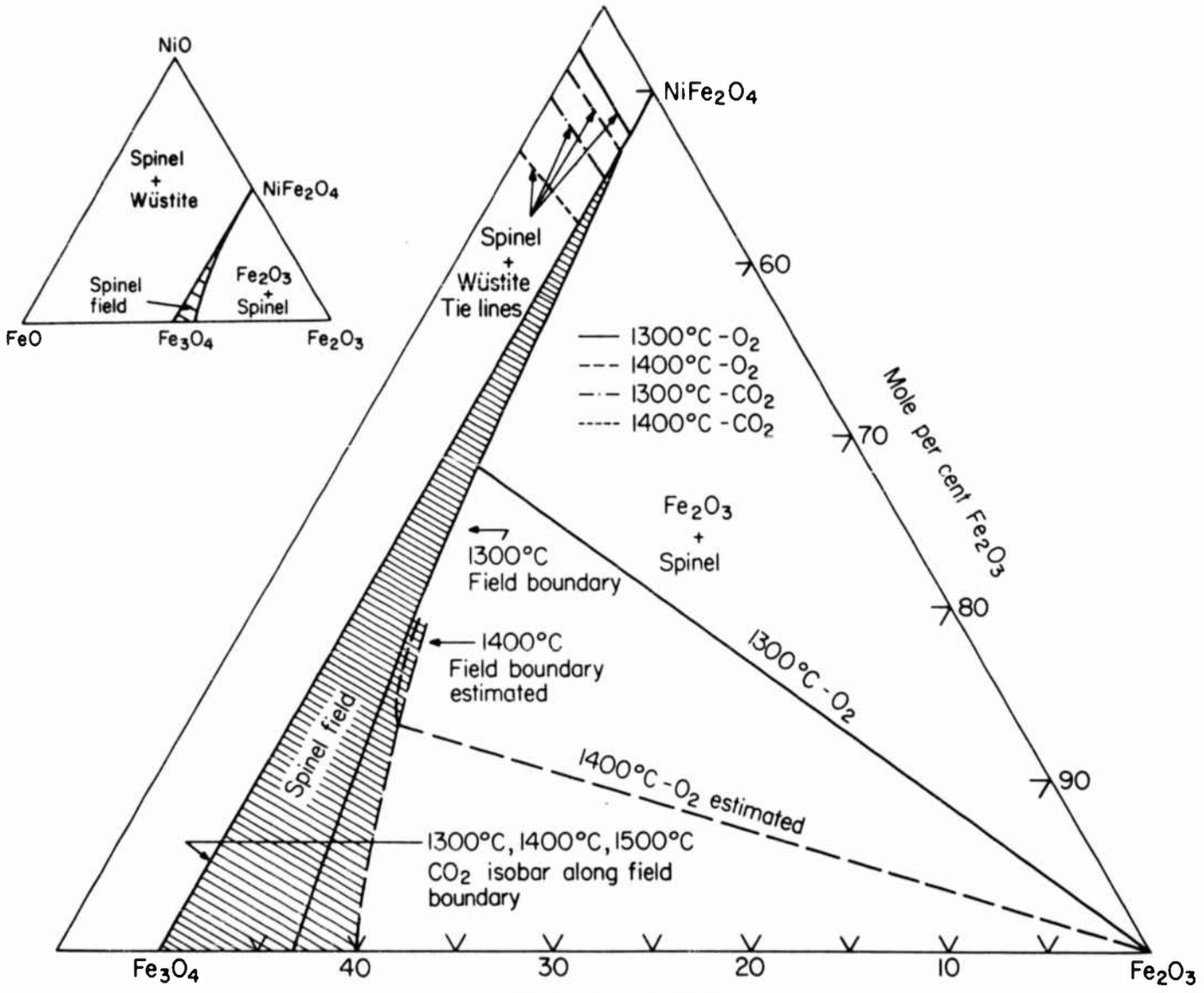


A PORTION OF THE FeO - NiO - $Fe_2O_3$ PHASE DIAGRAM

FIGURE 20

## TABLE II

### COMPOSITION OF THE SPINEL PHASE FOR THE SPINEL-WÜSTITE EQUILIBRIA

| Temperature | Atmosphere | x in $Ni_{1-x}Fe_xFe_2O_4$ | Mole % FeO |
|---|---|---|---|
| 1300°C | $O_2$ | 0.05 | 2.5 |
| 1400°C | $O_2$ | 0.07 | 3.5 |
| 1300°C | $CO_2$ | 0.10 | 5.0 |
| 1400°C | $CO_2$ | 0.15 | 7.5 |
| 1500°C | $CO_2$ | Melting occurred at x values of 0.1 and 0.2 | |

terms of x in $Ni^{2+}_{1-x}Fe^{2+}_{x}Fe^{3+}_{2}O_4$ and in terms of FeO mole percent for plotting the ternary diagram $NiO\text{-}FeO\text{-}Fe_2O_3$. The data for 1500°C at x values of less than 0.20 were not obtained because melting occurred with these compositions. Previously it had been shown that $NiFe_2O_4$ was stable at 1300°C in oxygen,[8] whereas the present results show the oxygen isobar emerging from the spinel field at an FeO content of 2.5%. The exact reason for this difference is not known, and because it is small, it will be neglected. At 1300°C and 1400°C the $CO_2$ isobar emerges at x equal to 0.10 and 0.15. At 1500°C melting occurred with the compositions at x values of 0.10 and 0.20, so that at best, samples at x values greater than about 0.30 can be prepared at this temperature. In pure oxygen, the isobar emerges at x values of 0.05 and 0.07 at 1300°C and 1400°C, respectively.

d. Conclusions

These results indicate that it is possible to prepare quenched samples of solid solutions of the form $Ni^{2+}_{1-x}Fe^{2+}_{x}Fe^{3+}_{2}O_4$. In pure $CO_2$ solid solutions containing x values greater than 0.10 at 1300°C and 0.15 at 1400°C can be prepared. For lower values of x, pure oxygen can be used to prepare compositions approaching $NiFe_2O_4$, but this would not be compatible with the requirements of dense, well sintered samples. Consequently, no effort was made to obtain low temperature phase equilibrium data.

2. The System Fe-Co-O

a. Introduction

As stated above, the substitution of $Co^{2+}$ for $Fe^{2+}$ in $Fe_3O_4$ occurs simply; the $Co^{2+}$ prefers the octahedral positions. However, this system provides an additional variation not possible in the previous one. A complete series of solid solutions exist between $Fe_3O_4$ and $Co_3O_4$ at elevated temperatures, so that substitutions are possible on both sides of the stoichiometric ferrite, $CoFe_2O_4$.

b. Experimental Procedure

The starting materials were prepared by a method described in detail by Wickham.[34] It consisted of co-precipitating the cations in the desired ratio from solution as oxalates followed by thermal decomposition of the oxalates to form the spinel. The source of the cobalt was Bakers Reagent Grade cobalt sulfate heptahydrate and the source of the iron was Bakers Reagent Grade ferrous sulfate heptahydrate. The oxalic acid and ammonium oxalate were also Bakers Reagent Grade material.

Specifically, a weighed amount of cobalt sulfate heptahydrate and ferrous sulfate heptahydrate to give the desired iron-cobalt ratio were dissolved together in demineralized water and added slowly by means of a separatory funnel to a hot solution containing ammonium oxalate and oxalic acid. Continuous stirring was maintained during the precipitation and for two more hours after all of the iron-cobalt solution had been added. The precipitated material was filtered, washed, and dried at 110°C. The material was then decomposed by heat lamps to form the oxides. The oxide material was then heated to 1300°C in an air atmosphere and held at this temperature for a period of six hours to increase the particle size. These precipitates were extremely fine and required this treatment. The material was allowed to cool to room temperature and then readily broken up using a mortar and pestle. It was passed through a 325 mesh screen and heated to a temperature of 850°C in an oxygen atmosphere and held at this point for a period of twelve hours and then cooled to room temperature in oxygen. The material was passed once more through a 325 mesh screen.

Each sample was analyzed by standard wet chemical methods to obtain the actual iron and cobalt contents, and the oxygen content was determined by the difference. The structure of all the samples prepared by this method was identified as the spinel structure using a General Electric Diffraction Unit with cobalt $K\alpha$ radiation.

The apparatus used to measure the equilibrium oxygen pressure has been previously described in detail[8] and is represented by a schematic diagram in Fig. 21. Briefly, it consists of a closed system of approximately 25 cc capable of maintaining pressures less than one atmosphere when the sample tube is at elevated temperatures (up to 1300°C). A calibrated mercury burette allows for expanding the system by definite increments of volume. All of the system outside the furnace is thermostated to within ±0.5°C. The system is calibrated for pressure as a function of the moles of gas in the system at different temperatures exclusive of the burette, so that at any given pressure and level in the burette, the moles of gas in the total volume is the sum of that in the calibrated portion of the system and the quantity in the burette calculated from the ideal gas law.

The operating procedure was as follows: An accurately weighed sample in a platinum crucible was placed in the tube and the system evacuated at room temperature by means of a mercury diffusion pump and fore pump down to $10^{-5}$ mm of mercury. The temperature of the furnace was raised to 800°C to cause any adsorbed gases on the sample to be evolved. This temperature is low enough to allow outgassing but no measurable decomposition. However, as an added precaution, dried oxygen was introduced into the system to reoxidize any of the samples that may have lost oxygen during the outgassing operation. The furnace was allowed to cool to room temperature. The system was again pumped down to $10^{-5}$ mm of mercury followed by the introduction of a given number of moles of oxygen. The number of moles of oxygen that was introduced was calculated using the ideal gas law. The sample was brought to the desired temperature and a series of equilibrium pressures were recorded by expanding the system after each equilibrium oxygen pressure was obtained. From this data, the moles of oxygen over the sample at a particular equilibrium pressure were calculated using the ideal gas law and previously calibrated curves of moles of oxygen versus pressure at the desired temperature. The original moles of oxygen introduced into the system was subtracted from the moles of oxygen over the sample at a particular equilibrium oxygen pressure to give the moles of oxygen lost by the sample. Since the original composition of the sample was known from chemical analysis, the equilibrium composition was calculated.

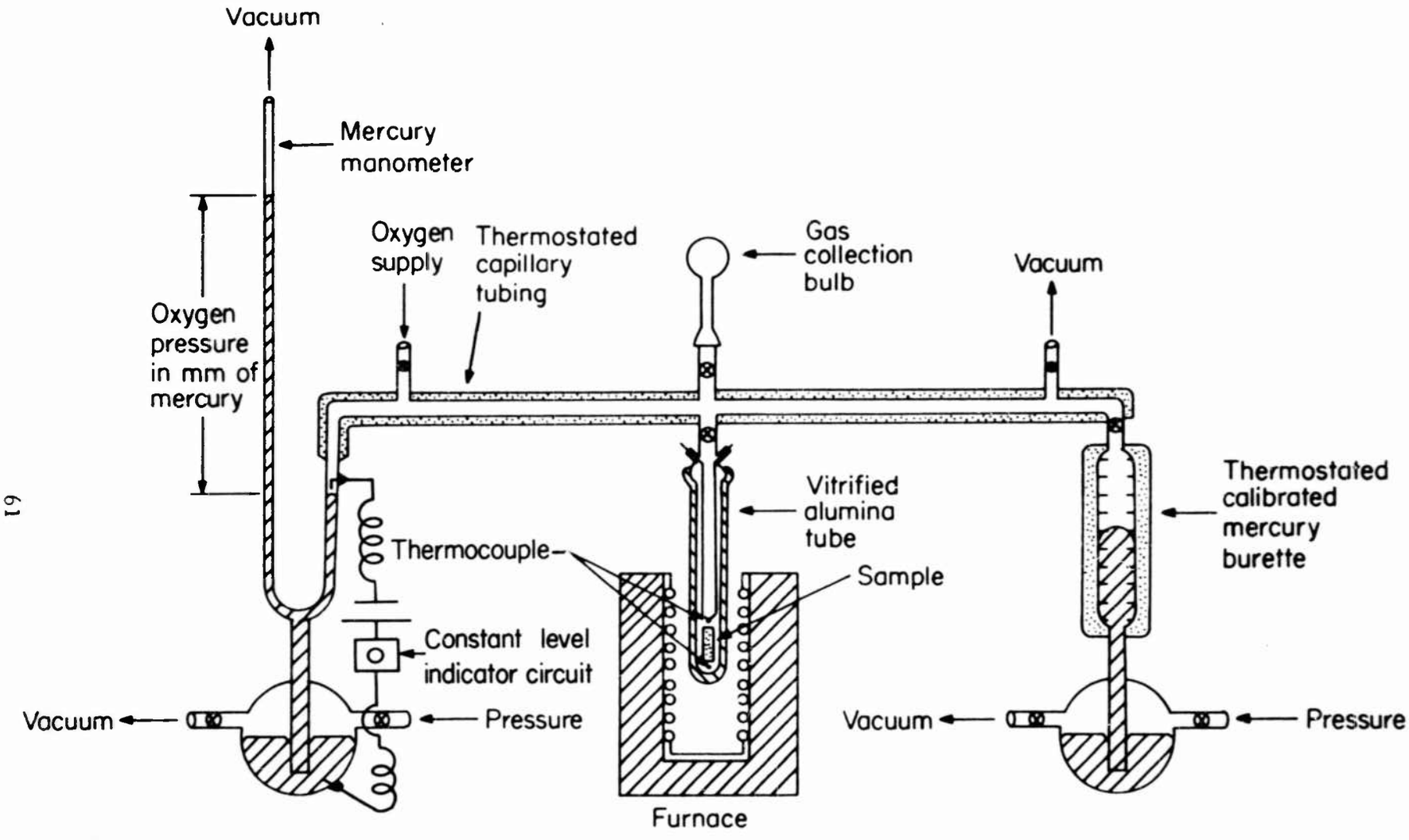


SCHEMATIC DIAGRAM OF THE DISSOCIATION APPARATUS

FIGURE 21

As a check on the reliability of the data obtained by the method described, a weight loss balance was used on identical samples to measure the loss of oxygen directly at 1000°C, 1100°C, 1200°C, and 1300°C in air. This method was not as sensitive as the oxygen pressure measuring technique, but it was much simpler in its operation and provided an alternate path for obtaining the same data. The balance was a standard two pan analytical balance with a capacity of 200 grams and a sensitivity of ±0.5 mg with full load. A 1 1/8 inch platinum crucible containing the sample was suspended from one pan of the balance to a point at the thermal center of a platinum-rhodium wound alumina tube furnace. The temperature at the thermal center was controlled to ±1°C by a saturable-reactor type controller. With the center of the platinum crucible placed in the thermal center of the furnace, a thermal gradient of 3°C existed over the length of the crucible.

The agreement between the two methods was excellent, so that only the results for the former approach are presented. Quenching experiments were run in conjunction with the equilibrium composition determinations to identify the phases present.

c. Discussion and Results

Prior to determining ternary phase relations, some information on the variability in composition of CoO and $Co_3O_4$ was needed to aid the construction of a larger diagram Fe-Co-O. Smiltens[35] has previously determined that in the vicinity of $CoFe_2O_4$ there is very little width to the spinel field so that it would be expected that for temperatures above the miscibility gap, the spinel field would extend with little width from the latter composition to $Co_3O_4$. If this were the case, then it would be an easy task to prepare starting materials lying on the 4/7 oxygen fraction line, or very close to it. Also, information on the CoO field would aid in the construction of the wüstite field from CoO to $Fe_xO$. As it developed, for the range of temperatures and pressures employed, the extension of the CoO field towards $Fe_xO$ was small.

A sample of cobalt oxide was heated to 1000°C and then cooled in oxygen so that it corresponded to the nominal composition $Co_3O_4$ as determined

by wet chemical analysis. The actual composition was not important; it was desired to determine whether there was any variability of the composition of this phase. A five gram sample was placed in the gas apparatus and enough oxygen introduced so that at any temperature the pressure would be high enough to prevent the decomposition to CoO. By a series of expansions of the system, the pressure was decreased and the change in composition followed in the manner previously discussed. At the decomposition pressure, the following equilibrium was established:

$$2\,Co_3O_4 \rightleftharpoons 6\,CoO + O_2 \qquad (7)$$

By repeated expansions, the $Co_3O_4$ was completely converted to CoO after which the composition of this phase would be followed as a function of pressure. Figure 22 presents the data obtained at 900°C. It is quite apparent that neither the spinel nor wüstite phase exist over a measurable oxygen content. This procedure was followed at temperatures up to that at which the equilibrium pressure is one atmosphere with the same results; the two phases are stoichiometric within experimental error. From the equilibrium pressure data, the enthalpy change for the above reaction was determined from the following relation:

$$\frac{d \ln K}{d (1/T)} = \frac{d \ln P_{O_2}}{d (1/T)} = \frac{-\Delta H^\circ}{R} \qquad (8)$$

From the fact that two solid phases are essentially pure, their activities were taken as unity. Figure 23 is a plot of this data from which the enthalpy change for the reaction was calculated to be 75.4 k cal/mole, as compared to 76.8 k cal/mole calculated from the heats of formation.[36]

Since $CoFe_2O_4$ and $Co_3O_4$ show no fieldwidth, it seems unlikely that spinels between $CoFe_2O_4$ and $Co_3O_4$ would exist over a range of oxygen content. Furthermore, at pressures up to one atmosphere of oxygen, it was not possible to exsolve $Fe_2O_3$ from their solid solutions. Consequently, starting samples slowly cooled in oxygen were assumed to be on the join between $CoFe_2O_4$ and $Co_3O_4$.

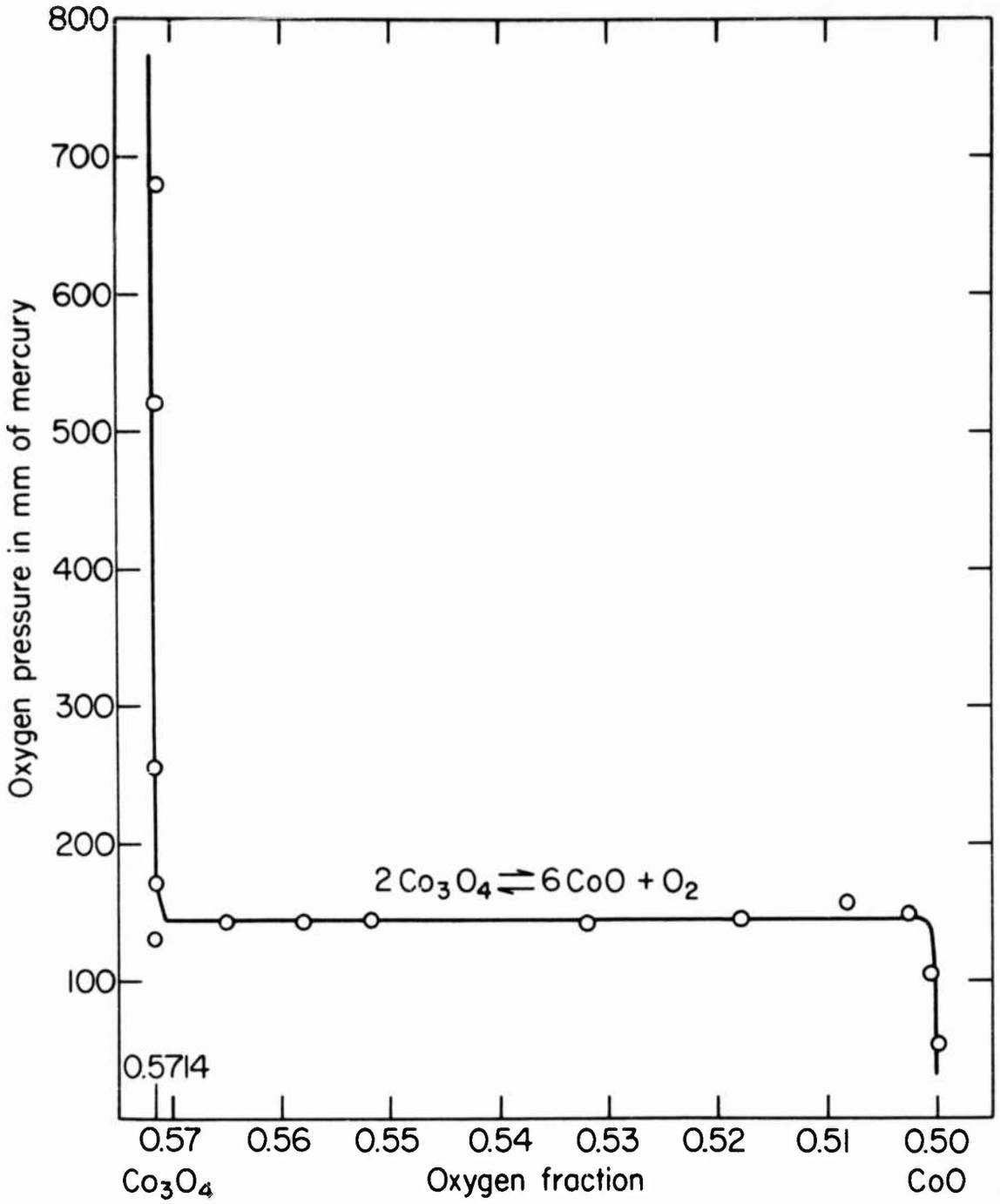


EQUILIBRIUM BETWEEN $Co_3O_4$, CoO, and $O_2$ at 900 °C ILLUSTRATING THE LACK OF FIELD WIDTH IN THE TWO SOLID PHASES

FIGURE 22

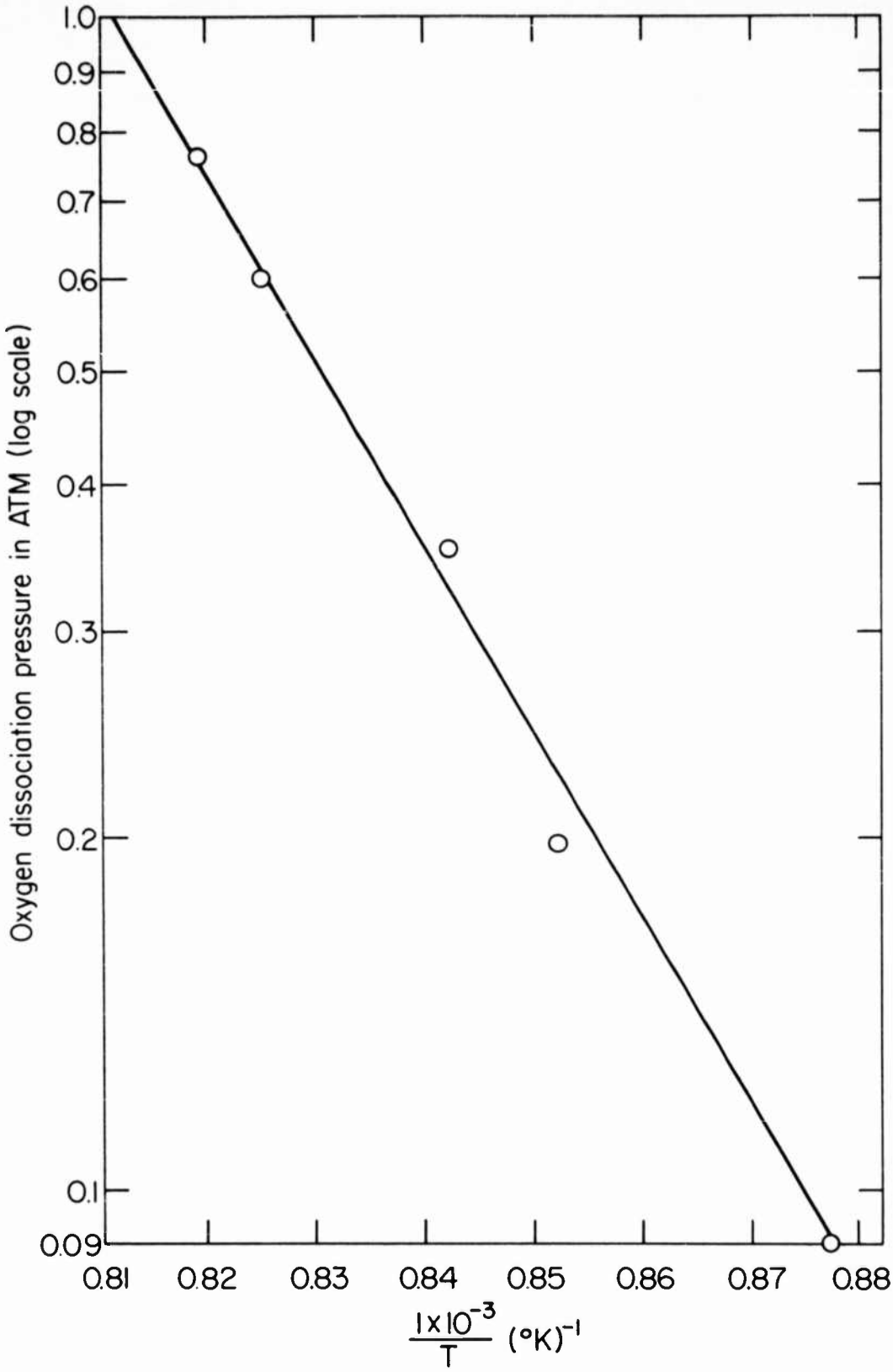


DISSOCIATION PRESSURE OF $Co_3O_4$ VS THE RECIPROCAL OF TEMPERATURE

FIGURE 23

The procedure for determining ternary compositions in this system has been described in section 2b, and Fig. 24 illustrates the data obtained on two compositions. (Constant metal ratio lines will be referred to as percent cobalt; $(\frac{Co}{Co + Fe} \times 100\%)$.) These curves are typical in their representation of such measurements. In addition to data obtained by this method up to the limiting pressure of the apparatus, namely one atmosphere, x-ray analysis was performed on samples quenched from elevated temperatures at pressures up to twenty atmospheres. Lattice parameter measurements allowed for estimating the composition of the spinel phase. This technique was only applicable on solid solutions lying between $CoFe_2O_4$ and $Co_3O_4$, and not on those between $Fe_3O_4$ and $CoFe_2O_4$. The reason for this is apparent upon examining Fig. 25 where the lattice constant is plotted for solid solutions from $Fe_3O_4$ to $Co_3O_4$. Changes in composition could not be followed by lattice parameter measurements between $Fe_3O_4$ and $CoFe_2O_4$ because it did not vary. However, the variation of the lattice constant between $CoFe_2O_4$ and $Co_3O_4$ is appreciable, so that measurements of this kind were quite useful in determining spinel composition at the higher pressures.

The ternary compositions for various pressures and temperatures are included in Table III, and the quench data for the air isobar in Table IV. Phase diagrams were constructed from this data and are included in Figs. 26 through 29. Only that portion of the larger system Fe-Co-O containing spinels between $CoFe_2O_4$ and $Co_3O_4$ is shown because phase relations between $Fe_3O_4$ and $CoFe_2O_4$ have been adequately described previously.[35] The insert is included in Fig. 26 to aid in locating the smaller section in the larger system, Fe-Co-O. At 1000°C, pressures somewhat less than five atmospheres are required to extend the spinel field from $CoFe_2O_4$ all the way to $Co_3O_4$. At one atmosphere, the isobar breaks out of the spinel field at about 58.4 percent cobalt and goes almost directly to CoO. Percent cobalt here refers to the ratio $(\frac{Co}{Co + Fe} \times 100\%)$ whereas in Table III, the complete composition of the spinel phase is given. This is somewhat surprising as it was anticipated that iron would extend the CoO field considerably towards FeO on the basis of Robin and Benard's data.[37] The composition of the spinel in equilibrium with the wüstite phase for the various pressures is given in Table V. The field is assumed to have negligible width for reasons discussed previously, so that the oxygen fraction throughout is assumed to be 4/7, or 0.5714.

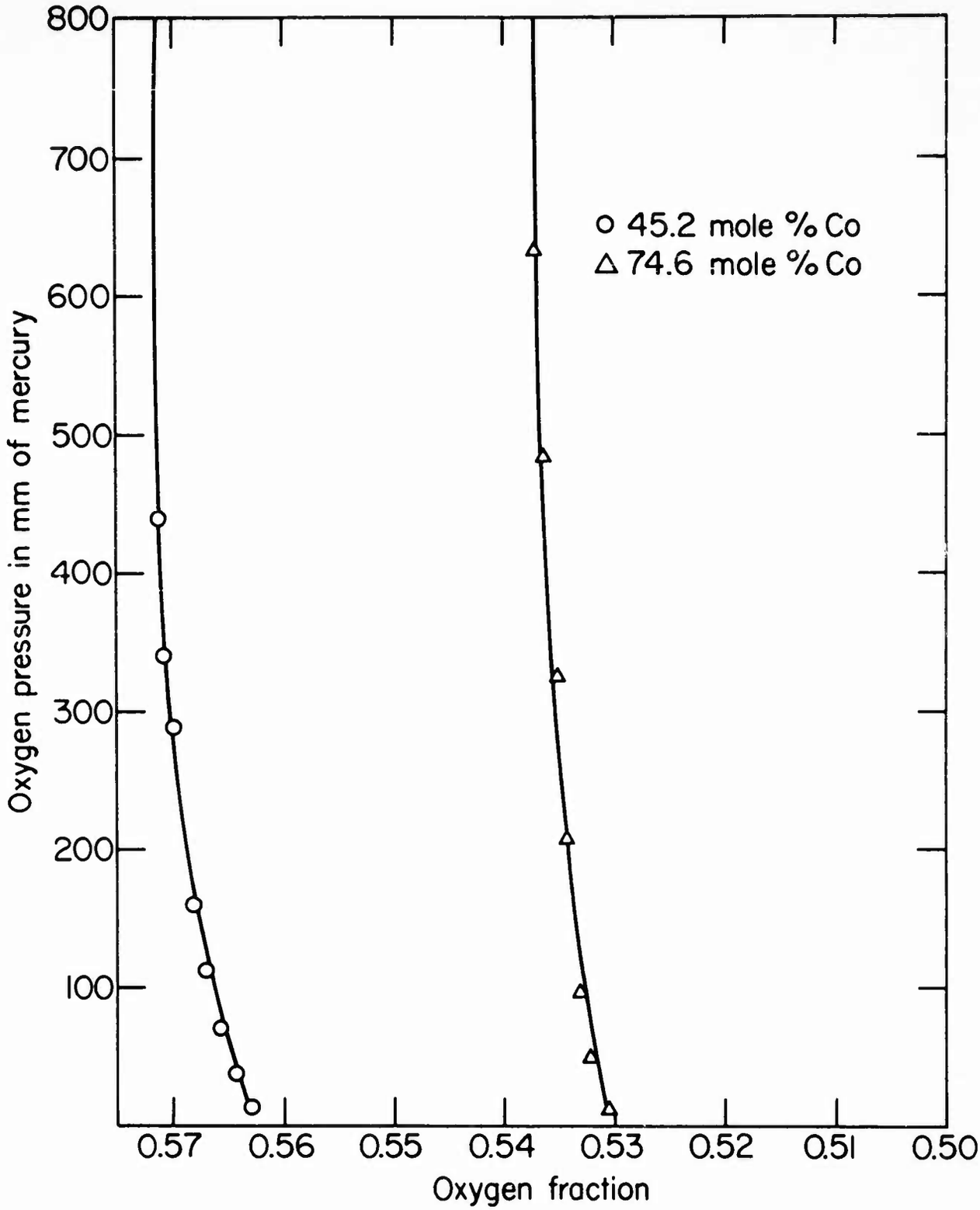


PRESSURE VS OXYGEN CONTENT FOR TWO COMPOSITIONS AT 1100 °C

FIGURE 24

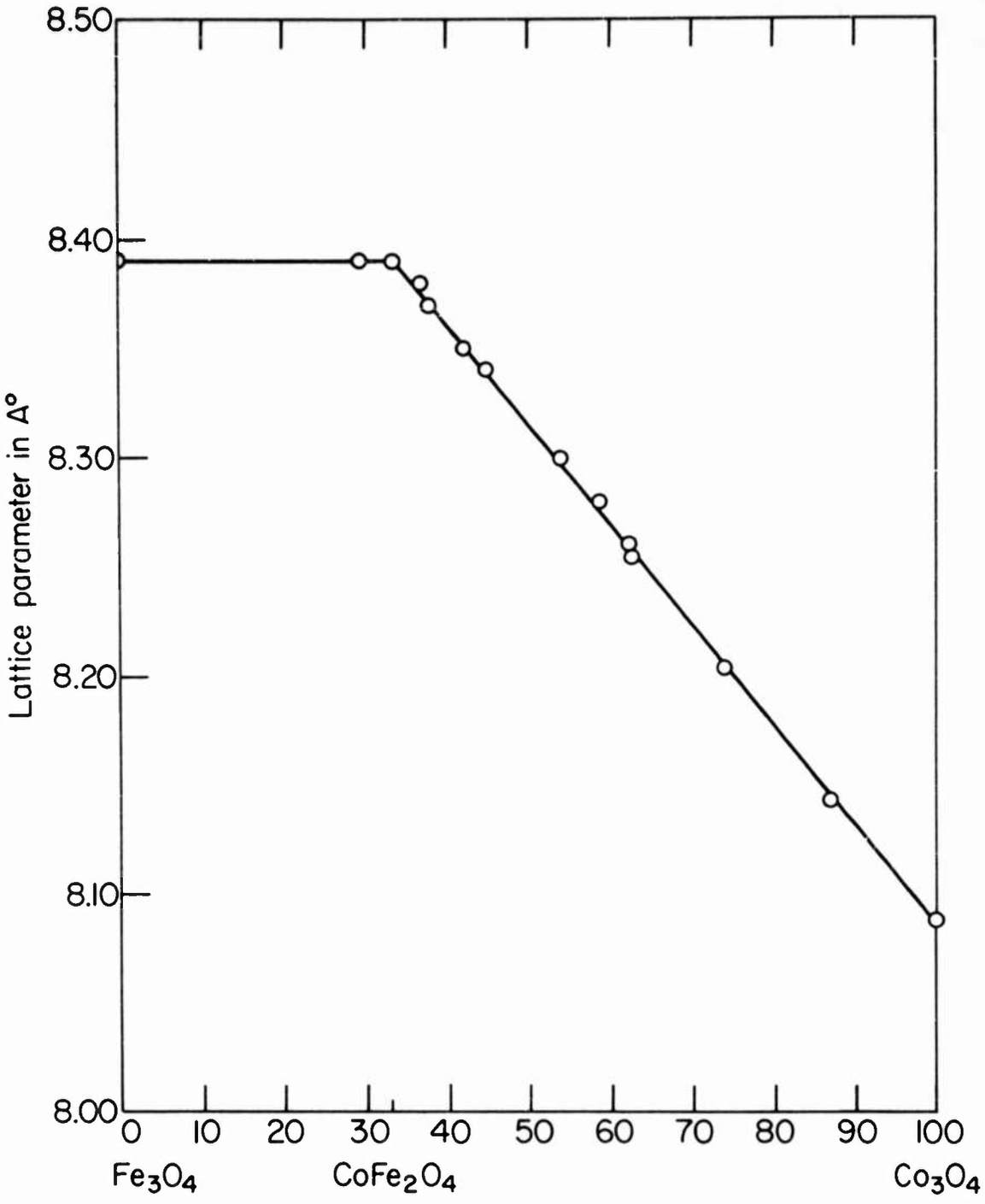


LATTICE PARAMETER VS COMPOSITION OF SPINEL IN THE SOLID SOLUTION SERIES $Fe_3O_4$-$Co_3O_4$

FIGURE 25

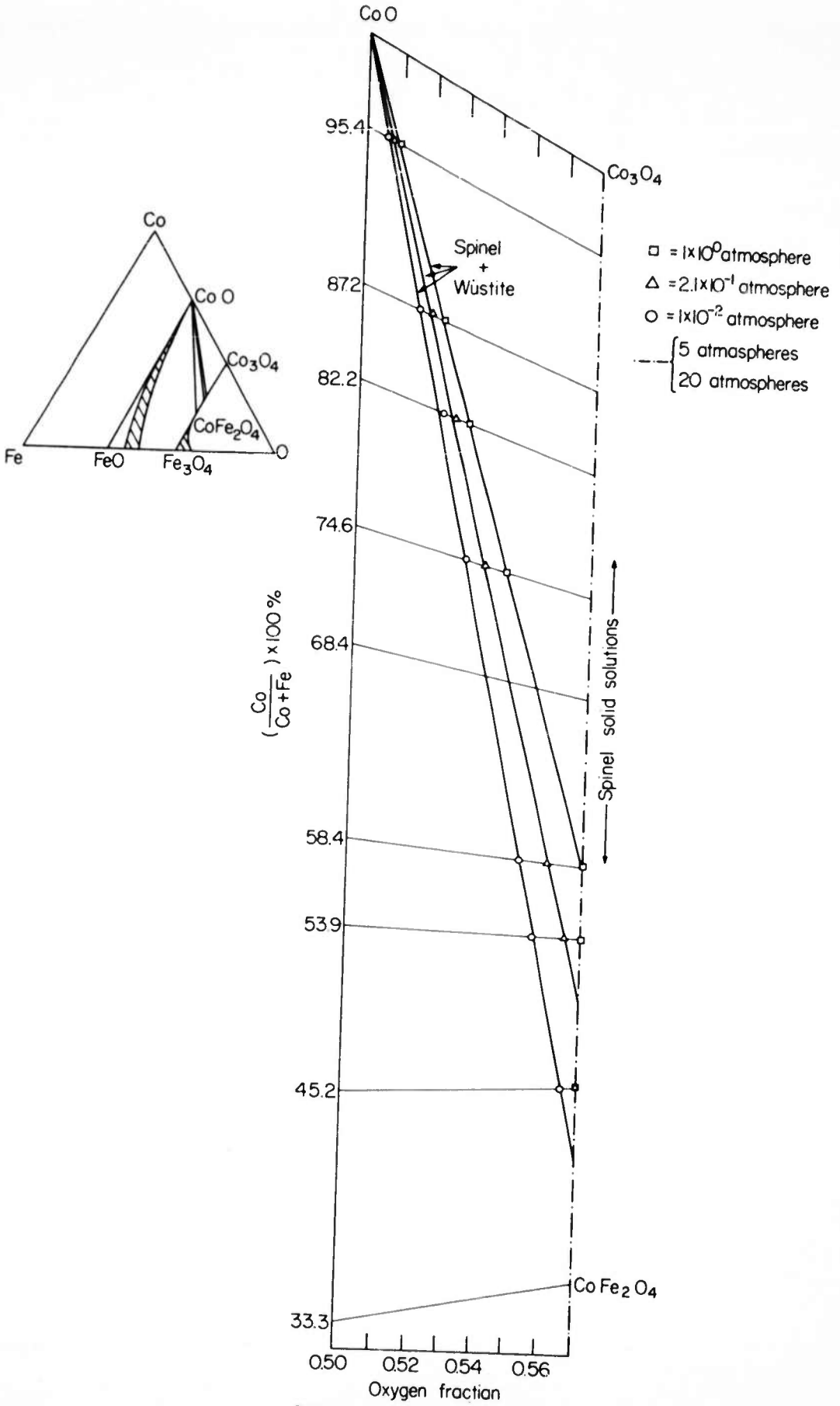


PHASE RELATIONS IN THE SYSTEM
Fe-Co-O AT 1000 °C

FIGURE 26

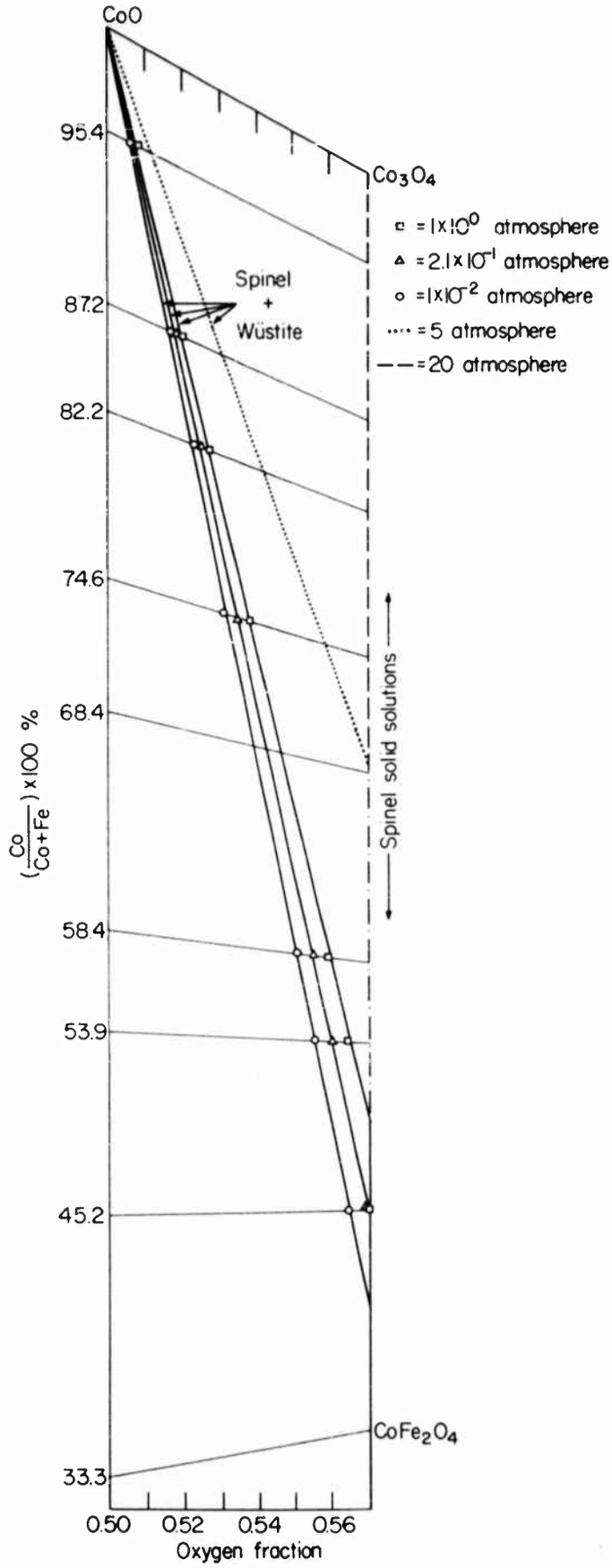


PHASE RELATIONS IN THE SYSTEM
Fe-Co-O AT 1100 °C

FIGURE 27

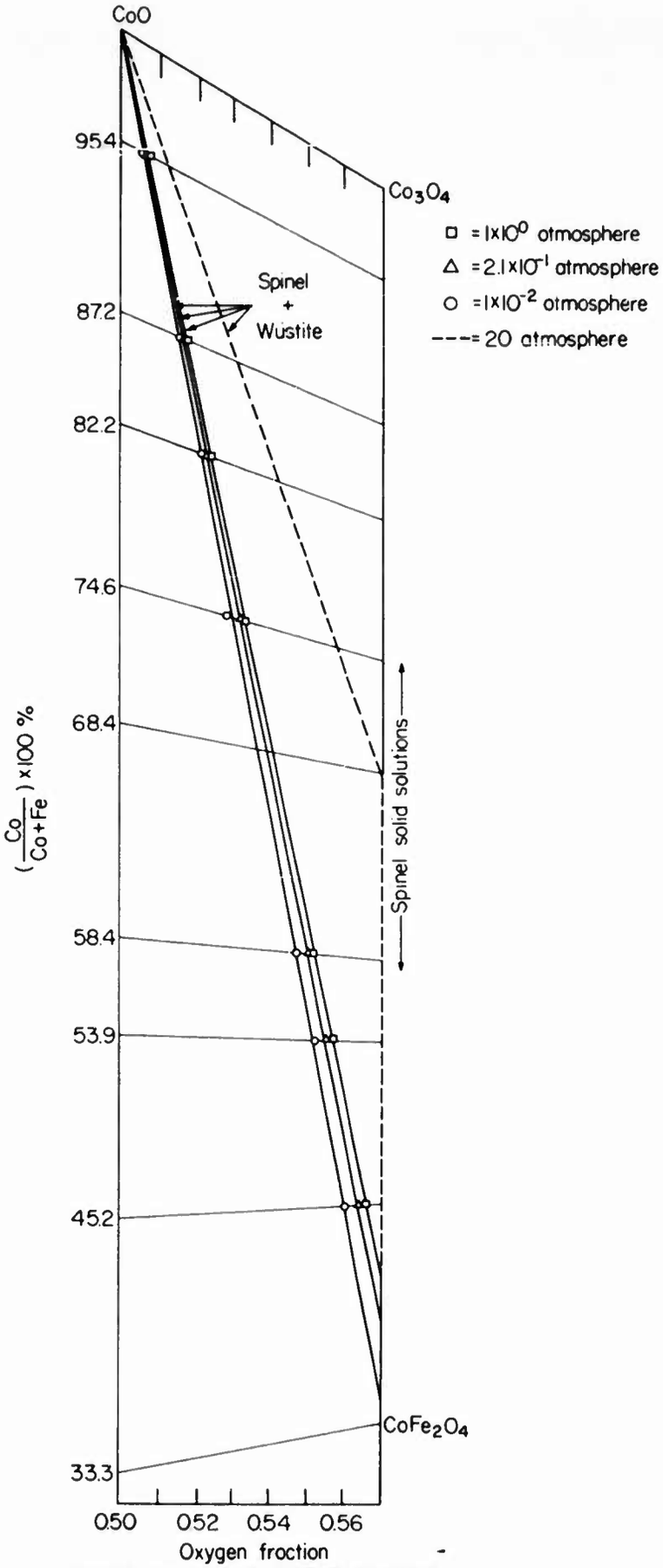


PHASE RELATIONS IN THE SYSTEM Fe-Co-O AT 1200 °C

**FIGURE 28**

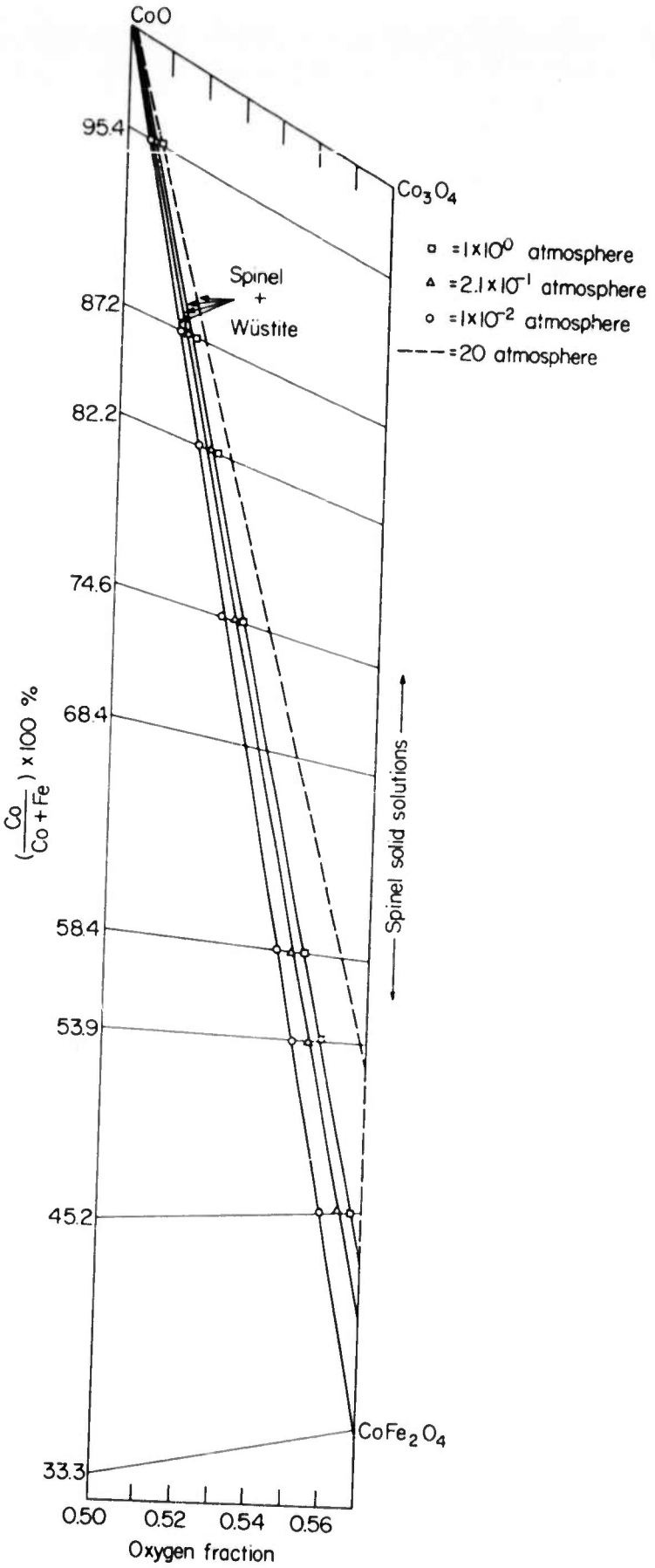


PHASE RELATIONS IN THE SYSTEM
Fe-Co-O AT 1300 °C

FIGURE 29

TABLE III

ATOMIC FRACTION OF OXYGEN AT EACH TEMPERATURE AND THREE ISOBARS FOR CONSTRUCTING THE TERNARY DIAGRAM, Fe-Co-O

| Composition Mole % Cobalt $\frac{Co}{Co+Fe} \times 100\%$ | 1000°C | | | 1100°C | | | 1200°C | | | 1300°C | | |
|---|---|---|---|---|---|---|---|---|---|---|---|---|
| | 10° | $2.1\times10^{-1}$ | $10^{-2}$ | 10° | $2.1\times10^{-1}$ | $10^{-2}$ | 10° | $2.1\times10^{-1}$ | $10^{-2}$ | 10° | $2.1\times10^{-1}$ | $10^{-2}$ |
| 95.4 | 0.5086 | 0.5084 | 0.5070 | 0.5084 | 0.5084 | 0.5074 | 0.5088 | 0.5084 | 0.5074 | 0.5088 | 0.5076 | 0.5074 |
| 87.2 | 0.5214 | 0.5204 | 0.5180 | 0.5202 | 0.5188 | 0.5169 | 0.5200 | 0.5188 | 0.5165 | 0.5198 | 0.5187 | 0.5161 |
| 82.2 | 0.5310 | 0.5298 | 0.5258 | 0.5273 | 0.5260 | 0.5240 | 0.5268 | 0.5258 | 0.5229 | 0.5256 | 0.5243 | 0.5211 |
| 74.6 | 0.5440 | 0.5382 | 0.5324 | 0.5376 | 0.5340 | 0.5300 | 0.5332 | 0.5327 | 0.5290 | 0.5318 | 0.5312 | 0.5272 |
| 58.4 | 0.5714 | 0.5680 | 0.5517 | 0.5598 | 0.5538 | 0.5498 | 0.5532 | 0.5516 | 0.5480 | 0.5524 | 0.5496 | 0.5460 |
| 53.9 | 0.5714 | 0.5660 | 0.5554 | 0.5644 | 0.5592 | 0.5544 | 0.5596 | 0.5564 | 0.5534 | 0.5570 | 0.5548 | 0.5510 |
| 45.2 | 0.5714 | 0.5714 | 0.5658 | 0.5714 | 0.5682 | 0.5624 | 0.5690 | 0.5656 | 0.5612 | 0.5666 | 0.5634 | 0.5596 |

TABLE IV

PHASE IDENTIFICATION OF QUENCHED SAMPLES - AIR ISOBAR

| Composition Mole % Cobalt $\frac{Co}{Co+Fe} \times 100\%$ | 1000°C | | 1100°C | | 1200°C | | 1300°C | |
|---|---|---|---|---|---|---|---|---|
| | Spinel | F. C. C. | Spinel | F. C. C. | Spinel | F. C. C. | Spinel | F. F. C. |
| 95.4 | - - - -* | 4.255 | - - - - | 4.255 | - - - - | 4.255 | - - - - | 4.255 |
| 87.2 | Present | Present | Present | Present | | | | |
| 82.2 | Present | 4.247 | Present | 4.244 | Present | 4.242 | - - - - | Present |
| 74.6 | 8.327 | 4.246 | 8.354 | Present | Present | Present | Present | Present |
| 62.2 | Present | Present | 8.354 | Present | 8.367 | Present | Present | Present |
| 58.4 | 8.326 | Present | 8.355 | Present | 8.367 | Present | 8.375 | Present |
| 53.9 | 8.326 | Present | 8.355 | Present | 8.367 | Present | 8.375 | Present |
| 45.2 | 8.343 | - - - - | 8.355 | Present | 8.366 | Present | | |
| 36.0 | 8.382 | - - - - | 8.382 | - - - - | 8.382 | - - - - | 8.382 | - - - - |

*- - - - Not detected.

Lattice constant precesion to ± 0.001 Å.

TABLE V

COMPOSITION OF THE SPINEL PHASE AT THE WÜSTITE - SPINEL FIELD BOUNDARY

| Temperature | Oxygen Pressure (Atm.) | Atomic Fraction Component Fe | Co | O* |
|---|---|---|---|---|
| | 20 | - - - | 0.4286 | 0.5714 |
| | 5 | - - - | 0.4286 | 0.5714 |
| 1000°C | 1 | 0.1786 | 0.2500 | 0.5714 |
| | 0.21 | 0.2146 | 0.2140 | 0.5714 |
| | 0.01 | 0.2586 | 0.1700 | 0.5714 |
| | 20 | - - - | 0.4286 | 0.5714 |
| | 5 | $0.18_8$ | $0.24_0$ | 0.5714 |
| 1100°C | 1 | 0.2186 | 0.2100 | 0.5714 |
| | 0.21 | 0.2446 | 0.1840 | 0.5714 |
| | 0.01 | 0.2666 | 0.1620 | 0.5714 |
| | 20 | $0.13_5$ | $0.29_4$ | 0.5714 |
| | 1 | 0.2506 | 0.1780 | 0.5714 |
| 1200°C | 0.21 | 0.2636 | 0.1650 | 0.5714 |
| | 0.01 | 0.2861 | 0.1425 | 0.5714 |
| | 20 | $0.20_6$ | 0.223 | 0.5714 |
| | 1 | 0.2566 | 0.1720 | 0.5714 |
| 1300°C | 0.21 | 0.2686 | 0.1600 | 0.5714 |
| | 0.01 | 0.2876 | 0.1410 | 0.5714 |

*From the discussion in the text, the spinel - wüstite boundary is assumed to be at exactly the 4/7 oxygen fraction line.

Figure 27 presents the 1100°C data. The five atmosphere isobar emerges from the spinel field at about 68.4 percent cobalt, whereas the twenty atmosphere isobar remains in the spinel field all the way to $Co_3O_4$. Again at this temperature, and at the 1200°C and 1300°C levels, the CoO field is not extended appreciably. In Table V the composition of the spinel phase in equilibrium with wüstite at the higher pressures is given with only two significant figures, the third being estimated because of the use of lattice parameter data only.

At 1200°C (Fig. 28) and 1300°C (Fig. 29) the three low pressure isobars have moved very little, whereas the twenty atmosphere tie line has moved down considerably towards $CoFe_2O_4$. At 1300°C, in fact, the twenty atmosphere isobar does not extend the spinel field towards $Co_3O_4$ a significant amount more than the one atmosphere isobar. Consequently, extremely high pressures would be required to prepare spinels between $CoFe_2O_4$ and $Co_3O_4$ in the temperature range necessary for sintering to dense compacts.

d. Conclusions

From the phase equilibria presented, it is apparent that very high oxygen pressures will be necessary to prepare single phase spinels between $CoFe_2O_4$ and $Co_3O_4$ at temperatures up to 1300°C. Most significantly, twenty atmospheres only allows for extending the spinel field to 52 percent cobalt (vs 33 percent Co in $CoFe_2O_4$) at 1300°C. In contrast, the preparation of spinels between $Fe_3O_4$ and $CoFe_2O_4$ will require low pressures, consistent with the phase relations presented by Smiltens.[35a] In fact, continuously changing pressures will be required if quenching cannot be used. Between $CoFe_2O_4$ and $Co_3O_4$ on the other hand, pressures can be kept constant but high over quite a temperature range before two phase situations would arise, viz., precipitation of $Fe_2O_3$. Although $Fe_2O_3$ did not appear as separate phase in twenty atmospheres of oxygen down to 900°C, higher pressures might cause separation of this phase. Finally, to obtain single phase spinel solid solutions between $CoFe_2O_4$ and $Co_3O_4$, quenching from temperatures above the closing of the miscibility gap will be required, viz., above 900°C.

## 3. The System $FeO-Fe_2O_3-Al_2O_3$

Investigation of the phase relations in the system $FeO-Fe_2O_3-Al_2O_3$ has been started and this part of the program will be continued on the contract extension. Only a very brief consideration of this system is warranted because of the limited data obtained to date.

### a. Introduction

Among the more pertinent investigations are those of Richards and White[7] and Muan and Gee.[38] Although neither of these considered the complete series of solid solutions between $Fe_3O_4$ and $FeAl_2O_4$, they both showed a rather unusual widening of the spinel field in the direction of oxygen excess as aluminum substituted for iron in the spinel phase. Beyond about 50 mole percent $Fe_3O_4$ and 50 mole percent $FeAl_2O_4$, the data were insufficient to indicate whether this extreme widening of the field continued of decreased. These previous investigations were carried out in air and oxygen up to about 1700°C, so that from these results one concludes that very low oxygen pressures will be required to prepare spinel solid solutions lying on the $Fe_3O_4$-$FeAl_2O_4$ join.

### b. Experimental Procedure

The starting mixtures of $Al_2O_3$ and $Fe_2O_3$ were made by co-precipitating the desired Fe:Al ratio as hydroxides. The precipitates were thoroughly washed, dried at 110°C and calcined at 1000°C for twelve hours in oxygen. The material was broken up and passed through a 270 mesh screen. Each sample was chemically analyzed for percent $Al_2O_3$ and $Fe_2O_3$. The samples were pressed into discs of approximately five grams, fired in air at 1300°C for twelve hours and slowly cooled in air. From the results of the investigations, no decomposition takes place at this temperature in air. A disc of a desired composition was accurately weighed on an analytical balance and then suspended by means of a thin alumina rod at the thermal center of the furnace. The other end of the rod extended well out of the hot zone of the furnace where it

was attached to a pan of the analytical balance by means of a platinum wire. The technique eliminated the use of a platinum crucible for containing the sample. This is desirable because significant losses in weight of platinum do arise through volatilization at high temperatures. The loss of oxygen from the sample was recorded automatically by a Maur automatic recording balance shown in Fig. 1.

By mixing the proper ratios of nitrogen and oxygen, the furnace atmosphere can be varied from one atmosphere oxygen to a partial pressure of oxygen of $1 \times 10^{-3}$ atmosphere. For oxygen partial pressures from $1 \times 10^{-10}$ atmosphere, mixtures of $CO_2$ and CO are necessary. The gases are purified, dried, and then mixed after passing through calibrated flow meters (Fig. 1). The gas mixing apparatus was calibrated against the $Fe_2O_3$-$Fe_3O_4$ decomposition as given by Darken and Gurry.[33a]

c. Discussion and Results

Weight loss measurements on several compositions at 1300°C in an oxygen pressure of $1 \times 10^{-6}$ atmosphere indicate that this isobar lies within the spinel field very close to the $Fe_3O_4$-$FeAl_2O_4$ join. Although the ternary diagram will eventually be constructed in terms of FeO-$Fe_2O_3$-$Al_2O_3$, it is more appropriate here to discuss the oxygen content in terms of its fraction of the components Al, Fe, and O. For compositions up to 40 mole percent Al, where mole percent here refers to $(\frac{Al}{Al + Fe} \times 100\%)$, the oxygen fraction varied between 0.5712 and 0.5717 as compared to the 0.5714 in $M_3O_4$. X-ray analysis performed on quenched samples of these same compositions revealed the presence of a single phase spinel structure. These preliminary results indicate that pressures well below $10^{-6}$ atmospheres will be required as the temperature is decreased to maintain the spinel at the stoichiometric oxygen content.

## B. CONDUCTIVITY STUDIES

### 1. Electrical Conductivity in Nickel-Ferrous Ferrites

#### a. Introduction

Electrical conductivity studies have been made on several sets of samples of nickel-ferrous ferrites ($Ni_{1-x}Fe_{2+x}O_4$) with $0.1 \leq x \leq 1$. To provide additional information for the interpretation of the conductivity data, thermoelectric measurements have recently been introduced and it is expected that future studies will involve both types of measurements.

#### b. Sample Preparation

Samples for resistivity measurements were prepared by mixing the desired ratios of Baker's Reagent Grade NiO and $Fe_2O_3$ in a methanol medium. Glass jars without balls were used rather than standard ball mills to maintain the reagent purity. After drying the powders under heating lamps, the materials were introduced into a tube furnace at 1300°C in a $CO_2$ atmosphere and held for twelve hours, then quenched. From the previously discussed phase equilibria data, it was shown that the $CO_2$ isobar lies on the $Fe_3O_4$-$NiFe_2O_4$ join (up to $x = 0.10$, III. A-1). Therefore, at this temperature and pressure, resulting compositions can be represented exactly by $Ni^{2+}_{1-x}Fe^{2+}_{x}Fe^{3+}_{2}O_4$. The powders were screened, mixed a second time, and reacted again at 1300°C in $CO_2$. Small pellets were pressed without binder and then sintered at 1400°C in $CO_2$ (except $x = 0.10$). These pellets were quenched, cut, and then ground into spheres. The spheres were heat treated again at 1400°C in $CO_2$ and quenched.

The electrical conductivity studies have been troubled by inconsistencies between measurements on materials prepared at different times by slightly different techniques from that described above. In addition, in some cases the measurements on a given set of samples were not consistent in themselves, e.g., the sample with $x = 0.7$ having a higher resistivity than the sample with $x = 0.6$. Improvement of sample quality is the subject of current and projected

studies. An attempt is being made to sinter the samples on the previously described thermobalance in a continuously changing atmosphere. This will allow for heating and cooling a sample under equilibrium conditions, rather than quenching the material. The analysis below, however, is based on two sets of samples already measured.

c. Resistivity Measurements

Resistivity measurements were carried out on small polycrystalline spheres at 10 kMc using the eddy current technique.[39, 40] It is believed that the resulting resistivities are those pertaining to the bulk material, independent of the grain boundaries; that is, the observed resistivities are those which would be measured at dc, if the resistance of the grain boundaries could be eliminated. The most self-consistent set of measurements thus far is shown in Fig. 30, which is a plot of measured $\rho/T$ on a log scale vs $1/T$, where $\rho$ is the resistivity and T the absolute temperature. This figure will be discussed further after consideration of the model taken for the conductivity.

The model is that of electron hopping; that is, the electrons are assumed to spend most of the time attached to specific ferrous ions, jumping across a potential barrier in a negligible time to an adjacent previously ferric ion. These jumps are activated by lattice vibrations, and the mean time of stay $\tau$ is related to the activation energy E by

$$\tau = \tau_0 e^{E/kT} \quad . \tag{9}$$

The diffusion constant D is related to $\tau$ by

$$D = \frac{d^2}{6\tau} = \text{const } e^{-E/kT} \quad , \tag{10}$$

where d is the jump distance. The mobility, $\mu$, according to the Nernst-Einstein relationship, is given by

$$\mu = \frac{qD}{kT} \quad , \tag{11}$$

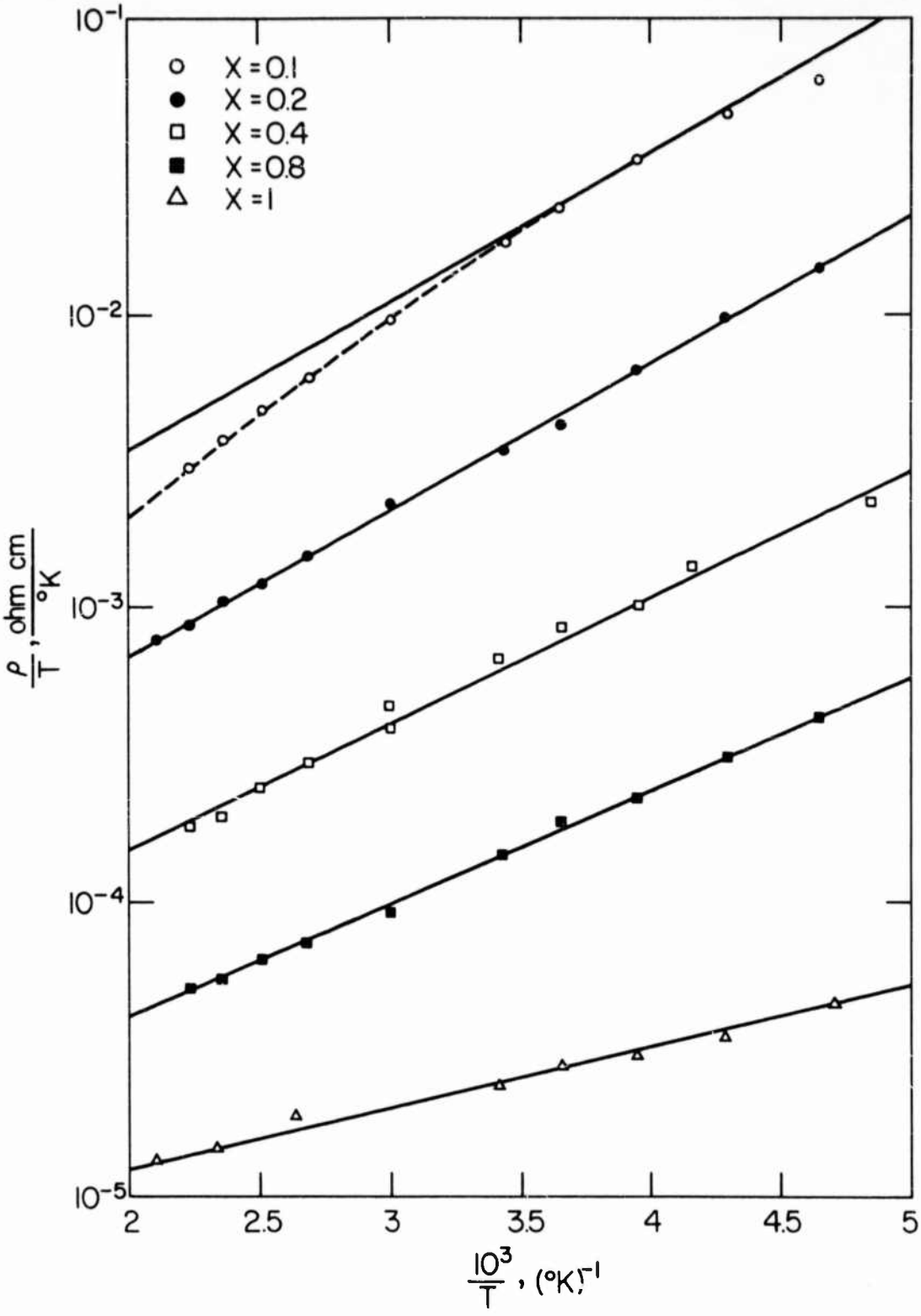


RESISTIVITY AS A FUNCTION OF RECIPROCAL TEMPERATURE FOR VARIOUS X VALUES IN $N^{2+}_{1-X}Fe^{2+}_{X}Fe^{3+}_{2}O_4$

FIGURE 30

where q is the electronic charge and k is Boltzmann's constant. Thus, if n is the density of carriers, the resistivity is

$$\rho = \frac{1}{nq\mu} = \frac{kT}{nq^2D} = \text{const}\ \frac{T}{n}\ e^{E/kT} \quad . \qquad (12)$$

Thus, if n is independent of temperature, a plot of log $\rho/T$ vs $1/T$ should be a straight line whose slope permits evaluation of the activation energy E. It is seen from Fig. 30 that very good straight lines result except for x = 0.1. The activation energies are given in Table VI.

TABLE VI

| x | E, ev |
|---|---|
| 0.2 | 0.099 |
| 0.4 | 0.085 |
| 0.8 | 0.076 |
| 1.0 | 0.042 |

With regard to the curve for x = 0.1, two facts may be noted. First, at low temperatures (large $1/T$), the slope of the curve falls off. This could arise from an additional conduction (or loss) mechanism, not thermally activated or having a smaller activation energy than the hopping process. Secondly, a rather steep slope is beginning to develop at the high temperature (low $1/T$) end. It appears that this effect may be explained by the appearance of intrinsic current carriers, in addition to those arising from the iron excess. At this point, it is appropriate to develop analytical expressions for the carrier densities.

We are concerned with those electrons capable of causing electrical conduction by moving among the octahedral cations. There is one such electron for each divalent cation. The energy of an electron when attached to a $Fe^{2+}$ ion is higher than when attached to an $Ni^{2+}$ ion. At very low temperatures, therefore, all the nickel ions will be divalent, and if there are N formula units of $(Fe^{3+})\left[ Ni^{2+}_{1-x}Fe^{2+}_{x}Fe^{3+} \right]O_4$ per unit volume, there will be Nx electrons moving among N (1 + x) iron sites. In general, however, we must consider the existence of thermally created $Ni^{3+}$ - $Fe^{2+}$ pairs. This not only permits the

existence of conduction through the nickel sites (hole conduction), but increases the number of electrons moving among the iron sites. Indeed, we will assume that the mobility of holes is negligible compared to the mobility of electrons among the iron sites, and consider only the influence of the increased number of divalent irons.

The fact that an electron attached to an $Fe^{2+}$ ion has an energy greater than one attached to an $Ni^{2+}$ ion is depicted in Fig. 31. Also shown is the Fermi

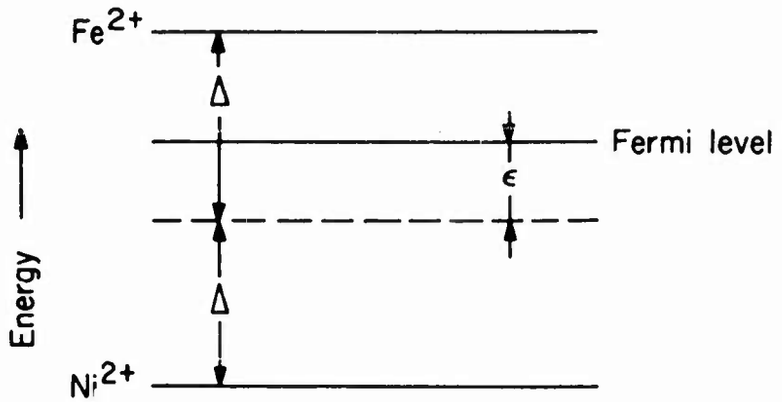


ENERGY LEVELS IN NICKEL FERROUS FERRITES
FIGURE 31

level, which will be discussed shortly. The dotted line is placed midway between the $Ni^{2+}$ and $Fe^{2+}$ levels and is chosen as the zero of energy. $\Delta$ and $\epsilon$ are then defined as the distance of the electronic levels and of the Fermi level from the center.

The statistical problem is now as follows: There are N electrons to be distributed between two types of sites: N (1 + x) Fe sites of energy $\Delta$ and N (1 - x) Ni sites of energy $-\Delta$. With the appropriate assumption that no more than one electron can be at a given site at any instant, the distribution of the electrons between the two types of sites is given by the Fermi-Dirac statistics as

$$n_{Fe} = \frac{N\,(1 + x)}{e^{(\Delta - \epsilon)/kT} + 1} \tag{13}$$

$$n_{Ni} = \frac{N\,(1 - x)}{e^{-(\Delta + \epsilon)/kT} + 1} \tag{14}$$

The Fermi energy, $\epsilon$, may be evaluated from the condition $n_{Fe} + n_{Ni} = N$. The result obtained is

$$e^{-\epsilon/kT} = \left[x^2 \sinh^2 (\Delta/kT) + 1\right]^{\frac{1}{2}} - x \sinh (\Delta/kT) \quad . \qquad (15)$$

Several special cases are now considered.

1. $x = 0$ (nickel ferrite): Then $\epsilon = 0$ for all T.
2. $x = 1$ (magnetite): $\epsilon = \Delta$ for all T.
3. $xe^{\Delta/kT} >> 1$: $\epsilon = \Delta + kT \ln x$. Then

$$n_{Fe} = \frac{N(1+x)}{e^{(\Delta - \epsilon)/kT} + 1} = \frac{N(1+x)}{e^{-\ln x} + 1} = \frac{N(1+x)}{\frac{1}{x} + 1} = Nx \quad . \qquad (16)$$

Thus condition (15) is the condition under which it is valid to assume that the number of carriers is given by the amount of ferrous iron indicated by the chemical formula.

Another equation which may be obtained from the above general relations is

$$e^{2\Delta/kT} = \frac{e^{(\Delta - \epsilon)/kT} - x}{e^{-(\Delta - \epsilon)/kT} - x} \quad . \qquad (17)$$

Use will be made of this formula below.

d. Correlation of Resistivity and Thermoelectric Data

Recently, thermoelectric measurements have been carried out in order to provide additional information for the interpretation of the conductivity data. Figure 32 is a plot of measured Seebeck coefficients at room temperature. (These measurements were made on a later set of samples than that whose resistivity data were discussed above. Unfortunately, the later material did not provide

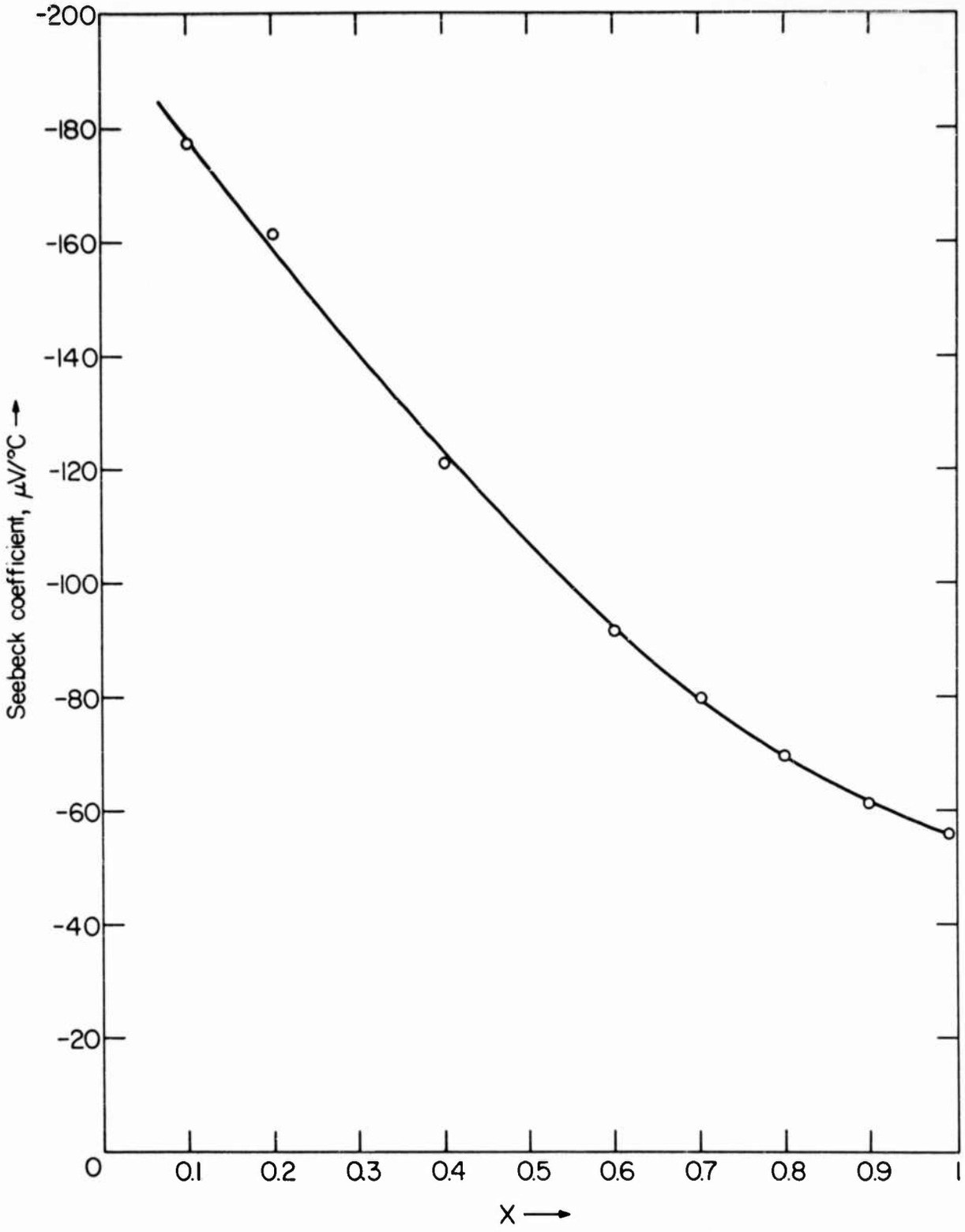


SEEBECK COEFFICIENT AS A FUNCTION OF X IN $Ni^{2+}_{1-x}Fe^{2+}_{x}Fe^{3+}_{2}O_4$ AT 300 °K

FIGURE 32

satisfactory samples for resistivity measurement.) The theory of the thermoelectric effect is complex, and what follows must be regarded as conjectural.

Figure 33 depicts the situation at the junction of a ferrite and a metal. The Fermi level is continuous across the junction. Electrons moving in the

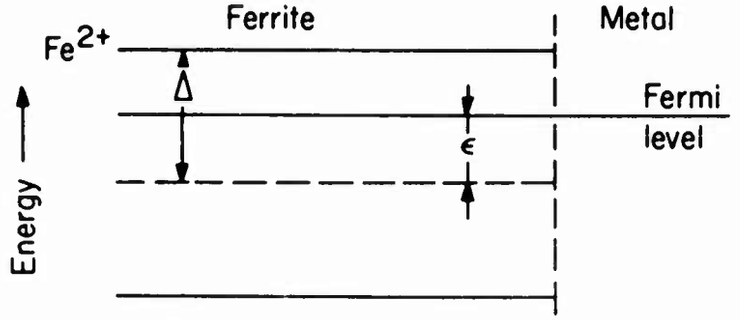


ENERGY LEVELS AT A JUNCTION OF A FERRITE AND METAL
FIGURE 33

ferrite have the energy corresponding to the $Fe^{2+}$ level while electrons conducting in the metal have energies near the Fermi level. Thus energy is released or absorbed as heat when an electron crosses the junction. The simplest assumption is that the energy released or absorbed is equal to the difference of the two transport levels, viz., $\Delta - \epsilon$. The heat per unit charge is $\pi = \frac{\Delta - \epsilon}{q}$ and is called the Peltier heat. In turn, $\pi$ is related to the Seebeck coefficient $\theta$ by the thermodynamic relationship $\pi = \theta T$. Thus

$$q\theta T = \Delta - \epsilon \quad . \tag{18}$$

At 300°K the measured value of Seebeck coefficient for $x = 0.1$ is 178 $\mu$ V/deg. Then $\Delta - \epsilon = 0.0534$ ev. From (17), $\Delta = 0.074$ ev. Since $\rho = 1/nq\mu$, it may be seen from (12) and (13) that

$$\rho = \text{const } T e^{E/kT} \left[ e^{(\Delta - \epsilon)/kT} + 1 \right] \quad . \tag{19}$$

We see from Table VI that the activation energies do not change rapidly at low x - values; a reasonable extrapolated value for $x = 0.1$ is $E = 0.1$ ev. The solid line in Fig. 30 is drawn for this value for constant n. If we take the above

mentioned $\Delta = 0.074$ ev and evaluate $\epsilon$ as a function of temperature from (15), a fair fit with the experimental points can be obtained using (19). A better fit results from using $\Delta = 0.09$ ev; this value was used to compute the broken line in Fig. 30. In view of several simplifications made in the analysis, the difference in the values of $\Delta$ is not too surprising. It should also be pointed out that the value of $\Delta = 0.09$ ev corresponds to a Seebeck coefficient of 191 $\mu$ V/deg, which is only 7% greater than the value of $\theta$ used to compute $\Delta = 0.074$. It should also be kept in mind that the resistivity measurements and the thermoelectric measurements were not made on the same set of samples. Needless to say, an analysis such as given above should be carried out on one set of samples when suitable materials are available.

## 2. Distribution Studies in Magnesium Ferrite

### a. Introduction

Prior to any attempt to measure electrical conductivity in magnesium substituted magnetites, determination of cation distributions will be required. It has been previously demonstrated that in this system, $MgFe_2O_4$ does not exist.[32] Magnesium extends the binary magnetite field to a nonstoichiometric (oxygen deficient) terminal composition. The object of this phase of the program is to determine cation distribution in the vicinity of the non-existent $MgFe_2O_4$.

The spinel lattice consists of approximately hexagonally close-packed oxygen layers which are stacked in the face-centered cubic sequence. Between the oxygen layers are interstitial lattice sites of both tetrahedral and octahedral coordination, which are partially occupied by metal ions. The unit cell contains eight molecules and has sixty-four tetrahedral and thirty-two octahedral interstitial positions. Of these, eight selected tetrahedral and sixteen selected octahedral sites are occupied. Writing the general formula, $A^{2+}B^{3+}{}_2O_4$, the cation distribution may vary from the so-called normal spinel in which the A ions are on tetrahedral and B ions on octahedral sites to the inverse spinel in which B ions are on the tetrahedral sites and the remaining A and B ions are distributed over the octahedral sites. A cation distribution between these two extreme cases may be described as a partial inversion and characterized by a distribution parameter $\lambda$ which is defined as the fraction of A ions on tetrahedral sites.

The crystallographic u parameter determines the degree of deviation from an ideal (u = .375) face-centered cubic close-packing of oxygens. In ferrite spinels u tends to be greater than 0.375 resulting in an enlargement of occupied tetrahedral sites relative to occupied octahedral sites so that their size become more nearly equal to each other than in the ideal case. The exact dimensions of these sites may be computed if u and the lattice parameter, a, are specified.

In magnesium ferrite both $\lambda$ and u may be established from the relative integrated intensities of several x-ray reflections. The present determinations are based on a least squares fit of calculated and observed integrated intensities. Two other parameters, an average Debye-Waller temperature factor and the normalization or scale factor, are adjusted in addition to $\lambda$ and u.

b. Discussion and Results

The objectives of the x-ray diffraction studies are the determination of a, $\lambda$, and u as a function of quench temperature for compositions of $Mg_{1-x}Fe_{2+x}O_4$ with $0.066 \leq x \leq 0.4$. Measurements have been completed for $Mg_{1.044}[Mg\Delta]_{0.22}Fe_{1.956}O_{4.000}$ with quench temperatures of 1100°C, 700°C, and 400°C. These results and a comparison with neutron diffraction values by Bacon and Roberts[41] for $MgFe_2O_4$ at 400°C are listed in Table VII. The notation [MgΔ] represents interstitial magnesium ions in other than the above mentioned selected positions, and are not included in the distribution determinations.*

The diffraction patterns were run on a Norelco diffractometer with Geiger counter detection using filtered $CoK_\alpha$ radiation and powdered samples. The lattice parameters, a, were derived from the peak positions of the (751) and (840) reflections which were calibrated using a silicon standard sample. Intensities were measured for several (hkℓ) reflections utilizing a fixed-count step-scanning device with intervals of 0.02° or 0.04° in 2θ and up to 25,600 counts per point. Geiger counter loss corrections were applied to the intensity at each point and the peak area above background was taken as a measure of the relative integrated intensity. Atomic scattering factors[42, 43, 44] for $Mg^{2+}$, $Fe^{3+}$, and $O^{2-}$ used in the intensity calculations were corrected for anomalous dispersion and the least squares fit was attained by an IBM 704 program for the determination of the cation distribution in spinel structures.

---

*The existence of interstitial Mg ions [MgΔ] has not been established and the actual formula may be $Mg_{1.060}Fe_{1.940}[O.V.]_{0.030}O_{3.970}$ where [O. V.] represents oxygen vacancies.

The study will be continued for compositions with $0 \leq x \leq 0.4$. $Fe^{2+}$ is substituted for $Mg^{2+}$ in these compositions and a complete determination would involve two cation distribution parameters, $\lambda$ and $\lambda'$, which are respectively the fractions of $Mg^{2+}$ and $Fe^{2+}$ occupying tetrahedral sites. Because of the nearly equal scattering factors of $Fe^{2+}$ and $Fe^{3+}$, an x-ray determination of $\lambda'$ is not feasible. However, $\lambda$ can be determined from x-ray data and since the saturation magnetization per formula weight should be $2[(2+\lambda')(1-x)+5\lambda x]$ Bohr magnetrons, combined x-ray and low temperature magnetic measurements could conceivably be used to find $\lambda'$.

TABLE VII

| Composition | Temperature (°C) | a(Å) | $\lambda$ | u |
|---|---|---|---|---|
| $Mg_{1.044}[Mg\Delta]_{0.22}Fe_{1.956}O_{4.000}$ | 1100° | $8.398_3$ | 0.28 | $0.38_1$ |
| " | 700° | $8.389_6$ | 0.22 | $0.38_0$ |
| " | 400° | $8.382_2$ | 0.09 | $0.38_2$ |
| $MgFe_2O_4$ [41] | 400° | | 0.1 | 0.382 ±0.002 |

## ACKNOWLEDGMENT

The authors would like to acknowledge the assistance of Messrs. C. R. Snider, F. G. Garabedian, R. B. Hawkes, and M. E. Nichols and Miss S. Georgian in the experimental work and Dr. B. D. Silverman for discussions on conductivity mechanisms.

## REFERENCES


1. E. J. W. Verwey, "Electronic Conduction of Magnetite ($Fe_3O_4$) and its Transition Point at Low Temperatures," Nature 144, 327 (1939).

2. G. H. Jonker, "Analysis of the Semiconducting Properties of Cobalt Ferrite," J. Phys. and Chem. Solids 9, 165-175 (1959).

3. H. J. Van Hook, "Single Crystal Growth of the Garnet Type Oxides. Part I Phase Relations in the System $Fe_2O_3$-$Fe_3O_4$-$YFeO_3$ in Air," AFCRC-TN-60-162 January 29, 1960; J. Am. Ceram. Soc. 44, 208-214 (1961).

4. H. J. Van Hook, "Single Crystal Growth of the Garnet Type Oxides, Part II Phase Relations in the Ternary System $Fe_2O_3$-FeO-$YFeO_3$," AFCRL 52 January 9 (1961).

5a. Arnulf Muan, "Phase Equilibrium in the System FeO-$Fe_2O_3$-$SiO_2$," Journal of Metals 7, 965-976 (1955);

b. Arnulf Muan, "Phase Equilibria at High Temperatures in Oxide Systems Involving Changes in Oxidation States," Am. J. Sci. 256, 171-207 (1958).

6. J. W. Greig, E. Posnjak, H. E. Merwin, and R. B. Sosman, "Equilibrium Relationships of $Fe_3O_4$, $Fe_2O_3$, and Oxygen," Am. J. Sci. 30, 239-316 (1935).

7. R. J. Richards and J. White, "Phase Relationships of Iron Oxide Containing Spinels," Brit. Ceram. Soc. Trans. 53, 233-270 (1954).

8. A. E. Paladino, Jr., "Phase Equilibria in the Ferrite Region of the System Fe-Ni-O," J. Am. Ceram. Soc. 42, 168-175 (1959).

## REFERENCES (Cont'd.)


9. J. W. Nielsen and E. F. Dearborn, "The Growth of Single Crystals of Magnetic Garnets," J. Phys. Chem. Solids 5, 202-207 (1958).

10. R. W. Ricker and E. F. Osborn, "Additional Phase Equilibrium Data on the System CaO-MgO-$SiO_2$," J. Am. Ceram. Soc. 37, 133-139 (1954).

11. J. White, "Equilibrium at High Temperatures in Systems Containing Iron Oxides," Iron Steel Inst. Carnegie Schol. Mem. 27, 1-75 (1938).

12. L. S. Kassel, "Thermodynamic Functions of Nitrous Oxide and Carbon Dioxide," J. Am. Chem. Soc. 56, 1838-1842 (1934).

13. S. Geller and E. A. Wood, "Crystallographic Studies of Perovskite-Like Compounds," Acta Cryst. 9, 563-568 (1956).

14. E. A. Maguire, "Ceramic and Magnetic Properties of Yttrium-Gadolinium-Iron Garnets," Raytheon Co., Research Div., Tech. Memo. T-221, March (1960).

15. I. Warshaw and R. Roy, "Stable and Metastable Equilibria in the Systems $Y_2O_3$-$Al_2O_3$ and $Gd_2O_3$-$Fe_2O_3$," J. Am. Ceram. Soc. 42, 434-438 (1959).

16. J. Bloem and F. A. Kröger, "The P-T-X Phase Diagram of the Lead-Sulphur System," Z. Physik. Chem. 7, 1-14 (1956).

17. W. D. Kingery, Introduction to Ceramics, (John Wiley and Sons, Inc. New York 1960).

18. F. C. Frank, "The Influence of Dislocations on Crystal Growth," Disc. Faraday Soc. 5, 48-54 (1949).

19. H. E. Buckley, Crystal Growth, (John Wiley and Sons, Inc., New York 1951).

## REFERENCES (Cont'd.)


20. W. B. Hillig and D. Turnbull, "Theory of Crystal Growth in Undercooled Pure Liquids," J. Chem. Phys. 24, 914 (1956).

21a. G. W. Sears, "The Effect of Poisons on Crystal Growth," in "Growth and Perfection of Crystals," R. H. Doremus, B. W. Roberts, D. Turnbull, Eds., (John Wiley and Sons, Inc., New York, 1958) 441-445;

b. G. W. Sears, "Investigation to Establish How Impurity Atoms Affect Crystal Nucleation," Final Report AFCRL-TR-60-35, April (1961).

22. R. Lacman and I. N. Stranski, "The Effect of Adsorption of Impurities on the Equilibrium Growth Forms of Crystals," in "Growth and Perfection of Crystals," R. H. Doremus, B. W. Roberts, D. Turnbull, Eds., (John Wiley and Sons, Inc., New York, 1958) 427-440.

23. W. A. Tiller, K. A. Jackson, J. W. Rutter and B. Chalmers, "The Redistribution of Solute Atoms During the Solidification of Metals," Acta Met. 1, 428-437 (1953).

24. Bruce Chalmers, "Melting and Freezing," Trans. AIME 200, 519-532 (1954).

25. R. C. L. Bosworth, Transport Processes in Applied Chemistry (John Wiley and Sons, Inc., New York, 1956) 387.

26. C. Wagner, "Theoretical Analysis of Solute During the Solidification of Alloys," Trans. AIME 200, 154-160 (1954).

27. A. Carlson, "The Fluid Mechanics of Crystal Growth from Solution," in "Growth and Perfection of Crystals," R. H. Doremus, B. W. Roberts, D. Turnbull, Eds., (John Wiley and Sons, Inc., New York, 1958) 421-426.

## REFERENCES (Cont'd.)


28. R. A. Laudise, "Hydrothermal Crystallization," in "Growth and Perfection of Crystals," R. H. Doremus, B. W. Roberts, D. Turnbull, Eds., (John Wiley and Sons, Inc., New York, 1958) 458-464.

29. R. C. DeVries, "Observations on Growth of $BaTiO_3$ Crystals from KF Solutions," J. Am. Ceram. Soc. 42, 547-558 (1959).

30. R. G. Rudness and R. W. Kebler, "Growth of Single Crystals of Incongruently Melting Yttrium Iron Garnet by Flame Fusion Process," J. Am. Ceram. Soc. 43, 17-22 (1960).

31. L. L. Abernethy, T. H. Ramsey and J. W. Ross, "Growth of Yttrium Iron Garnet Single Crystals by the Floating Zone Technique," J. Appl. Phys. 32, 376S-378S (1961).

32. A. E. Paladino, Jr., "Phase Equilibria in the Ferrite Region of the System $FeO-MgO-Fe_2O_3$," J. Am. Ceram. Soc. 43, 183-191 (1960).

33a. L. S. Darken and R. W. Gurry, "The System Iron-Oxygen, II Equilibrium and Thermodynamics of Liquid Oxide and Other Phases," J. Am. Chem. Soc. 68, 798-816 (1945);

b. J. Smiltens, "The Standard Free Energy of Oxidation of Magnetite to Hematite at Temperatures Above 1000°C," Laboratory for Insulation Research, Massachusetts Institute of Technology. Technical Report 116, January (1957).

34. D. E. Wickham, "The Synthesis of Ferrites and Preparation of Cobalt Ferrite Single Crystals," Laboratory for Insulation Research, Massachusetts Institute of Technology. Technical Report 89 (1954).

35a. J. Smiltens, "Investigation of the Ferrite Region of the Phase Diagram Fe-Co-O," J. Am. Chem. Soc. 79, 4881 (1957);

## REFERENCES (Cont'd.)


b. R. E. Carter, "Dissociation Pressures of Solid Solutions from $Fe_3O_4$ to $0.4\ Fe_3O_4 \cdot 0.6\ CoFe_2O_4$," J. Am. Ceram. Soc. 43, 448-452 (1960).

36. F. D. Rossini, D. D. Wagman, W. H. Evans, S. Levine, I. Jaffe, "Selected Values of Chemical Thermodynamic Properties," N. B. S. Circular 500, 252 (1952).

37. J. Robin and J. Benard, "Recherches sur la Structure et la Stabilité des Phases dans le System $Fe_2O_3$-$Co_3O_4$," Comptes Rendus 234, 734-735 (1952).

38. A. Muan and C. L. Gee, "Phase Equilibrium Studies in the System Iron Oxide-$Al_2O_3$ in Air and at 1 Atm. $O_2$ Pressure," J. Am. Ceram. Soc. 39, 207-214 (1956).

39. T. Kohane and M. H. Sirvetz, "Measurement of Microwave Resistivity by Eddy Current Loss in Spheres," Rev. Sci. Instr. 30, 1059 (1959).

40. T. Kohane, "The Measurement of Microwave Resistivity by Eddy Current Loss in Small Spheres," IRE Transactions on Instrumentation I-9, 184 (1960).

41. G. E. Bacon and F. F. Roberts, "Neutron Diffraction Studies of Magnesium Ferrite - Aluminate Powders," Acta Cryst. 6, 57 (1953).

42. J. Berghuis, et al., "New Calculations of Atomic Scattering Factors," Acta Cryst. 8, 478 (1955).

43. R. E. Watson and A. J. Freeman, "Hartree-Fock Atomic Scattering Factors for the Iron Transition Series," Acta Cryst. 14, 27 (1961).

44. A. J. Freeman, private communication.

## DISTRIBUTION LIST

| Code | Organization | No. of Copies |
|---|---|---|
| AF 5 | AFMTC (AFMTC Tech Library - MU-135)<br>Patrick AFB, Fla. | 1 |
| AF 18 | AUL<br>Maxwell AFB, Ala. | 1 |
| AF 43 | ASD (ASAPRL)<br>Wright-Patterson AFB, Ohio | 1 |
| AF 139 | AF Missile Development Center (MDGRT)<br>Holloman AFB, New Mexico | 1 |
| AF 244 | OAR<br>Attn: AFOSR Library<br>Washington 25, D. C. | 1 |
| AF 318 | OAR (ARL, Tech Library)<br>Building 450<br>Wright-Patterson AFB, Ohio | 1 |
| AF 319 | ARDC (RDRS)<br>Andrews AFB<br>Washington 25, D. C. | 1 |
| Ar 5 | U. S. Army Signal Engineering Laboratories<br>Technical Documents Center<br>Evans Signal Laboratory<br>Belmar, New Jersey | 1 |
| AR 9 | Chief of Research and Development<br>Department of the Army<br>Washington 25, D. C.<br>Attn: Scientific Information Branch | 1 |
| Ar 67 | Army Rocket & Guided Missile Agency<br>Redstone Arsenal, Ala.<br>Attn: ORDXR-OTL, Technical Library | 1 |
| G 2 | ASTIA<br>Arlington Hall Station<br>Arlington 12, Virginia | 10 |

DISTRIBUTION LIST (Cont'd)

| Code | Organization | No. of Copies |
|---|---|---|
| G 68 | National Aeronautics & Space Agency<br>1520 H Street, N. W.<br>Washington 25, D. C.<br>Attn: Library | 1 |
| G 109 | Director<br>Langley Research Center<br>National Aeronautics & Space Administration<br>Langley Field, Virginia | 1 |
| M 6 | AFCRL, Office of Aerospace Research (CRRELT)<br>L. G. Hanscom Field, Bedford, Mass. | 20 |
| N 1 | Director, Avionics Division (AV)<br>Bureau of Aeronautics<br>Department of the Navy<br>Washington 25, D. C. | 2 |
| N 29 | Director (Code 2027)<br>U. S. Naval Research Laboratory<br>Washington 25, D. C. | 2 |
| 1 292 | Director, USAF Project RAND<br>Via: AF Liaison Office<br>The Rand Corporation<br>1700 Main Street, Santa Monica, Cal. | 1 |
| AF 127 | Boston Sub Office<br>Patent Prosecution Branch (Hq. AMC)<br>Murphy General Hospital, Building 133<br>424 Trapelo Road, Waltham 54, Mass. | 1 |
| AF 253 | EOARDC<br>Shell Building<br>47 Rue Cantersteen<br>Brussels, Belgium | 1 |
| Ar 107 | U. S. Army Aviation Human Research Unit<br>U. S. Continental Army Command<br>P. O. Box 438, Fort Rucker, Ala.<br>Attn: Maj. Arne H. Eliasson | 1 |

DISTRIBUTION LIST (Cont'd)

| Code | Organization | No. of Copies |
|---|---|---|
| G 8 | Library<br>Boulder Laboratories<br>National Bureau of Standards<br>Boulder, Colorado | 2 |
| M 63 | Institute of the Aeronautical Sciences<br>2 East 64th Street<br>New York 21, New York<br>Attn: Librarian | 1 |
| N 73 | Office of Naval Research<br>Branch Office, London<br>Navy 100, Box 39<br>F. P. O. New York, N. Y. | 10 |
| U 32 | Massachusetts Institute of Technology<br>Research Laboratory of Electronics<br>Building 26, Room 327, Canbridge 39, Mass.<br>Attn: John H. Hewitt | 1 |
| AF 328 | Hq. ARDC (RDR-62)<br>Reference 4608 - CA<br>Andrews AFB, Washington 25, D. C. | 3 |
| Ar 105 | Commanding Officer<br>U. S. Army Signal R&D Lab.<br>Fort Monmouth, New Jersey<br>Attn: SIGFM/EL-PEM, Mr. I. Bady | 1 |
| G 97 | Advisory Group on Electron Parts<br>Moore School Building<br>200 South 33rd Street<br>Philadelphia 4, Penn.<br>Attn: Col. A. E. Mickelsen | 3 |
| G 53 | Advisory Group on Electronic Parts<br>Moore School Building<br>200 South 33rd Street<br>Philadelphia 4, Penn.<br>Attn: Working Group on Electronic Materials | 4 |

## DISTRIBUTION LIST (Cont'd)

| Code | Organization | No. of Copies |
|---|---|---|
| G 70 | Advisory Group on Electron Tubes<br>346 Broadway, 8th Floor<br>New York 13, N. Y.<br>Attn: Secretary, Working Group on Semiconductor Devices | 4 |
| M 60 | ESD (ESRRI, Maj. James Van Horn)<br>L. G. Hanscom Field, Bedford, Mass. | 1 |
| I 439 | International Tel. & Tel. Corp.<br>I. T. T. Laboratories Division<br>500 Washington Avenue<br>Nutley 10, New Jersey<br>Attn: Mr. P. E. Lighty, Executive Engineer | 1 |
| I 608 | Westinghouse Electric Corp.<br>Materials Engineering Department<br>501 Highland Avenue<br>East Pittsburgh, Penn.<br>Attn: Mr. J. A. Osborn | 1 |
| I 817 | Varian Associates<br>611 Hansen Way<br>Palo Alto, California<br>Attn: Morris Feinleib | 1 |
| U 281 | Massachusetts Institute of Technology<br>Laboratory for Insulation Research<br>Cambridge 39, Mass.<br>Attn: Prof. A. Von Hippel | 1 |